Synchronization in the suprachiasmatic nucleus through gap junction and neuromodulator coupling

O.O. Heerkens Thijssen

Technische Universiteit Delft

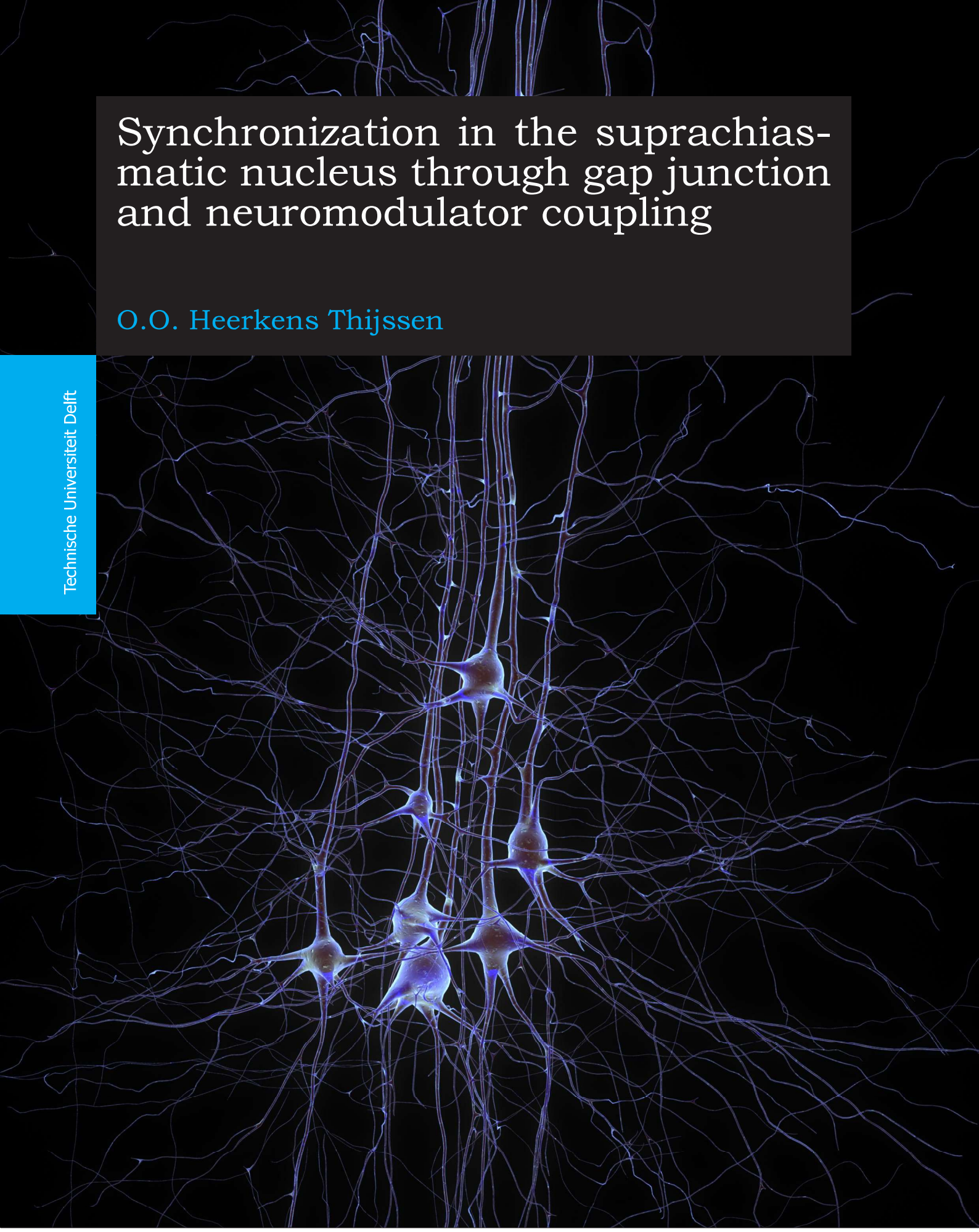

TU Delft Delft University of Technology

Challenge the future

Synchronization in the suprachiasmatic nucleus through gap junction and neuromodulator coupling

by

O.O. Heerkens Thijssen

in partial fulfillment of the requirements for the degree of

Master of Science
in Systems & Control

at the Delft University of Technology,
to be defended publicly on Tuesday October 8, 2019 at 14:00.

Supervisor:	Dr. E. Steur,	TU Delft
Thesis committee:	Prof. dr. ir. B. De Schutter,	TU Delft
	Dr. ir. K. Batselier,	TU Delft
	Dr. J. Rohling,	Leiden University

TU Delft Delft University of Technology

Preface

This thesis titled "Synchronization in the suprachiasmatic nucleus through gap junction and neuromodulator coupling" is the result of a research on synchronization through neuronal coupling in the suprachiasmatic nucleus. It has been written to fulfill the graduation requirements of the MSc Systems & Control at the TU Delft. I was engaged in researching and writing this dissertation from April 2018 until September 2019.

I would like to thank my supervisor Erik Steur for his excellent guidance and support. In addition, I wish to thank Jos Rohling for sharing his biological knowledge and for shaping this research on an early stage. In addition, I wish to thank my peers in the Systems & Control department for reading and commenting on the developing report.

Oscar Heerkens Thijssen

Delft, 23-09-2019

Abstract

A better understanding in the biological clock is important to help reduce stress on shift workers. Moreover, in the field of medication it will allow for more effective treatments as certain types of medication are more effective when applied at certain moments in the 24-hour cycle.

The mammalian biological clock is controlled by a tiny area in the brain called the suprachiasmatic nucleus (SCN). The neurons in the SCN are able to synchronize their clock gene expression to each other through coupling. However, it is unclear how different types of coupling affect the synchronizing property of the SCN. This research explores how two types of coupling, namely gap junction coupling and neuromodulator diffusion shape the synchronous behaviour of a network of SCN neurons.

Since data collection in the biological system is challenging, this research is done using a modeling approach. A mathematical single SCN neuron model was analyzed and scaled to a network representation. The individual neuron models in this network were coupled using gap junction and neuromodulator models.

In this research, it was found that gap junction coupling is a precise and strictly local form of coupling. However, in a network there is a maximum number of neurons that can be synchronized, assuming that the number of gap junctions per neuron is limited. Therefore, it was concluded that in large SCN networks gap junction coupling is not able to completely synchronize the network.

Neuromodulator coupling is imprecise, slow and global. It can effectively synchronize large phase errors, however, as phase errors become small, neuromodulator coupling loses much of its synchronizing ability. Therefore, it can only synchronize the daily pattern and cannot synchronize on the level of action potentials. Furthermore, it was shown that neuromodulator diffusion can synchronize SCN networks of arbitrary size.

As a final conclusion, the combination between gap junctions and neuromodulator diffusion is able to synchronize a network completely, perfectly, and rapidly. The neuromodulator component ensures complete synchronization while the gap junctions guarantee perfect synchronization (in the absence of noise). Furthermore, the combination ensures effective synchronization for both small and large phase errors. Therefore, the combination of these two types of coupling is vital in the establishment of network with versatile synchronization properties.

Contents

List of Figures

List of Tables

Chapter 1

Introduction

Every cell in the human body oscillates on a near 24-hour cycle. This oscillation is controlled by the circadian clock. This is a complex biochemical system that allows organisms to predict and adjust to one of the biggest environmental changes on earth: the day/night cycle. At the heart of this system lays the suprachiasmatic nucleus (SCN), located at the base of the hypothalamus. The SCN not only ensures that all cells in the human body oscillate in synchrony with respect to each other, but also that this oscillation is entrained to the external light/dark cycle; it acts as a master clock for all body processes [2].

The SCN is a neural network of about 20,000 cells. The nucleus consists of two almond shaped parts that are located on opposite sides of the third ventricle. The left and right part that form the SCN are similar. The SCN is situated just above the optic chiasm (hence the name), and receives input from the retina. Photosensitive ganglion cells in the retina send information about the external light intensity to the SCN cells, to which the neurons synchronize.

Every single SCN neuron has an intrinsic cycle with an approximate 24 hour period. This period is established by a genetic feedback loop involving several genes. Individual cells are coupled electrically by so called gap junctions and chemically by neuromodulator diffusion. Through this coupling the activity of individual neurons is constantly delayed or advanced, leading to a synchronized genetic feedback loop.

1.1 Problem statement

Some states of the genetic feedback loop can be measured. At the Leiden University Medical Center a biomarker was attached to one of the genes in the feedback loop such that the expression of this gene becomes observable. The resulting Figure 1.1 shows the expression of a clock gene in a slice of SCN tissue. Approximately 140 cell containing regions are measured over a time span of 150 hours. It can be seen that the phase of the cycles is (to some extend) uniform, indicating the occurrence of synchronization.

Figure 1.1 raises the question how the neurons synchronize the internal genetic feedback loop. Because of the internal nature of the feedback loop, the neurons cannot directly communicate this state to other neurons. Instead, communication happens at the electrochemical level via synaptic interactions (gap junctions and chemical synapses) and neuromodulator diffusion. The objective of this research is to investigate how gap junction coupling and neuromodulator coupling shape synchrony in the genetic feedback loop in a network of SCN neurons. The following research question was formulated:

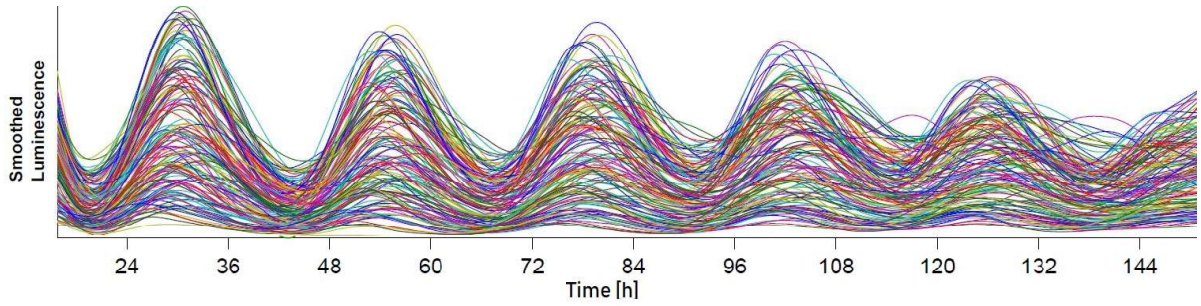

Figure 1.1: Gene expression of about 140 cell containing regions

"How do gap junction and neuromodulator coupling synchronize the gene expression of a network of SCN neurons?"

Since it is challenging to answer this question in totality, six sub questions were formulated. These sub questions are:

1. Can two SCN neurons synchronize when they are only coupled by gap junction coupling?
2. Can two SCN neurons synchronize when coupled only by neuromodulator coupling?
3. Does the combination of neuromodulator coupling and gap junction coupling enhance synchronization between two SCN neurons?
4. Can a network of SCN neurons synchronize when coupled only by gap junction coupling?
5. Can a network of SCN neurons synchronize when coupled only by neuromodulator coupling?
6. Does the combination of neuromodulator coupling and gap junction coupling enhance synchronization in a network of SCN neurons?

The sub questions separate the research question by type of coupling and network size. The first two sub questions focus on the emergence of synchronization in the most basic setting: a network of just two neurons with only one type of coupling. The third sub question combines both types of coupling in a basic two neuron network. The fourth and fifth sub question both consider one type of coupling but in an extended network. The sixth sub question aims to combine both coupling mechanisms in an extended network setting.

This research is focused on a network of SCN neurons without an external light input. Therefore, only synchronization between the intrinsic cycles of neurons are considered without any external influences. Besides, all neurons in the SCN network are considered to be identical.

This research will be conducted using a modeling approach. This is done because biological data collection techniques are limited. Most of the neuron states are simply not measurable (unlike the data from Figure 1.1). For instance, it is very challenging to

measure the individual coupling mechanisms. Therefore, we turn to single cell models, coupling models, and network models.

The research results are meant to guide the direction of biological research and provide insights in how the biological clock might work. As the methods of this research are purely mathematical, the aim is not to make definite claims about the biological model of the SCN.

1.2 Relevance

Understanding synchrony in the human clock is important. In the field of medication it will allow for more effective treatments. Certain types of medication are more effective when applied at certain moments in the 24-hour cycle. For instance, tumor cells can be affected by chemotherapy more effectively during the most active part of the sleep/wake cycle [3].

Better insight in the biological clock can also help reduce stress on shift workers. Some professions in places like hospitals, power plants or emergency services demand from people to work in shifts that are not synchronized to the natural light/dark cycle. People are more likely to make mistakes when working in these shifts [4]. For safety reasons, it is therefore important to investigate the circadian rhythm and find ways to make shift work less error-prone.

1.3 Structure

The organization of this report is as follows. In Chapter 2 a biological model of the SCN is discussed. This is done to familiarize the reader with the biological processes at play. It will help understand the mathematical (single cell, coupling, and network) models introduced later. In case the reader is already acquainted with the firing of neurons and the circadian genetic feedback loop, feel free to skip Chapter 2.

In Chapter 3 the Diekman2013 model is discussed. This is the mathematical single SCN neuron model that is used for this research. The goal of this chapter is to get the reader acquainted with the model and to highlight some of its special features. Besides the Diekman model the so-called *switch model* is introduced here. This model is a representation of the Diekman2013 model on the circadian time scale.

With Chapters 2 and 3 complete sufficient insights are gained to start discussing the sub question. This is done in Chapters 4 and 5.

The case of two coupled neurons is discussed in Chapter 4. This case is highly valuable as it allows us to analyze the behaviour of two neurons without any network effects. The stability region of the synchronized state as well as other non-synchronized states are discussed. Insights from this chapter are used to answer the first three sub questions.

In Chapter 5, the two neuron network is scaled to a network of arbitrary size. This will be done by analyzing the network parameters of several plausible networks. Insights from this chapter are used to answer the last three sub questions.

Thereafter, in Chapter 6 a general conclusion is provided. In this chapter the main research question will be answered. Also, some recommendations for further research are given.

Chapter 2

Biological model

A biological representation of the suprachiamatic nucleus is provided in this chapter. The goal is to present a brief and up-to-date view of the workings of the SCN. This is done by describing a single SCN neuron, the coupling between neurons, and the network structure. A more comprehensive description can be found in the corresponding literature study [5].

In order to build a mathematical model, an adequate understanding in the biological system it represents is essential. This is especially the case for the mathematical SCN models since researchers in this field go to great lengths to create biologically plausible models with physiologically meaningful states. Therefore, in order for us to understand the mathematical models of the SCN, adequate insights in the biological representation of the SCN is required.

The outline of the chapter is as follows. First, the biological processes that play at single cell level are discussed in section 2.1. Then, the interaction between neurons is described in section 2.2. Finally, in section 2.3, the network in which the neurons couple is discussed.

2.1 Single Cell

The SCN is comprised of neurons which are electrically excitable cells that can process and transmit information through electrical and chemical signals. The neurons themselves consist of dendrites, a soma and an axon. The cell body, or soma, is the core of the cell and contains most of the organelles and the nucleus. The cell body is the part where genes are located and proteins are built. The cell body is surrounded by dendrites and an axon which receive and transmit electrical signals [6]. Figure 2.1 provides a graphical representation of a neuron.

A single SCN neuron can be represented by two different systems: the electrical and molecular system. The molecular system creates the cell intrinsic circadian oscillation and the electrical system is able to communicate this rhythm to the other neuron. In the following subsections both parts are discussed.

2.1.1 Electrical part

A neuron is enclosed by a cell membrane, which separates the inside of the cell from its outside. The region directly inside of the cell membrane is called the cytosol while the region outside of the cell is known as the extracellular space. The cytosol and extracellular space differ in ion concentrations. This causes an electro-chemical potential across the

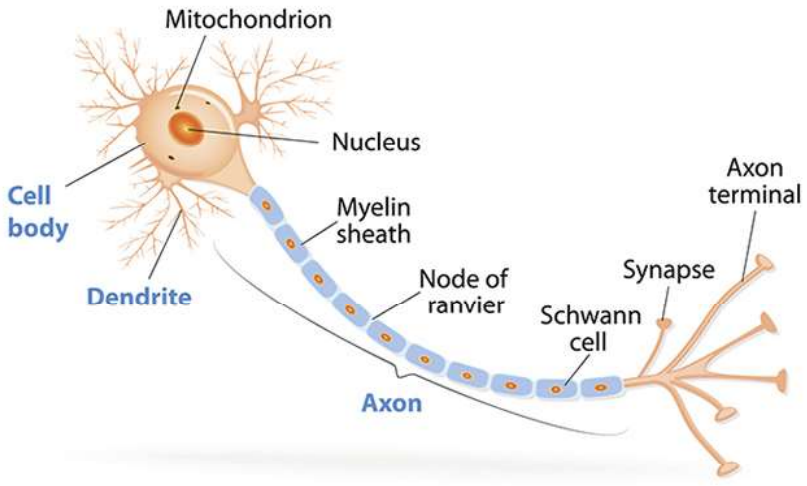

Figure 2.1: Anatomy of a neuron https://qbi.uq.edu.au/brain/brain-anatomy/axons-cable-transmission-neurons

membrane. Most of the time the potential is kept polarized near a constant -70 millivolt, which is called the resting membrane potential.

The neuron is able to stay polarized because the ions cannot diffuse through the lipid membrane. However, there are gates in the membrane called ion channels through which diffusion according to the electro-chemical gradient is possible. When the membrane depolarizes across a certain threshold, gates in the membrane open allowing positively charged sodium ions to rush in. These channels are known as voltage gated ion channels since the membrane voltage determines whether they open or not. This is in contrast to ligand gated channels, for which a particular particle is needed to trigger the opening of the gates.

Due to the intake of positively charged sodium ions the cell depolarizes further resulting in the opening of the potassium gates. This allows positively charged potassium ions to flow out of the cell according to the diffusion gradient. The leading role of the sodium gates and the delay of the potassium gates results in a short period of extreme depolarization. This is known as an action potential, which acts like a wave that travels down the axon to the synapses [6]. Upon the arrival of the action potential at the synapse the presynaptic membrane releases neurotransmitters that open the ligand gated sodium channels on the postsynaptic membrane [7]. If enough neurotransmitter is released the action potential propagates to the next neuron. After the event the sodium-potassium pump restores the original equilibrium by transporting sodium out of the cell and potassium into the cell. In this way the neuron restores for the next action potential. This cycle of firing an action potential and recovering has a period in the order of milliseconds.

To summarize, different ion concentration in the cytosol and extracellular space result in an electro-chemical gradient. This gradient allows a neuron to shoot electrical pulses called action potentials. These fast pulses can be transmitted to other neurons.

2.1.2 Molecular clock

Apart from the electrical activity of a neuron the molecular clock is of great importance. The neurons have an intrinsic rhythm of approximately 24 hours, which is established by a genetic feedback loop comprised of several genes that are rhythmically expressed [8].

Before discussing the circadian feedback loop the general process of genetic feedback is described. In a neuron, a string of genetic code (DNA) is copied to a string of mRNA in a process called transcription [9]. Unlike the DNA, mRNA is able to travel out of the nucleus to the endoplasmic reticulum where proteins are synthesized according to the genetic information carried by the mRNA. The step of protein synthesis is called translation [9]. The proteins can enhance or block transcription of genes that code for themselves or other proteins. In the case of positive feedback the protein is called a transcription factor for a certain gene. In case the protein blocks the transcription it is called a repressor. In the previously described process several genes and proteins can interact in a so called transcriptional translational feedback loop (TTFL).

Let us now have a look at the circadian TTFL more specifically. The most important genes involved in generating the circadian rhythm are Period (Per), Cryptochrome (Cry), Clock, Bmal1 and Rev-Erbα. However, nearly a thousand genes that affect the amplitude of the rhythm and about one hundred that influence the period have been identified [10]. In the following a brief explanation will be provided about how the formerly introduced circadian genes interact [11, 2, 8, 12, 13]. In this report genes are written with a single capital letter and their protein products are written with all capital letters.

The Clock gene is more or less expressed continuously. It is transcribed and its mRNA is translated such that the CLOCK protein forms. It binds with BMAL1 protein to form a compound protein, a heterodimer. These BMAL1/CLOCK heterodimers are transcription factors for the Per and Cry genes which means that the heterodimer enhances the transcription of Per and Cry. Subsequently, mRNA concentration of the Per and Cry genes rises. The Per and Cry mRNA travels out of the nucleus to form PER and CRY proteins.

The PER and CRY protein form a complex that binds with the BMAL1/CLOCK heterodimers which disables the BMAL1/CLOCK from enhancing Per and Cry transcription. Without BMAL1/CLOCK enhancing the transcription of the Per and Cry gene the production of Per and Cry mRNA drops. Subsequently the PER and CRY protein gradually decay over time leading the decay in complexes. The cycle starts over again.

BMAL1 levels are also oscillatory. The BMAL1/CLOCK heterodimers also act as a transcription factor on the Rev-erbα gene. The REV-ERBα protein binds to the promotor region of the Bmal1 gene and inhibits the transcription of the Bmal1 gene. Subsequently translation of Bmal1 drops followed by a drop in BMAL1 protein concentration. REV-ERBα protein consequently drops and the cycle starts over again. In this way the REV-ERBα concentration follows Per and Cry concentrations. Figure 2.2 gives a schematic representation of the feedback loop.

To summarize, clock genes and their products interact in a feedback loop. This feedback loop results in a oscillation of approximately 24 hours. Therefore the molecular process is considered to be very slow compared to the electrical part.

2.1.3 Interaction between electrical and molecular clock

There is a coupling between the electrical and molecular part of a neuron. The molecular part is coupled to the electrical part via mRNA and protein concentrations which appear to alter the permeability of the membrane [14, 15]. For example, the K^+ channels are believed to block with high concentrations of Per [16]. Subsequently, the electrical activity is coupled to the molecular part via Ca^{2+} ion concentrations. During action potential

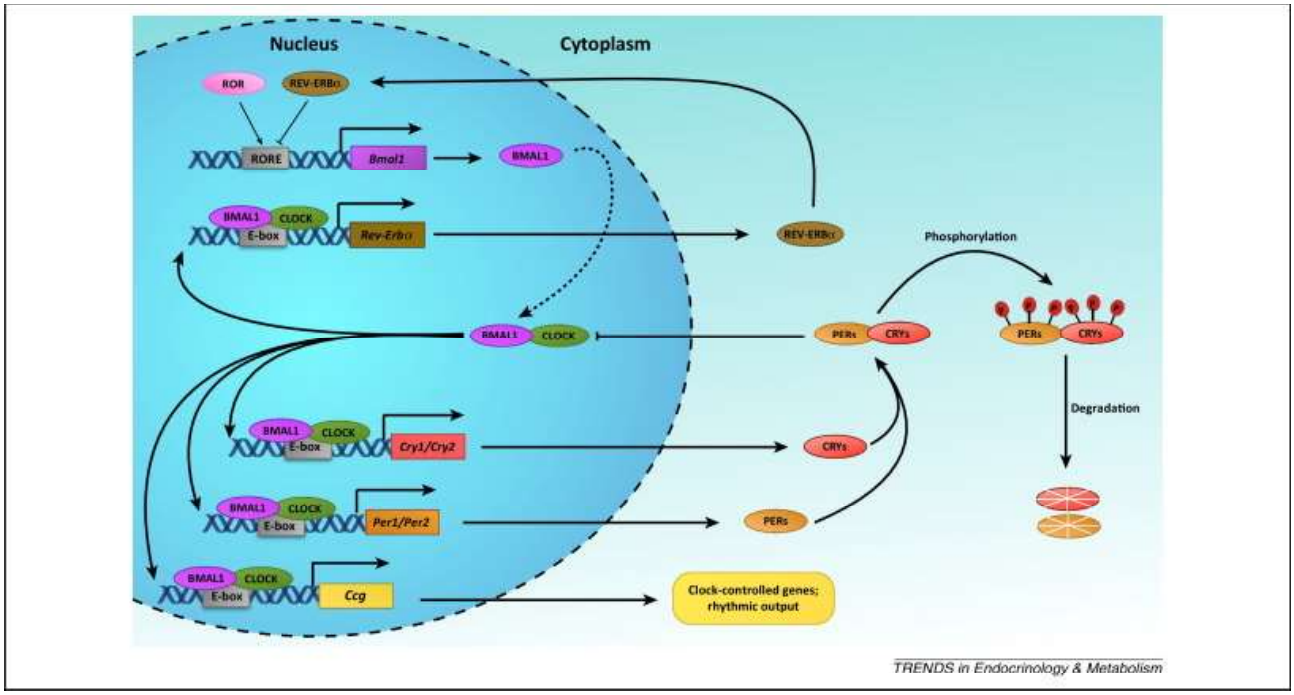

Figure 2.2: Schematic representation of the circadian transcriptional translational feedback loop [1]

firing ions cross the membrane. The Ca^{2+} net influx is enhanced by a depolarized membrane potential. High concentrations of Ca^{2+} enhance the transcription of the Period gene.

In this section (2.1) it was shown that a neuron has an electrical part and a molecular part. The electrical part, which acts on the time scale of milliseconds is very fast while the molecular part, which acts on the time scale of hours is slow. The two parts are coupled to represent a single neuron.

2.2 Interaction between neurons

So far only a single neuron was discussed. However, the SCN is a network of coupled neurons. Therefore, the ways in which two neurons couple needs to be discussed.

At the cell membrane a neuron can interact with other neurons (and its environment). This is done through electric and chemical signals. Most notable are gap junctions and neuromodulator diffusion. Both will be discussed in the following sections.

2.2.1 Gap junction

A gap junction is a channel connecting two neurons which allows ions and small molecules to diffuse from one cell to the other. It allows for nearly instantaneous pulse transmission in neighboring SCN neurons [17]. The importance of gap junctions in establishing a stable circadian rhythm is demonstrated by mice lacking the connexin36 protein that forms gap junctions. These mice have distorted circadian behavioural and electrical rhythms [18]. Moreover, these mice also showed a rhythm with lower amplitude and a delayed onset of activity.

2.2.2 Neuromodulators

Another important form of coupling is coupling by neuromodulator diffusion. Neuromodulators are "drifting" particles that can alter the state of a neuron. After secretion (by some neurons), neuromodulators diffuse through the extracellular space. When arriving at receptors on a cell membrane they alter the state of a neuron in many different ways. Neuromodulators can alter the permeability of the membrane of an observing neuron or influence the cell's TTFL through secondary messengers. There are many different neuromodulators, but only vasoactive intestinal peptide (VIP) is discussed here as it is believed to be the most important neuromodulator in synchronizing the SCN [12]. VIP alters the TTFL by raising the cAMP concentration which in turn enhances the transcription of the Period gene. VIP secretion again is rhythmically expressed with the Period gene.

Note that there is arguably another important coupling mechanism: synaptic coupling. This type of coupling is believed to act on the fast electrical system in a small-world like network, which is a nearest neighbour network with random links across the network (see corresponding Literature study [5]). Though important, synaptic coupling is not considered in this research since its characteristics are believed to lay in between those of gap junctions and neuromodulators. It can couple both electrically and chemically with the fast time scale characteristic of gap junctions but with the more global network characteristic of neuromodulator diffusion.

2.2.3 Conclusion

At the cell membrane two neurons can interact. This is done electrically, through gap junctions and chemically, through neuromodulator diffusion. The electrical coupling is fast (milliseconds) while neuromodulator coupling is very slow (hours). Gap junctions couple locally while neuromodulator coupling spans the entire network.

2.3 Network structure

With adequate understanding in how two neurons couple a network of coupled neurons can be evaluated. In constructing a reliable rhythm the network plays a key role.

One of the most important attributes of the network is the ability to synchronize the neurons. Without this phase synchronization the average SCN output is (nearly) constant since the phases of individual cells are uniformly spread over the 24-hour period. This behaviour has been observed in dispersed cell cultures [13]. Here, the neurons are uncoupled and no network oscillation was observed. Therefore, synchrony is needed to create a rhythmic SCN output.

Moreover, it has been shown that while phases of individual neurons can be as far apart as 2.5 hours the resulting average output is reliable and close to 24 hours [19]. This demonstrates the normalizing property of the network. By averaging over many neurons the SCN output is reliable even though the individual cells are not.

Not only can the phases of individual cells be far apart, but also the period of a single neuron is not constant. The revolution of a single cell might take 23 hours one cycle but 25 hours the next cycle. The period of total SCN output, being the average of many cells is far more reliable. This way the cumulative ability of the network also ensures a reliable period [19].

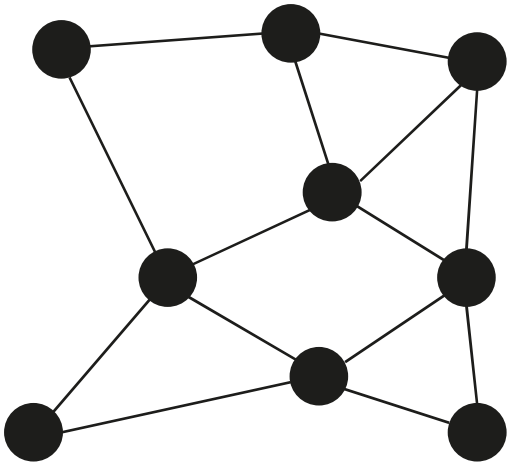

(a) Local coupling in a distributed network

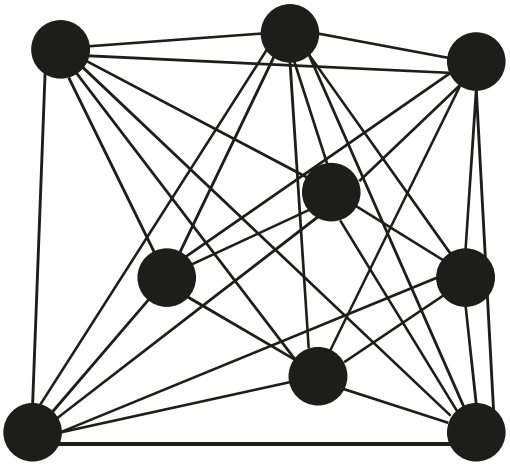

(b) Global coupling in an all-to-all network.

The robustness properties demonstrate the importance of the network. However, mapping the network structure is challenging. Even if one were to know exactly which neuron couples to which neuron than still the strength of every specific link would be unknown. Moreover, the network changes over time with new connections being made at any moment (synaptic plasticity) [20].

However, the basic network structures at which interaction takes place is known. Gap junctions couple in an undirected distributed network, an example of which can be seen in Figure 2.3a. Neuromodulator diffusion coupling creates an all-to-all network (or some-to-all depending on receptor mismatch), an example of which is shown in Figure 2.3b.

2.4 Conclusion

The goal of this chapter was to familiarize the reader with the biological model of the SCN. In order to do so, a single neuron, coupling between two neurons, and the network were discussed.

The single neuron can be partitioned in a fast electrical and a slow molecular part. Both parts interact via the membrane permeability and the calcium ion concentration. Two neurons couple electrically and chemically through two important coupling mechanisms: gap junction coupling and neuromodulator diffusion. Gap junction couple locally, electrically and fast while neuromodulator diffusion couples globally, chemically, and slowly.

The network is crucial in creating a reliable oscillating output. The precise network is not well understood. However, it is believed that gap junction couple in a distributed network while neuromodulator coupling couples in an all-to-all network.

Chapter 3

Single Diekman neuron

Since data collection in the biological system is very challenging, a mathematical model of the SCN is used for this research. One of these is the Diekman model which is highly suitable for this research due to its biological plausibility and simplicity. This chapter provides an analysis of the single Diekman neuron. The goal of this analysis is to find out what causes an oscillating output, how to separate timescales, and creating models for each timescale.

Firstly, an overview of the model is given in section 3.1. The different parts of the model are discussed and the different states are introduced. Secondly, the *time scale separation principle* is introduced in section 3.2. Using the time scale separation principle the model is split in a fast and a slow system. The fast electrical subsystem is analyzed in section 3.3 while the slow molecular subsystem is treated in section 3.4. Next, the interaction between the time scales is discussed in section 3.5. Finally, an alternative model for the slow dynamics is derived in section 3.6.

3.1 Overview of the model

As discussed in Chapter 2 there are two cell processes, namely the electrical and genetic (or molecular) of interest when describing the circadian rhythm of an SCN neuron. The Diekman model describes exactly those processes by combining a Hodgkin-Huxley-like electrical model [21] with a Goodwin-like molecular model [22]. For readers not familiar with the model a brief introduction is provided here while a more extensive analysis follows in sections 3.3 and 3.4.

The Diekman model has 13 states of which 10 represent electrical variables and 3 represent molecular variables [23]. The states are listed in Table A.1. The full model can be found in Appendix A. The electrical model describes the potential across a membrane (x_1) using Ohm's law with nonlinear resistances. The resistances are determined by gating variables x_2 to x_8 which represents the fraction of membrane channels that are open or closed. In addition, the Diekman model also describes two calcium concentration states (x_9 and x_{10}). The first of these states represents the concentration near the cell membrane while the later represents the concentration in the cytosol. The molecular model describes the transcription and translation of a single gene in mRNA (x_{11}), its corresponding protein (x_{12}), and activated protein (x_{13}). The electrical part manipulates the molecular part through the calcium concentration (x_{10}). The molecular part influences the electrical part by altering the permeability of the membrane through the activated protein concentration (x_{13}). Note that this is conform with our biological representation

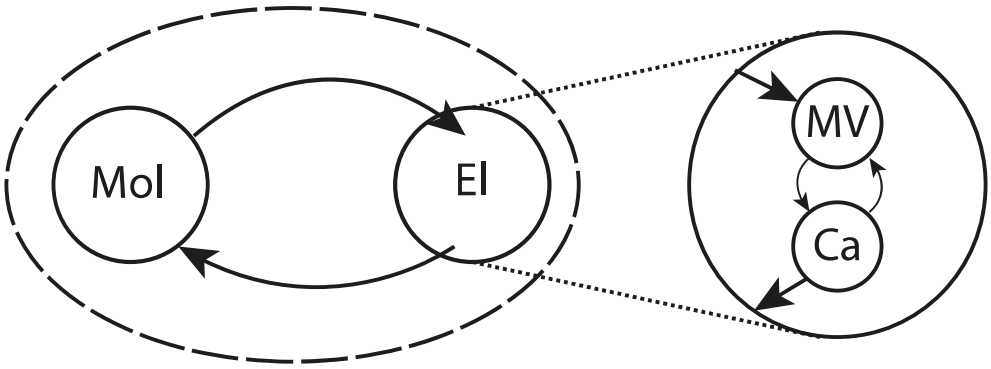

Figure 3.1: Schematic representation of the interaction between the electrical (El) and molecular (Mol) subsystems. The electrical subsystem can subsequently be split in a part describing the membrane states (MV) and the calcium states (Ca).

Table 3.1: State numbers to names

State number	Symbol	Unit	Description
x_1	Vm	mV	Mebrane voltage
x_2	m	-	a Na gating variable
x_3	h	-	a Na gating variable
x_4	n	-	K gating variable
x_5	rL	-	Ca^{2+} long lasting gating variable
x_6	rNonL	-	a Ca^{2+} not long lasting gating variable
x_7	fNonL	-	a Ca^{2+} not long lasting gating variable
x_8	s	-	Ca^{2+}-dependent potassium gating variable
x_9	Ca_s	mM	Ca^{2+} concentration near the cell membrane
x_{10}	Ca_c	mM	Ca^{2+} concentration in the rest of the cytosol
x_{11}	mRNA	mM	mRNA concentration of a general clock gene
x_{12}	P	mM	Protein concentration
x_{13}	P*	mM	Phosphorilated protein concentration

given in Chapter 2. Figure 3.1 shows a graphical representation of the interaction in the model in which the molecular subsystem affects the membrane states (MV) which alter the calcium concentration. In turn the calcium states affects the molecular subsystem.

To summarize, the Diekman model consists of an electrical and a molecular part. The two subsystems influence each other through states x_{10} and x_{13}. In the following section the electrical and molecular subsystem are split using the time scale separation principle. This will allow for a more effective analysis.

3.2 Time scale separation principle

Recall from Chapter 2 that the molecular system is very slow with a period of approximately 24 hours while the firing of action potentials is a very fast process on the time scale of milliseconds. This double time scale property has also been incorporated in the Diekman model. However, the double time scale makes analysis both analytical and numerical challenging. For a more effective analysis the Diekman model is split into two parts: the fast dynamics and the slow dynamics. This is known as time scale separation. The goal of this section is to understand the concept of time scale separation and why

it is useful for the Diekman model. In order to do so, first, an example demonstrating both time scales is provided. Thereafter, the time scale separation principle is discussed mathematically.

3.2.1 Example of the dual time scale property

In order to demonstrate the dual time scale property of a Diekman neuron a simulation was conducted. A single Diekman neuron was implemented in MATLAB and the state trajectories were estimated (for initial conditions near the periodic orbit). Figure 3.2A shows the evolution of the x_1 state (the membrane voltage) over a period of 10 hours, corresponding to the active phase of a neuron (day time). At the beginning of the simulation the membrane is said to be hyperpolarized. The membrane is at rest at approximately -67mV. As time increases (during day time) the membrane potential of a neuron slowly rises to a point at which the neuron starts firing action potential. This can be observed between hour 2 and hour 4 in the simulation. The average membrane potential increases further and between hour 5 and hour 6 in the simulation the neuron is at a highly-depolarized constant state. Thereafter, the neuron returns towards the hyperpolarized state by going back through the spiking phase.

During these 10 hours a very slow cycle can be observed. For clarity, the slow cycle is isolated (by increasing the stepsize of the MATLAB iteration) and plotted in Figure 3.2C. The cycle has a period of approximately 24 hours of which Figure 3.2C shows 10 hours containing one peak. In the report, the slow 24-hour time scale is referred to as the *circadian time scale*. On this slow cycle seen in Figure 3.2A very fast oscillations can be observed between hours 2-4 and hours 7-8. When zooming in on these oscillation, to the order of milliseconds, Figure 3.2B emerges in which the firing of action potentials can be seen. In the report this time scale is referred to as the *millisecond time scale*. To conclude, the oscillation of the membrane potential consists of a slow oscillation, with very fast oscillations on top. This is what is meant by the double time scale.

One can imagine that analysis of the system on both time scales is challenging both numerically and analytically. Numerically, a single cycle with the double time scale is rather difficult to estimate using bifurcation software (such as MATCONT and AUTO). Analytically, the double time scale makes analysis needlessly complicated. Therefore the system is split into a fast and a slow system using the so-called *time scale separation principle*.

3.2.2 Separating the time scales

The goal of this section is to derive a method for splitting the time scales. This is done by applying the time scale separation principle to a general fast slow system. Thereafter, a more intuitive description is provided which demonstrates the applicability of the principle on the Diekman model.

Consider a system with fast variable x and a slow variable y:

$$\begin{aligned} \dot{x} &= f(x, y) \\ \dot{y} &= \epsilon g(x, y), \quad \text{with } 0 < \epsilon << 1 \end{aligned} \tag{3.1}$$

Here ϵ is a time constant representing the fast/slow ratio of the system. Since ϵ is near zero the y dynamics (in (3.1)) are very slow relative to the x dynamics.

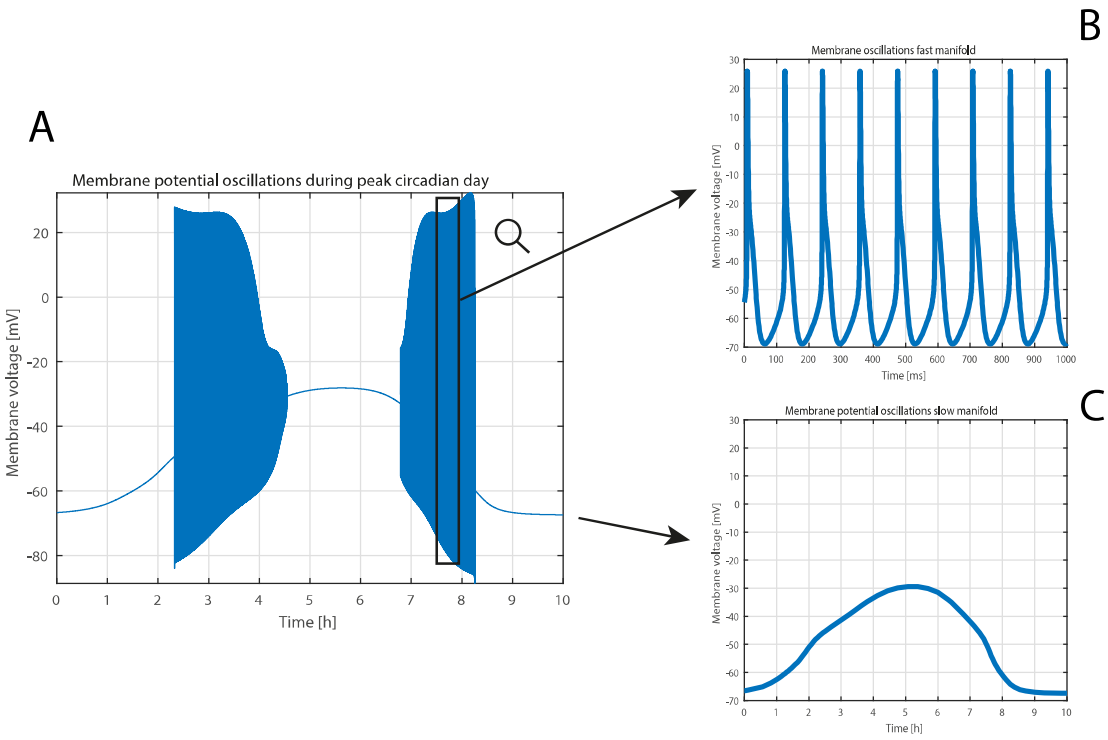

Figure 3.2: (A) Membrane oscillations during peak of circadian day showing both oscillations on the slow circadian time scale as on the fast millisecond time scale. The result is a slow oscillation with very fast oscillations on top. (B) Zoomed in on oscillations on the millisecond time scale. (C) Single oscillation of the slow time scale.

Let us first evaluate the system on the fast time scale. This is encompassed by taking the limit of ϵ to zero for Equation (3.1) such that:

$$\lim_{\epsilon \to 0} \dot{y} = 0 \tag{3.2}$$

The solution of (3.2) is a constant. Therefore, on the fast manifold the slow system can be represented as a constant while the system (3.1) can be represented on the fast manifold as:

$$\begin{aligned} \dot{x} &= f(x, c), \\ \dot{y} &= 0 \end{aligned} \tag{3.3}$$

where c represents the solution of $\dot{y} = 0$.

Now the fast system is evaluated on the slow time scale. The dynamics of the fast system on the slow time scale can be represented as the average of the fast system. In this representation the *method of averaging* [24] is useful. Consider the fast system oscillating in time t with period T then the average of x is defined as:

$$\bar{x}(t) = \frac{1}{T} \int_0^T x(t) dt \tag{3.4}$$

where $\bar{x}$ represents the average of x. Therefore on the slow time scale the system of (3.1) can be represented as:

$$\begin{aligned} \bar{x} &= \frac{1}{T} \int_0^T x(t) dt \\ \dot{y} &= \epsilon g(\bar{x}, y) \end{aligned} \tag{3.5}$$

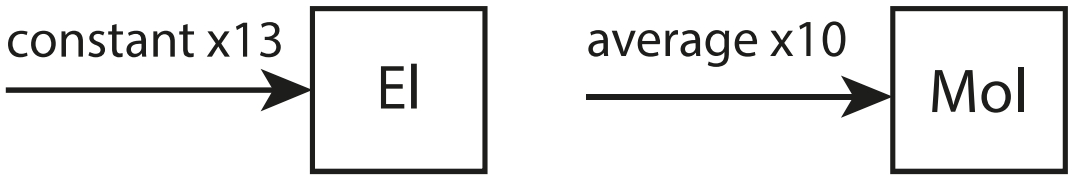

(a) Constant x_{13} in fast electrical system

(b) Average of x_{10} in slow molecular subsystem

Figure 3.3: Time scale separation in block scheme.

The usefulness of the time scale separation principle for the Diekman model can be understood intuitively. The molecular model hardly changes on the timescale of seconds or even milliseconds. Therefore, the molecular states can be assumed constant when analyzing the electrical model on the millisecond time scale. On the other hand, a single action potential is too fast for the molecular subsystem to track. Therefore, a single action potential is not relevant for the molecular model on the circadian time scale. However, it is the sum (or average) of these small oscillations that affects the molecular state. Therefore, the average of the electrical output will be considered when analyzing the molecular clock. Figure 3.3 shows the idea in a block scheme.

To summarize, in order to allow for effective analysis the Diekman model is to be split into a fast and a slow system. This can be done by providing the fast electrical Diekman model with a constant molecular input (x_{13}) and providing the molecular Diekman model with the average of the electrical signal (x_{10}).

3.3 Electrical subsystem

This section aims to provide an in-depth analysis of the electrical part of the Diekman model using the time scale separation principle. First, some of the differential equations that result in oscillations seen in Figure 3.2 are discussed. Thereafter, the time scale separation principle is used to split the fast and slow systems. Subsequently, the electrical subsystem is analyzed using a numerical bifurcation analysis.

3.3.1 Differential equations of the Diekman electrical subsystem

Recall that, as discussed in Chapter 2, the different ion concentrations on either side of the membrane result in an electro-chemical gradient. Ions flow in and out of the cell through special channels in the membrane according to the gradient. The Diekman model represents this system as the electrical circuit, shown in Figure 3.4. Here the membrane is modeled as a capacitor, the electro(chemical) potentials as voltage sources, and the channels as nonlinear conductances (inverse resistance).

The dynamics of the circuit shown in Figure 3.4 can be caught in differential equations. Using the capacitor equation one can derive the first differential equation of the Diekman model:

$$\frac{dV_m}{dt} = \frac{\sum I_c}{C_m} \tag{3.6}$$

This is an equation describing the membrane potential depending on the capacitance parameter C_m and the net current across the membrane. The Diekman electrical model

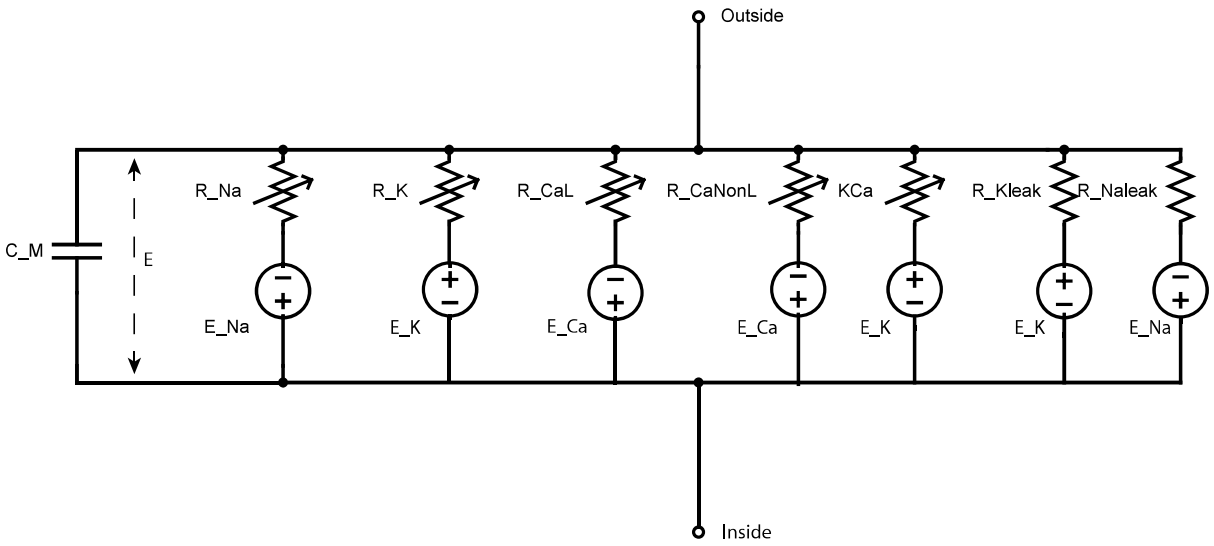

Figure 3.4: Electrical circuit of the electrical Diekman model

describes 7 different currents through the membrane:

$$\sum I_c = I_{Na} + I_K + I_{CaL} + I_{CaNonL} + I_{KCa} + I_{Kleak} + I_{Naleak} \tag{3.7}$$

Currents I_{KCa} and I_{Kleak} take the x_{13} molecular state as an input (to the electrical subsystem). Through this input the molecular subsystem is able to affect the electrical subsystem.

The currents of Equation 3.7 are calculated using Ohm's law. One of these currents is given here as an example (the rest can be found in Appendix A).

$$I_{Na}(x_1, x_2, x_3) = \bar{g}_{Na} x_2^3 x_3 (x_1 - E_{Na}) \tag{3.8}$$

Here I_{Na} represents the sodium current across the membrane. The $(x_1 - E_{Na})$ factor represents the potential while $\bar{g}_{Na} x_2^3 x_3$ represents the conductance (inverse resistance). The states x_2 and x_3 represent the gating variables which take values between zero to one depending on x_1 (and initial conditions). When x_2 or x_3 is zero all channels are closed resulting in $I_{Na} = 0$ while if x_2 and x_3 take the value of one all channels are open and the maximum conductivity of $\bar{g}_{Na}$ is reached resulting in $I_{Na} = \bar{g}_{Na}(x_1 - E_{Na})$.

Similar to equation 3.8 states x_4 to state x_8 are used to calculate the other ion currents. The ion currents alter the ion concentrations in the cell. Out of all ion concentrations only the Ca^{2+} concentration are of interest as high Ca^{2+} concentrations enhance the production of the Period gene (Chapter 2). The currents can be used to calculate the concentrations of calcium such that state x_{10} is described by

$$\dot{x}_{10} = -k_{10}(I_{CaL} + I_{CaNonL}) - x_{10}/\tau_{10} + b_{10} \tag{3.9}$$

As can be seen, the state x_{10} is a function of the calcium currents, a decay, and a base (b_{10}). The electrical x_{10} state forms the input to the molecular subsystem which will be discussed later.

To summarize, the electrical subsystem can be represented as a circuit in which the membrane represents a capacitor an the channels nonlinear resistors. Using the capacitor equation and Ohm's law the currents and the membrane potential are calculated. Subsequently, the calcium currents can be used to calculate the calcium concentration in the neuron. The resulting Diekman electrical model consists of ten states with one "external" input x_{13}, provided by the molecular part.

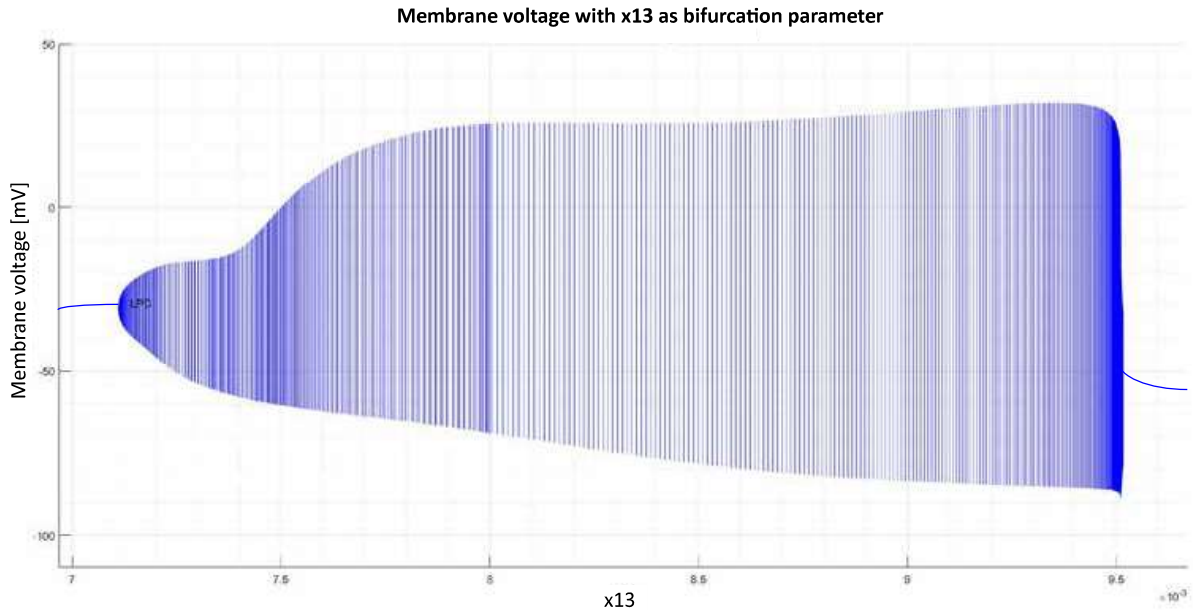

Figure 3.5: Membrane potential depending on x_{13}

3.3.2 Response of the fast subsystem

The goal of this section is to investigate the emergence of the fast action potential spiking seen in Figure 3.2B and to understand how the molecular x_{13} input effects this event. In order to do so, the time scale separation principle was applied in combination with a bifurcation analysis.

Recall that Figure 3.2 shows that only for certain time periods the electrical subsystem is oscillatory on the millisecond time scale. Since slow state x_{13} is the only input to the fast electrical subsystem, it was hypothesized that only for certain x_{13} inputs the membrane potential is oscillatory on the millisecond time scale.

In order to investigate this hypothesis, a bifurcation analysis was conducted using MATCONT. Recall that x_{13} is very slow such that when analyzing the fast electrical system a constant x_{13} can be used. Therefore, the input constant x_{13} is taken as bifurcation parameter. The bifurcation parameter was initiated at zero and slowly increased. Two Hopf bifurcations were found. One at $x_{13} \approx 0.00711$ and one at $x_{13} \approx 0.00952$. The stable equilibrium disappears through the first bifurcation only to reemerge through the second. Figure 3.5 show the membrane potential as a function of x_{13}. It can be observed that the subsystem indeed oscillates for a range of x_{13} inputs while resulting in constant steady state anywhere else. Moreover, it can be observed that the amplitude of the signal greatly varies with different x_{13} inputs.

Let us now zoom in on different areas of Figure 3.5 and view the solutions in time (rather than in x_{13}). Figure 3.6 describes the responses in time for four different x_{13} inputs. For high x_{13} the membrane potential is at a low constant steady state seen in Figure 3.6a. When x_{13} is decreased the constant steady state gives way to oscillation seen in Figure 3.6c. In case x_{13} decreases further the amplitude and period drop resulting in trajectories such as seen in Figure 3.6b. For yet lower x_{13} inputs the subsystem undergoes the Hopf bifurcation resulting again in a constant steady state.

To conclude, the emergence of fast oscillations in the electrical subsystem results from the state x_{13} crossing a region bounded by two Hopf bifurcation. In between these

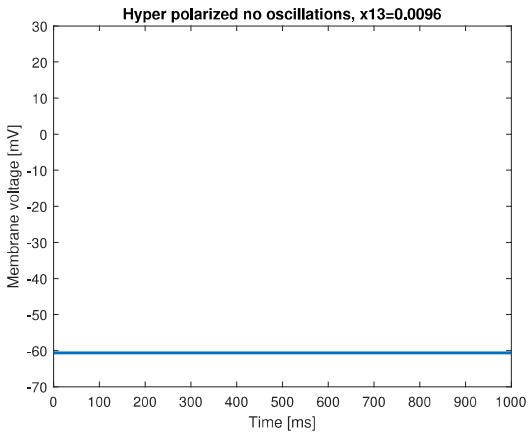

(a) High concentration of $x_{13} = 0.0096$

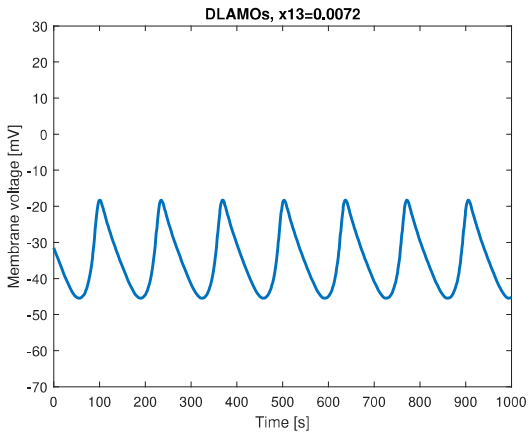

(b) Medium low concentration of $x_{13} = 0.0072$

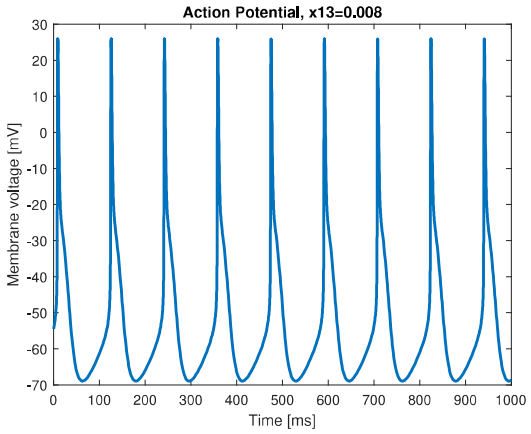

(c) Medium high concentration of $x_{13} = 0.0080$

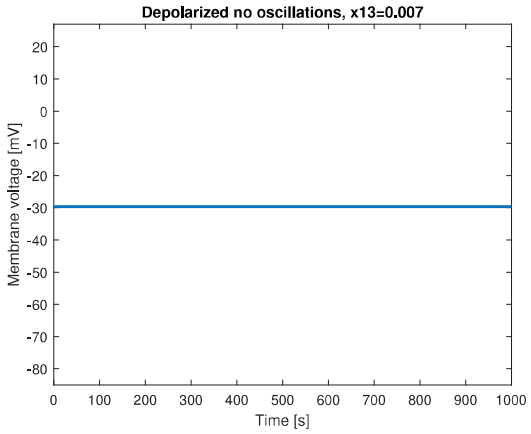

(d) Low concentration of $x_{13} = 0.0070$

Figure 3.6: Different modes of the membrane potential depending on x_{13}.

thresholds the solutions oscillate while outside these thresholds the solutions reach a constant steady state. When looking at Figure 3.2 it can be concluded that the circadian oscillations of x_{13} cross the Hopf bifurcations twice every circadian cycle resulting in a time period characterized by fast action potential spiking.

3.4 Molecular subsystem

This section aims to provide an in-depth analysis of the molecular subsystem. In doing so, first some trajectories of the molecular states in a Diekman neuron are evaluated. Thereafter, the differential equations are addressed. Finally, the response to an x_{10} input is discussed.

3.4.1 Trajectories of the molecular states

A single Diekman neuron with initial conditions near the periodic orbit was simulated in MATLAB. Figure 3.7a shows the trajectories of the three molecular states for a time period of approximately 70 hours. Every cycle consists of a peak in mRNA concentration

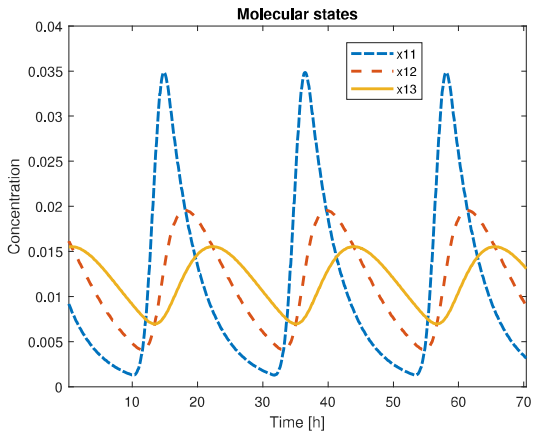

(a) Freerunning molecular states in combined model

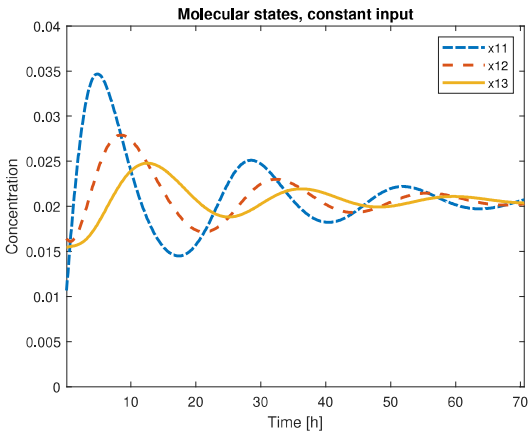

(b) Molecular trajectories with constant CRE input

Figure 3.7: Molecular states trajectories

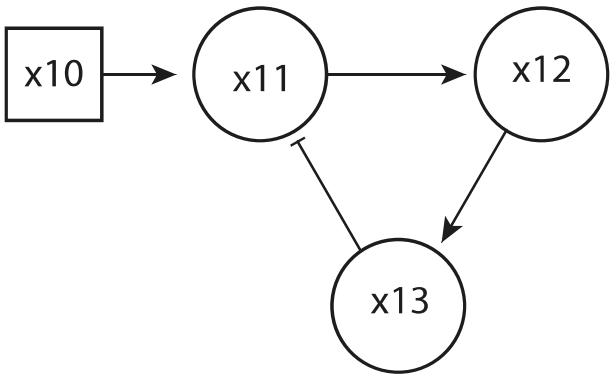

Figure 3.8: Interaction of the molecular states with input x_{10}. Sharp arrows indicate enhancement while blunt arrows indicate repression.

(x_{11}), followed by a peak in protein concentration (x_{12}), followed by a peak in activated protein (x_{13}). Note that this corresponds with our biological representation from Chapter 2. The period of the circadian oscillations is approximately 21.5 hours. This is a little low with respect to biological observations which are in the range of 21-26h [13].

3.4.2 Differential equation of the Diekman molecular subsystem

The molecular states interact in a feedback loop represented by Figure 3.8. The external x_{10} state represents an external input to a feedback loop of states x_{11}, x_{12}, and x_{13}. The Equations (3.10),(3.11),(3.12) describe the interaction of the states more precisely:

$$\dot{x}_{11} = a\left(CRE(x_{10})Ebox(x_{13})^n - x_{11}\right), \tag{3.10}$$

$$\dot{x}_{12} = a(x_{11} - x_{12}), \tag{3.11}$$

$$\dot{x}_{13} = a(x_{12} - x_{13}), \tag{3.12}$$

$$CRE(x_{10}) = \max(0, 10^6 \cdot x_{10} - 75), \tag{3.13}$$

$$Ebox(x_{13}) = \left(\frac{k_i}{k_i + x_{13}}\right) \tag{3.14}$$

Here $CRE(x_{10})$ is a nonlinear function describing the maximum rate at which the mRNA (state x_{11}) can be produced. The electrical state x_{10} is an external input to the molecular subsystem. *Ebox* is a measure of how strongly x_{13} inhibits x_{11}. If x_{13} is low the fraction *Ebox* becomes close to 1 meaning that the maximum transcription rate $CRE(x_{10})$ of mRNA (in Equation (3.10)) is asymptotically reached. However, if x_{13} is high the fraction *Ebox* becomes close to zero meaning that the transcription of mRNA is low. In the *Ebox* function k_i is equal to the concentration of x_{13} at which x_{11} production is half the maximum value. The value a in Equations (3.10),(3.11),(3.12) describes a time constant. The value of a ($a = 5.6 \cdot 10^{-8}$) can be seen as the very small value of ϵ used for the time separation principle seen in Equation 3.1. The Hill coefficient, n, is a number that represents the amount of protein that is needed to bind to the promotor.

To conclude, the molecular subsystem describes the concentration of three substances that interact in a feedback loop. The only external input to the molecular subsystem is the electrical state x_{10}.

Remark The $CRE(x_{10})$ function used in this report is a different function that the original Diekman $CRE(x_{10})$ function. The original $CRE = 10^6 \cdot Ca_c - 75$ ([23] p.9) is changed to $CRE = \max(0, 10^6 \cdot Ca_c - 75)$. This is done such that the $CRE(x_{10})$ function only yields a positive term. This alteration is validated by the insight that the function $CRE(x_{10})$ is an activation and therefore cannot take negative values. Moreover, a negative $CRE(x_{10})$ forces the molecular states to become negative as well. Since these states describe concentrations this cannot be the case. When referring to the Diekman model in this report this alteration is included.

Remark This section may have given the impression that the parameters of the Diekman model can be chosen at will. The Diekman model, however, comes with a specific parameter set which has been validated using biological data. For the sake of biological plausibility this parameter set is not altered throughout this report. The Diekman parameter set can be found in Appendix A.

3.4.3 Response of the slow subsystem

The uncoupled molecular Diekman model is now evaluated in much the same way as the electrical subsystem. The time scales are split and the model is analyzed using a bifurcation analysis. The molecular subsystem has three states and one external input x_{10}. Using the time scale separation principle it was demonstrated that the fast x_{10} input is perceived by the slow system as the average of x_{10}, represented by $\bar{x}_{10}$. Recall that the bifurcation analysis of the fast electrical system was relatively easy as only one constant input needed to be considered. This is not the case for the slow molecular system. On the circadian time scale the input $\bar{x}_{10}$ is not restricted to constant $\bar{x}_{10}$. The input can also be of oscillatory nature (on the circadian time scale). Therefore, the analysis is split into the case for which $\bar{x}_{10}$ is constant and the case for which $\bar{x}_{10}$ is oscillatory.

Constant x_{10} input

First, the case for which the input $\bar{x}_{10}$ is constant is evaluated. The molecular model was implemented in MATCONT and a bifurcation analysis was performed using $\bar{x}_{10}$ as

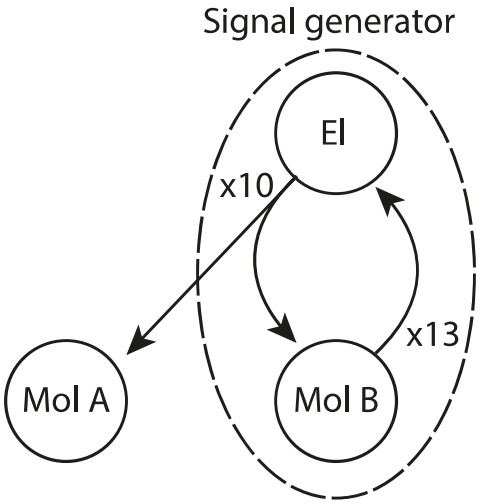

(a) Graphical representation of an x_{10} signal that oscillates on the circadian time scale feed into a molecular subsystem

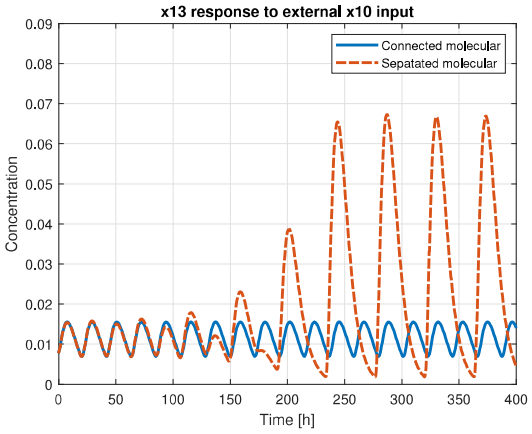

(b) Trajectories of x_{13} of the connected and the drive molecular subsystems. Initial conditions of both subsystems are set identical.

Figure 3.9: A molecular system is driven with an x_{10} signal oscillating on the circadian time scale.

a bifurcation parameter. The bifurcation parameter was varied over the range $[0,\ 100]$. The molecular subsystem was found not to oscillate (in steady state) for any $\bar{x}_{10}$ input. Figure 3.7b shows an example for the trajectories with arbitrary constant $\bar{x}_{10} = 0.2$ and arbitrary initial conditions. Since a constant $\bar{x}_{10}$ for which the molecular oscillates cannot be found numerically it was hypothesized that the Diekman molecular subsystem does not oscillate for any constant $\bar{x}_{10}$ input.

In order to investigate this hypothesis, a local stability analysis was performed analytically. This was done by evaluating the stability of the system around its unique equilibrium. It was demonstrated that for any constant input a unique and stable equilibrium exists (using the Diekman parameter set). The calculations can be found in Appendix B.

Oscillatory x_{10} input

When evaluating the response to an oscillatory $\bar{x}_{10}$ input is evaluated, all kinds of frequencies and amplitudes can be chosen. However, a good start would be evaluating the autonomous circadian oscillation of x_{10} of a combined (electrical and molecular) neuron. In this analysis the x_{10} input is chosen as the x_{10} that a molecular subsystem would perceive in a combined (electrical and molecular) system.

The configurations of the simualton are represented in Figure 3.9a. The initial conditions of the combined model are chosen near the periodic orbit. The separated molecular system A is initiated identical to the combined molecular system B.

Figure 3.9b shown the trajectories of both subsystems. At the start of the simulation the separated subsystem A appears to oscillate identical to connected subsystem B. After some time the separated subsystem A starts oscillating with double period and an increased amplitude. The separated molecular system A seems to be unable to track the circadian oscillations of $\bar{x}_{10}$. Instead, it only peaks every other cycle compared to $\bar{x}_{10}$ (which peaks approximately every 24 hours). This is a interesting result for two reasons.

First, identical molecular systems respond differently to identical $\bar{x}_{10}$ input signals. It was therefore hypothesized that the molecular subsystem needs feedback through the electrical subsystem to oscillate properly. Second, applying the circadian $\bar{x}_{10}$ input to the molecular subsystem does not result in a model for the slow system.

The objectives of this section were to find the origin of the circadian oscillations and to create a model of the slow dynamics. First of all, it was found that the molecular subsystem does not oscillate for constant input $\bar{x}_{10}$. Recall from section 3.3 that the electrical subsystem does not oscillate on the circadian time scale. Consequently, the origin of the circadian oscillations was not found. Therefore, it is hypothesized that the circadian oscillations must be the result of coupling between the two subsystems. Second, at the start of this section it was assumed that feeding the molecular subsystem with the average of $\bar{x}_{10}$ results in a model of the slow dynamics. However, this is not the case as feeding $\bar{x}_{10}$ into the molecular model does not mimic the slow Diekman oscillations seen in Figure 3.9b. Consequently, it is hypothesized that in order for the molecular subsystem to express circadian oscillations, a feedback through the electrical subsystem is needed.

3.5 Emergence of oscillations on the slow time scale

In the previous section it was discussed that the molecular model requires an oscillatory input to exert oscillations. In addition, the electrical system also requires a driver to oscillate on the circadian time scale. Both the electrical and the molecular system are not self-oscillatory on the circadian time scale. Therefore, it was hypothesized that the oscillations on the circadian time scale originate from coupling between the two subsystems. The goal of this section is to find out if the interaction results in circadian oscillations.

In order to evaluate the interaction, the time scale separation principle is used to determine the steady state solutions per time scale. The electrical system was given 130 different constant x_{13} inputs equally spaced between 0 to 0.013. The steady state values of x_{10} were derived for every corresponding x_{13} input. In case the constant input resulted in an oscillating x_{10} input the average of x_{10} was taken. The data points were collected and plotted in Figure 3.10. Now the constant steady state values of the slow system for any given $\bar{x}_{10}$ input were calculated. The result was also plotted in Figure 3.10.

Figure 3.10 describes the lines to which the two subsystems are attracted. When starting at a certain point in the phase plane and alternately exciting the fast and slow system one can draw the arrow graph in Figure 3.10b. First the slow system is simulated for hours in order to reach its steady state: a point on the molecular steady state line. Thereafter the fast system is excited for just a second. The fast system shoots towards its steady state on the electrical steady state line. Then this $\bar{x}_{10}$ is used to excite the molecular system. Note that the solutions start rotating in a clockwise manner demonstrating the emergence of oscillations. There appears to be an unstable equilibrium where the steady state lines cross. The steady states deviate from the equilibrium towards the limit cycle shown in Figure 3.10b.

In summary, both the molecular and electrical system are individually not oscillatory on the circadian time scale. However, when coupled the combined system exerts oscillations due to the revolution in steady state solutions.

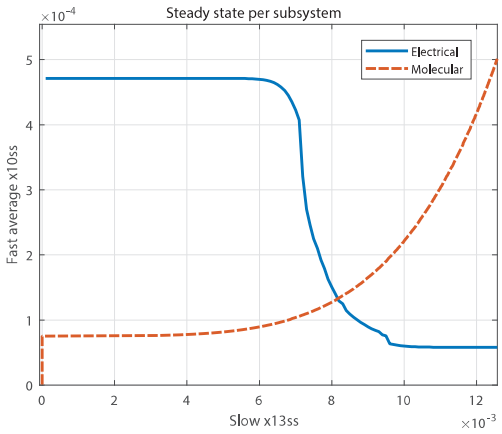

(a) Steady states per system

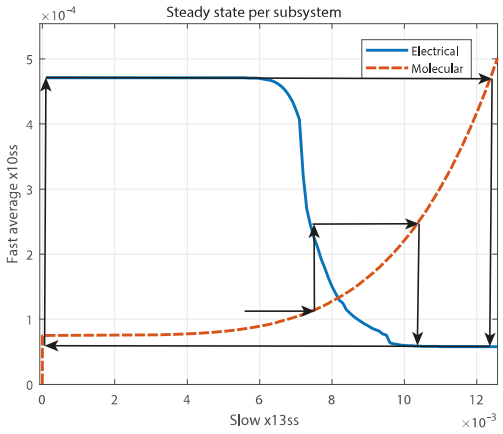

(b) Steady state revolution

Figure 3.10: Steady state per system

3.6 Switch models

The goal of this section is to derive a model of the slow dynamics of the Diekman neuron. Previously, it was hypothesized that feedback through the electrical system is needed for the molecular system to oscillate on the circadian time scale. Therefore, deriving a model for the slow dynamics is believed to be equivalent to describing this feedback.

3.6.1 A model for the slow dynamics

Let us start by looking at Figure 3.10 once more. The figure suggest a strong relationship between state x_{10} and state x_{13}. Instead of feeding the molecular state x_{13} through the electrical system to find the corresponding $\bar{x}_{10}$ value Figure 3.10 can be used as a lookup table. On the slow time scale this makes sense since the molecular subsystem is not interested in x_{10} but rather in $\bar{x}_{10}$. Moreover, $\bar{x}_{10}$ is fast (compared to x_{13}) and therefore is assumed to be at steady state instantly ($\bar{x}_{10} \approx \bar{x}_{10,ss}$). The result is a model of the slow dynamics that uses Figure 3.10 to bridge output x_{13} to input x_{10}.

The $\bar{x}_{10}$ curve in Figure 3.10 is just a set of data point. In order to use the data set, it has to be translated to the continuous domain. Using the MATLAB curve fitting toolbox equation $g(x_{13})$ was fitted on the data set.

$$\begin{aligned} g(x_{13}) = d \cdot (-1/(1+\exp(-a \cdot (x-b))) + 1) + c, \quad \text{with} \\ a = 2665 \\ b = 0.007473 \\ c = 6.184e-05 \\ d = 0.0004121 \end{aligned} \tag{3.15}$$

Subsequently the *smooth switch model* was derived:

$$\begin{aligned} \dot{x}_{11} &= a\,(h(x_{13}) - x_{11}) \quad \text{with } h(x_{13}) = CRE(g(x_{13}))Ebox(x_{13})^4, \\ \dot{x}_{12} &= a(x_{11} - x_{12}), \\ \dot{x}_{13} &= a(x_{12} - x_{13}), \end{aligned} \tag{3.16}$$

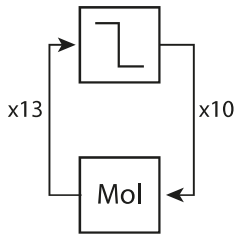

Figure 3.11: Schematic representation of the switch model

Here $h(x_{13})$ includes the newly created $g(x_{13})$ function. It is a monotonically decreasing function such that when x_{13} is low $h(x_{13})$ is high and vise versa.

The newly created smooth switch model is an elegant and very simple representation of the circadian dynamics of the Diekman model. However, the smooth switch model can be further simplified. Instead of a logistic function a heaviside step function can be used. Namely, $\bar{x}_{10} \approx 4.72 \cdot 10^{-4}$ for $x_{13} < 8 \cdot 10^{-3}$ and $\bar{x}_{10} \approx 5.78 \cdot 10^{-5}$ for $x_{13} > 8 \cdot 10^{-3}$. Depending on the value of x_{13} the model switches between $\bar{x}_{10} = 4.72 \cdot 10^{-4}$ and $\bar{x}_{10} = 5.78 \cdot 10^{-5}$. When the output of the system is low the input is switched on. When the output subsequently becomes high, the input is switched off. Using the MATLAB curve fitting toolbox the following heaviside function was found:

$$g_{\text{heaviside}}(x) = 4.72 \cdot 10^{-4} - (4.1420 \cdot 10^{-4}) \cdot \text{heaviside}(x - a), \quad \text{with} \quad a = 0.0073 \tag{3.17}$$

The molecular subsystem with a heaviside switch results in the so called *switch model*. A graphical representation of the switch model is given in Figure 3.11.

3.6.2 Trajectories of the switch models

In order to demonstrate the switch models, the trajectories of both models are evaluated and compared to the original Diekman trajetories. The trajectories of the switch and smooth switch model seen in Figure 3.12 are similar to those of the combined Diekman model seen in Figure 3.7a. The periods as well as the amplitudes of both switch models appear to be similar. The first state of the switch model (x_{11}) is a little more "spiky". However, after integrating this signal twice in order to come up with state x_{13} this is hardly visible anymore.

To conclude, the smooth switch and the switch model represent the Diekman model on the circadian time scale. Both models vastly simplify the electrical Diekman model while preserving the molecular subsystem. Both switch models are extremely useful as they allows for analysis using bifurcation software.

3.7 Summary and conclusion

The goal of this analysis was to find out what causes an oscillating output, how to separate timescales, and creating a model for each timescale. First, the time scale separation principle was discussed. It was shown that the fast time scale can be represented by replacing the slow variables with a constant. The slow time scale can be represented by replacing the fast variables with their average.

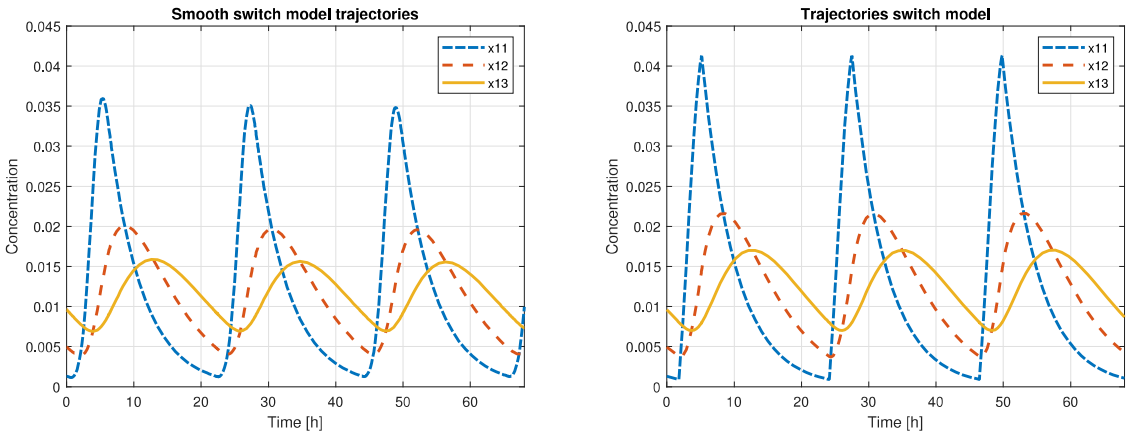

(a) Trajectories of the smooth switch model (b) Trajectories of the switch model

Figure 3.12: Comparison between the trajectories of the smooth switch and the switch model

Thereafter, the Diekman model was split in a fast and a slow part. The fast system was analyzed with a constant x_{13} input conform with the time scale separation principle. Two Hopf bifurcations spanning a domain of oscillations were found. The electrical subsystem starts oscillating when it is exited with values of x_{13} in between the Hopf points.

Subsequently, the slow molecular subsystem was considered. It was found that the molecular subsystem is not self-oscillatory. Besides, it does not oscillate with a constant x_{10} input. Moreover, the molecular subsystem does not represent the circadian oscillations of the Diekman model when an oscillatory x_{13} input is given. Therefore, it was concluded that coupling with the electrical subsystem is needed for the emergence of circadian oscillations. Using this insight the switch and the smooth switch model were derived. These models describe the Diekman model on the circadian time scale.

Chapter 4

Two coupled neurons

As discussed in Chapter 2, many of the interesting properties of the SCN such as synchronization do not appear in a single neuron but rather in a network of coupled neurons. Therefore, the single Diekman neuron case is extended to a network setting. As a first step towards more complex networks, this chapter analyzes the most basic network: two coupled neurons. The goal of this chapter is to find out if two neurons can synchronize when coupled by gap junctions, neuromodulator coupling, or both. This coincides with the first three research questions.

In order to understand these questions first a few definitions of synchronization are discussed as well as a general coupling model. Thereafter, diffusive coupling, a model for gap junction coupling is discussed. Thereafter, neuromodulator coupling is discussed using the Gonze model [25]. Finally, the combination of gap junction coupling and neuromodulator coupling is discussed.

4.1 Coupling and synchronization

Since we are dealing with a mathematical model of a single neuron, the coupling needs to be defined mathematically. Moreover, an important result of this coupling is the synchronization the neuron outputs. Therefore, a few mathematical definitions regarding synchronization are provided here.

Coupling

First the coupling is discussed in a very general sense. Consider two identical coupled neurons i and j. The dynamics of the i-th neuron can be described using a state space representation such that:

$$\dot{x}_i = f(x_i) + Bu_i \tag{4.1}$$
$$y_i = Cx_i \tag{4.2}$$

Here, $x_i \in \mathbb{R}^n$ represents the statevector of the i-th neuron and n represents the number of states. The vector $f(x_i)$ contains n functions translating the state values x_i of the i-th neuron to the rate of change $\dot{x}_i$ of the i-th neuron. The input $u_i \in \mathbb{R}^m$ describes the input of the i-th subsystem with m being the number of inputs. The output $y_i \in \mathbb{R}^p$ represents output of the i-th neuron with p being the number of outputs. $B \in \mathbb{R}^{n\times m}$ represents the control matrix which determines how the system input affects the state change. The

output matrix $C \in \mathbb{R}^{p \times m}$ determines the relationship between the system states and the system output. The neurons are identical, hence f, B, and C do not depend on i.

In our SCN network model any external inputs to the network are absent. In this research the network is considered to be autonomous, so the only input to any neuron is the output of other neurons. In our two coupled neuron network this simply means that the output of neuron i influences the input of neuron j and vise versa such that:

$$\begin{aligned} u_i &= g_{ij}(y_i, y_j), \\ u_j &= g_{ji}(y_j, y_i) \end{aligned} \tag{4.3}$$

where $g_{ij}(y_i, y_j)$ represents the coupling function of any two coupled neurons i and j depending on outputs y_i and y_j. So, the input of a neuron is a function of the outputs of individual neurons. The coupling function g_{ij} describes a specific type of coupling. In the following sections this function will be specified for both forms of coupling (gap junctions and neuromodulator diffusion).

Synchronization

Through the coupling function the outputs y_i and y_j can be altered. A special case emerges when the coupling function drives the state error between two neurons to zero. The two systems are now said to synchronize.

From a mathematical perspective this means that the states of two neurons of a networked dynamical system, x_i and x_j converge to the same synchronized state x_s such that

$$x_i(t) \to x_s(t) \text{ and } x_j(t) \to x_s(t) \text{ as } t \to \infty \tag{4.4}$$

The result is that:

$$\lim_{t \to \infty} |x_i(t) - x_j(t)| = 0 \tag{4.5}$$

However, when applying this general notion of synchronization to the Diekman neuron problems are encountered. As a start, the $t \to \infty$ condition is confusing. On the fast time scale $t \to \infty$ can be estimated by taking t in the order of minutes whereas on the slow time scale the limit is estimated by taking t in the order of weeks. Therefore, the notion of output synchronization is provided.

Definition 4.1.1. Consider system 5.2-5.3 with output $w_i = x_{n,i}$ where $x_{n,i}$ is any observable state n of neuron i. Neurons i and j *output synchronize* in case w_i and w_j converge to the same synchronized state w_s such that

$$w_i(t) \to w_s(t) \text{ and } w_j(t) \to w_s(t) \text{ as } t \to \infty \tag{4.6}$$

The result is that:

$$\lim_{t \to \infty} |w_i(t) - w_j(t)| = 0 \tag{4.7}$$

Note that the output y_i is used in coupling the neurons whereas output w_i is used to measure synchronization.

Definition 4.1.1 is useful when analyzing synchronization in a analytical way. However, using a numerical approach it will not be of much help. Due to numerical errors the output error does not reach zero, but instead becomes small. In order to accommodate this case a more practical definition of synchronization is given.

Definition 4.1.2. Consider output $w_i = x_{n,i}$ where $x_{n,i}$ is the observable n-th state of neuron i. Neurons i and j oscillate in *practical output synchrony* in case

$$||(w_i - w_j)(t)|| \leq \beta(t, ||(w_i - w_j)(0)||) + \delta, \text{ with } \beta \in \mathcal{KL} \tag{4.8}$$

where β is a class-$\mathcal{KL}$ function [1], $f(t)$ is a function of time, and δ is sufficiently small.

To summarize, a general coupling setting as well as some definitions of synchronization were discussed. First, it was demonstrated that in an autonomous (two cell) network the collective of outputs of the neurons form the inputs to the individual neurons. Thereafter, a definition for synchronization was provided. In addition, two definitions for output synchronization were provided.

4.2 Diffusive coupling

One of the important means of coupling, discussed in Chapter 2, is gap junction coupling. This section aims to investigate diffusive coupling, which is a model for gap junction coupling. The goal is to evaluate the first research question: "Can two SCN neurons synchronize when they are only coupled by gap junction coupling?"

In order to do so, first the diffusive coupling model is introduced. This model provides a function for the coupling function g_{ij} from Equation (4.3). In section 4.2.2 it is demonstrated that two Diekman neurons coupled by diffusive coupling can synchronize. However, this is not always the case and hypotheses regarding the stability of the synchronous solution are formed. Thereafter, the electrical subsystem is analyzed in section 4.2.4. Finally, the molecular subsystem is analyzed in section 4.2.5.

4.2.1 Diffusive coupling as a model for gap junctions

The goal of this section is to introduce diffusive coupling and implement it into the Diekman model. In order to do so, the input and output of the Diekman system are defined. Thereafter, the coupling function (from Equation (4.3)) is derived. Finally, some implications of diffusive coupling on the Diekman model are addressed.

Recall from Chapter 2 that a gap junction was represented as an ion channel between two neurons. Several ions can flow through this channel and alter the local membrane voltage of a neuron. As discussed a local depolarization of the membrane voltage increases the permeability of the membrane resulting in an action potential. The action potential can subsequently result in a depolarization of the membrane voltage of another neuron across a (different) gap junction. In this way electrical signals can be transmitted from one neuron to the next.

In diffusive coupling the gap junction is represented as an electrical resistance. The input u to a neuron is the current though the channel and can be summed with the other

[1] Consider class-$\mathcal{KL}$ function $\beta(r, s)$ then [26]:

$$\beta(r, \cdot) \in \mathcal{K}: \text{ strictly increasing and } \beta(0, \cdot) = 0$$
$$\beta(\cdot, s) \in \mathcal{L}: \text{ strictly decreasing and } \lim_{s \to \infty} \beta(\cdot, s) = 0$$

ionic currents in the first differential equation of the Diekman model (see Appendix A) such that:

$$\dot{x}_1 = \frac{I_{tot}(x)}{Cm}, \quad \text{with } I_{tot} = \sum I_{ion} + u \tag{4.9}$$

The current across the channel is determined by the difference in membrane potential between the two neurons (and the resistance). The membrane potential of a neuron is taken as an output. Using Ohm's Law the current across is calculated by multiplying the conductance (inverse of the resistance) with the difference in membrane potential of the neurons. The result is the diffusive coupling equation for neurons i and j [27]:

$$\begin{aligned} u_i &= \sigma(y_j - y_i), \quad \text{with } \; y_j = x_{j,1} \\ u_j &= \sigma(y_i - y_j) = -u_i \end{aligned} \tag{4.10}$$

The coupling strength σ represents the conductance of the membrane. Note that Equation (4.10) is a specification of the general coupling equation (4.3).

Now that a mathematical gap junction model has been introduced the model is evaluated more intuitively. When the output y_j in (4.10) is lower than the output y_i a negative input u_i will be received by the i-th neuron. In case $y_i < y_j$ a positive input will be received by the i-th neuron. Consequently the input for $u_{ij} = -u_{ji}$. In a biological representation this means that when the membrane potential of neuron i is lower than the membrane potential of neuron j ($y_i < y_j$), a current from j to i occurs. Subsequently, when the membrane potential of neuron j is lower than the membrane potential of neuron i ($y_j < y_i$), a current from i to j occurs. Note that when both membrane potentials are equal the coupling functions becomes zero. In fact, when a network of identical neurons coupled by diffusive coupling is synchronized, the coupling disappears.

To summarize, for diffusive coupling a difference in membrane voltage drives a current from one neuron to the other. The in flow from neuron i to neuron j is equal the out flow from neuron j to neuron i. In this way, the difference in membrane voltages and the conductance dictate the input to a neuron.

4.2.2 Exploratory simulations and hypotheses

With diffusive coupling defined and implemented in the Diekman model, the dependence of the network solution on the coupling strength σ is investigated. The goal of this section is to explore the network solutions numerically, and to form a conjecture on how the coupling affects the network solutions.

Exploratory simulations

Two Diekman neurons were coupled by diffusive coupling and simulated using MATLAB. Both neurons were initiated with a phase delay of 7 hours. The synchronizing property was investigated by varying the coupling strength between the neurons. Figure 4.1 shows the trajectories of electrical states x_1 and molecular states x_{11} of both neurons on the circadian time scale for three different coupling strengths. It is observed that for a coupling strength of $\sigma = 0.001$ both neurons do not synchronize as can be seen in Figure 4.1a. For this coupling strength (and these initial conditions) a non-synchronized solution is observed. For a coupling strength of $\sigma = 0.1$ both neurons synchronize in the sense of definition 4.1.2. This can be observed in Figure 4.1b. Finally, for a high coupling strength

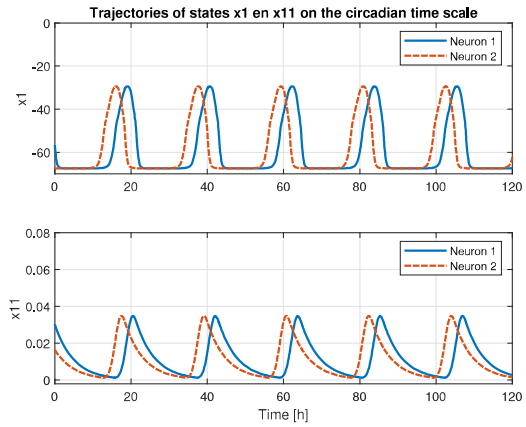

(a) Coupling strength $\sigma = 0.001$

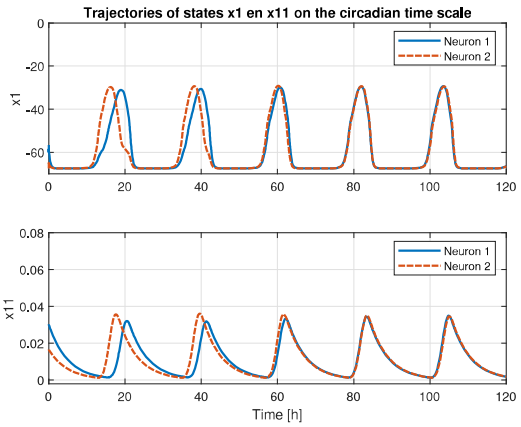

(b) Coupling strength $\sigma = 0.1$

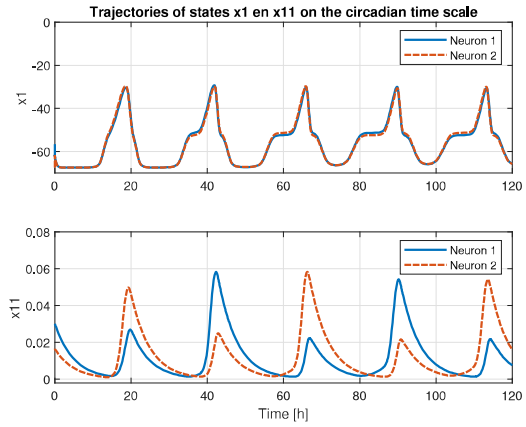

(c) Coupling strength $\sigma = 5$

Figure 4.1: State trajectories of x1 and x11 for low, middle, and high coupling strength.

of $\sigma = 5$ only the electrical x_1 states synchronize (in the sense of definition 4.1.2) while the molecular states x_{11} states do not synchronize.

The previous simulation indicates that for low coupling strengths two neurons do not necessarily synchronize, for certain coupling strength both neurons synchronize while for high coupling strength the neurons only some states synchronize. For high coupling strengths the electrical states synchronize while the molecular states do not synchronize.

Hypotheses

Considering the results of the previous simulations it is hypothesized that:
1) For coupling strengths below a certain threshold two neurons do not necessarily synchronize.
2) There is an upper threshold above which two neurons do not synchronize.
Since the electrical state do not appear to synchronize for a low coupling strengths, it is hypothesized that:
3) The electrical subsystem has a lower threshold on the coupling strength for which the synchronized solutions are globally stable.
4) The electrical subsystem does not have an upper threshold on the coupling strength for which the synchronized solutions are globally stable.
Since the molecular states do not appear to synchronize for low coupling strengths and

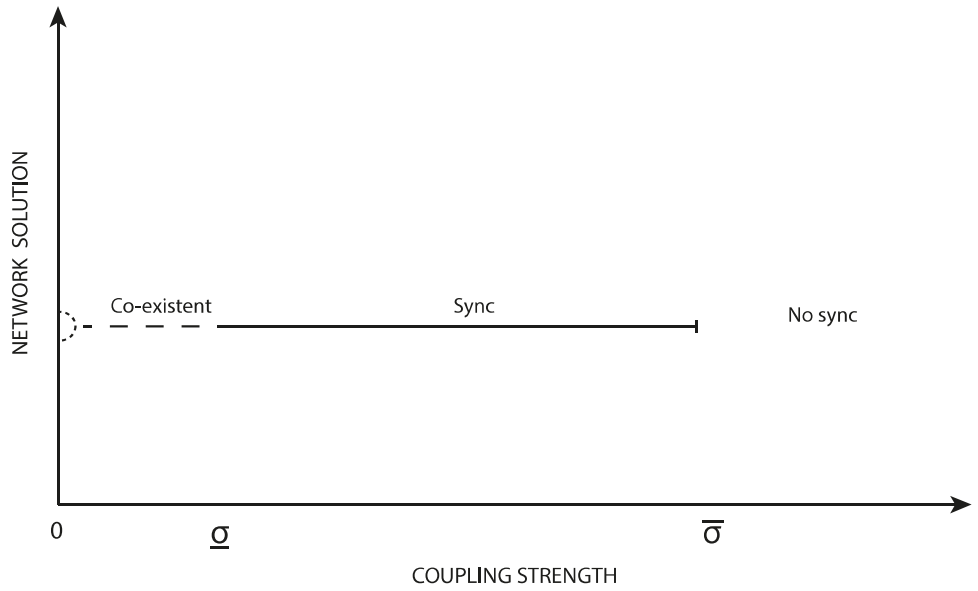

Figure 4.2: Hypothesized network solution depending on coupling strength

for high coupling strengths, it was hypothesized that:
5) The molecular subsystem has a lower threshold on the coupling strength for which the synchronized solutions are globally stable.
6) The molecular subsystem has an upper threshold on the coupling strength for which the synchronized solutions are globally stable.

The hypotheses can be summarized in Figure 4.2 which represents the steady state solution depending on the coupling strength σ. The lower threshold on the coupling strength is represented by $\underline{\sigma}$ while the upper threshold is represented by $\overline{\sigma}$.

To summarize, the dependence of the solutions on the coupling strength was explored using some simulations. The results indicated that different coupling strengths result in different network solutions. Therefore, six hypotheses were formed regarding the dependence of the solution on the coupling strength.

4.2.3 Estimating thresholds on the circadian time scale

The objective of this section is to investigate the first two hypotheses. Recall that due to the double time scale property it is challenging to analyze the network solutions using bifurcation software. Therefore, the solutions are further investigated in several MATLAB simulations. The goal of the simulations is to evaluate the (global) stability of the synchronized solutions depending on the coupling strength.

In general, all simulations have the same setup. Two Diekman neurons were initiated at a particular steady state solutions and the coupling strength was varied. The goal is to find the coupling strengths for which the initial state oscillation becomes unstable. In order to do so, MATLAB was used to simulate the two-neuron network for a simulation time of 30,000 hours. After 30,000 hours the neurons were assumed to have reached their final states.

First, the initial conditions of two coupled neurons were chosen randomly. The coupling strength was set low and simulations started. It was observed that depending on the initial conditions the neurons either synchronize or not. For initial conditions that

do not result in synchrony the neurons do influence each other. It was observed that there are several stable (non synchronous) solutions depending on the coupling strength and the initial conditions. One of these solutions was found to be particularly persistent with increasing coupling strength. The following simulations were initiated in this state. The coupling strength was set to a constant value and the trajectories were estimated using MATLAB for 30,000 hours. In case the neurons synchronized the coupling strength was lowered and the simulation was done again. It was found that a coupling strength $\sigma > 0.0024$ (± 0.0001) is needed for the system to jump from this non-synchronized attracting state to a synchronized state (in a time span of 30,000 hours). Subsequently, the initial conditions were set to the synchronized state and the coupling strength was lowered. In this case no coupling strength was found for which the synchronized state becomes unstable (in a time span of 30,000 hours).

Finally, the upper bound on the coupling strength was evaluated. First, the initial conditions were set at the synchronized state, the coupling strength was set at a low constant, and the trajectories were estimated for 30,000 hours. In case the molecular states stay synchronized, the coupling strength is increased. In case the synchronous state persisted, the coupling strength was increased. It was found that the synchronized state breaks down for $\sigma > 1.02$ (± 0.01). Finally, the experiment was reversed such that the initial conditions were set to the solution that was found for high coupling strength. The coupling strength was set at a high constant value and the trajectories were calculated for 30,000 hours. In case the neurons did not synchronize the coupling strength was lowered. It was found that for $\sigma < 0.98$ (± 0.01) both neurons synchronize.

Considering the results of the previous simulations it was concluded that for lower coupling strengths the solutions depend on the initial conditions. For these lower coupling strengths the solutions of the network either synchronize or are attracted to a non synchronous solution. Therefore, the first hypothesis was considered validated. Moreover, there is also an upper threshold, above which the synchronized solutions becomes unstable. Therefore, the second hypothesis was considered validated.

Obviously, the values limits found in the previous experiments are a little arbitrary since they depend on the simulation time, the accuracy, and the precision of the simulation. These numerical limitations unable us to draw any definite conclusions. However, the experiments provides us with workable thresholds for which synchronized trajectories can be simulated.

Besides the numerical limitations, these simulations paint a rather local picture. Since it is impossible to evaluate all possible initial conditions, only a very limited number of initial conditions were tested in the previous simulations. Therefore, there might be more types of network solutions than previously found. Moreover, only coupling strengths in the range of $\sigma < 1.02$ were evaluated. Higher coupling strengths were not used. Therefore, possible alteration in stability for coupling strengths $\sigma > 1.02$ are not explored.

4.2.4 Two coupled electrical subsystems

Previously six hypotheses regarding the network solutions of the network dynamic system were formed. The goal of this section is to evaluate the hypotheses regarding the electrical subsystem. Recall the hypotheses:

1. The electrical subsystem has a lower threshold.

2. The electrical subsystem does not have a upper threshold.

In order to evaluate the hypotheses, two coupled electrical subsystems are evaluated on the millisecond time scale. First, a numerical analysis using MATCONT will investigate the coupled electrical subsystem case. Thereafter, an analytical approach is used.

Numerical analysis

In order to evaluate the hypotheses, some simulations were conducted using MATLAB. In addition, a bifurcation analysis was done using MATCONT.

First, two electrical subsystems were coupled in MATLAB. The goal is to derive the dependency of the solution on the coupling strength on the millisecond time scale. In order to represent the fast dynamics the x_{13} input was set to a constant $x_{13} = 0.008$ such that action potentials firing (see Chapter 3) with a period of approximately 117ms occurs. The initial conditions of both neurons were set 45ms apart (near/on the periodic orbit). Figure 4.3a shows the initial oscillations for two uncoupled electrical subsystem. The simulation time was set to 2 minutes and every simulation the coupling strength was varied.

It was found that for low coupling strength the solutions are attracted to a non synchronous steady state. Figure 4.3b shows the steady state oscillations for a coupling strength of $\sigma = 5 \cdot 10^{-5}$. Since for low coupling strengths it take a long time to reach steady state, Figure 4.3b only shows the last 700 milliseconds containing the steady state oscillations.

When the coupling strength was increased this non-synchronized steady state solution was not found, but instead a synchronized solution was reached. Figure 4.3b shows an example for a coupling strength of $\sigma = 0.005$.

When the coupling strength is increased further both subsystems converge towards the synchronized state rapidly. Figure 4.3d shows the trajectories for $\sigma = 50$. Note that the difference in initial conditions is hardly visible. Both subsystems synchronize almost instantaneously.

Considering the results of the previous simulation it was concluded that there is at least one attracting non-synchronized state at low coupling strengths. Besides, it was found that for higher coupling strengths two electrical subsystems synchronize. It seems that there is no upper limit to the coupling strength for which the synchronized state is stable.

Before analyzing the synchronized steady state this non synchronous attracting steady state is briefly addressed. The goal is to estimate the threshold for which the non synchronous steady state becomes unstable. In another MATLAB simulation two coupled electrical subsystems were initiated in the non synchronous state found previously. The simulation time was set to 1 hour and the coupling strength was initially low but increased with every simulation. It was found that for $\sigma > 3 \cdot 10^{-4}$ the non-synchronized steady state solution disappeared and only the synchronized steady state solution was found.

The stability of the synchronized state is analyzed by evaluating the Floquet multipliers of the system. In Floquet theory the multipliers determine the orbital stability of a system [28]. Among the multipliers there is always one equal to one. For a stable orbit the others are smaller that one. Calculating the multipliers of high dimensional nonlinear systems such as the Diekman model is challenging. However, MATCONT can be used to estimate the multipliers. The goal is to derive conditions on the coupling strength for which the synchronized state is stable. In order to do so, two coupled electrical sub-

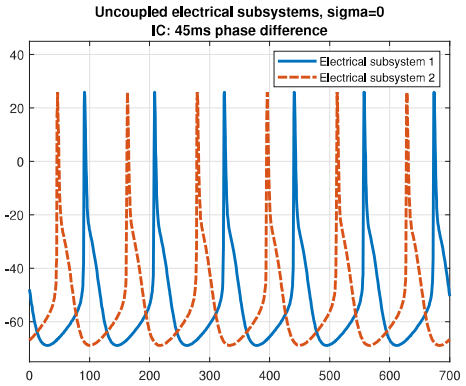

(a) Uncoupled electrical subsystems. Phases set 45ms apart.

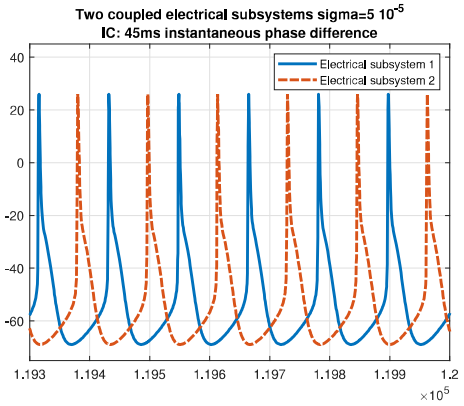

(b) Steady state solution of two coupled electrical subsystems with coupling strength $5 \cdot 10^{-5}$ and initial conditions set 45ms apart.

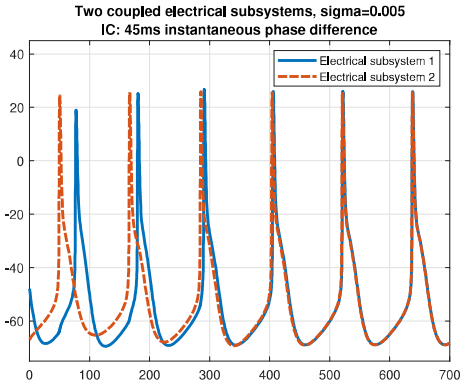

(c) Trajectories of two coupled electrical subsystems with coupling strength 0.005 and initial conditions set 45ms apart.

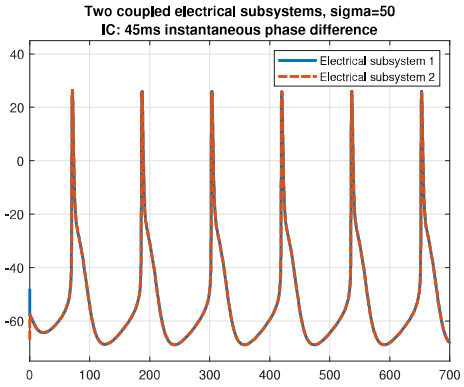

(d) Trajectories of two coupled electrical subsystems with coupling strength 50 and initial conditions set 45ms apart.

Figure 4.3: Two electrical subsystems coupled by diffusive coupling for various coupling strengths.

systems were implemented in MATCONT with both x_{13} set to $x_{13} = 0.008$ such that action potentials firing (see Chapter 3) with a period of approximately 117ms occurs. The coupling strength was taken as a bifurcation parameter. The initial state was set to the synchronized state and the coupling strength was varied from 0 to the arbitrary value of 100 with a maximum step size of 0.1. For every iteration the multipliers were estimated. The largest multiplier found was $\mu = 0.9356$. Therefore, it was concluded that the orbit is stable in the range $(0, 100]$. Therefore, it was concluded that there is no upper threshold on the coupling strength for which the synchronized state becomes unstable (for $\sigma \in (0,\ 100]$). Moreover, no lower threshold for which the synchronized state becomes unstable was found.

To summarize, it was found that for low coupling strengths there is at least one attracting non synchronous steady state. Moreover, the synchronized state is also stable for low coupling strengths. Therefore, it was concluded that for low coupling strengths multiple solutions exist. In this co-existence region, the solutions depends on the initial conditions. Therefore, in this region two electrical subsystems do not necessarily end up in a synchronized state. However, if a certain threshold on the coupling strength is crossed only synchronized solutions are found. Moreover, no upper threshold on the stability of the synchronized state could be found. However, only a limited range of initial conditions and coupling strength can be tested. Therefore, analytical analysis will have to provide a more definite answer.

Analytical approach

The numerical analysis of the two coupled electrical subsystems did not falsify the hypotheses. However, in order to truly validate the hypotheses an analytical approach is desired. The goal of this section is to prove that two coupled electrical subsystems synchronize if the coupling strength is above a certain threshold. In order to do so, the *synchronization theorem*, that proves the emergence of synchrony for diffusely coupled oscillators analytically, is used. In this section, first the synchronization theorem and then the subordinate lemmas are introduced. Thereafter, the synchronization theorem is tested for the electrical subsystem.

Theorem 4.2.1. [29] Consider two diffusely coupled subsystems and suppose that its solutions are confined to a closed and bounded set $\Omega^2 \subset (\mathbb{R}^n)^2$. Furthermore, let the subsystems be *internally exponentially convergent*. Then, for the synchronized subspace $\mathcal{S}$, there exists a constant $\underline{\sigma} \in \mathbb{R}_+$ such that if

$$\sigma > \underline{\sigma}$$

the $\mathcal{S}$ contains a globally (in Ω) exponentially stable subset.

The synchronization theorem tells us that, given some conditions, the synchronous state is globally exponentially stable if the coupling strength is large enough. Considering the exploratory simulation of section 4.2.2, it is hypothesized that Theorem 4.2.1 holds for the electrical subsystem but Theorem 4.2.1 does not hold for the molecular subsystem and combined Diekman neuron.

According to Theorem 4.2.1 the problem of examining the asymptotic stability of the synchronized state is reduced to

1. Validating that the solutions of the individual neurons are bounded.

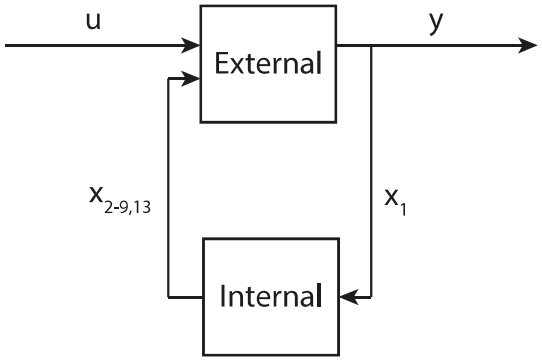

Figure 4.4: Internal and external dynamics of a Diekman neuron

2. Evaluating the internally convergence property of the neurons.

The reader might be unfamiliar with both properties. Therefore, both properties are addressed one at a time.

Definition 4.2.1. Consider a system consisting of n states. The solutions are said to be forward invariant if there exists a compact set $\Omega \subset \mathbb{R}^n$ such that $x(t) \in \Omega$, then $x(t+T) \in \Omega$ for all $T \geq 0$.

Definition 4.2.1 can be tested by calculating the equilibrium points of every state and validating the vector field at the equilibrium points inwards (into Ω).

Before discussing the internal convergence property, the internal and external dynamics of a system are separated. In order to do so, consider system

$$\begin{aligned} \dot{x} &= f(x) + Bu \\ y &= Cx \end{aligned} \tag{4.11}$$

Using an invertible coordinate transformation $x_i \to (z_i, y_i)$ system (4.11) can be separated in internal and external dynamics such that

$$\dot{z}_i = q(z_i, y_i), \tag{4.12}$$

$$\dot{y}_i = a(y_i, z_i) + CBu_i = a(y_i, z_i) + u_i, \quad \text{if } CB \text{ is invertible} \tag{4.13}$$

Equation (4.12) describe the internal dynamics and (4.13) describes the external dynamics.

By splitting the internal and external dynamics, a Diekman neuron is divided as seen in the block scheme of Figure 4.4. The external dynamics process the input and generate the output. The internal dynamics represent a feedback that steers the external dynamics. For the Diekman neuron the external state is $y = x_1$. The internal states are states $z_{1-12} = x_{2-13}$. Note that the split in internal and external states is different that the split in electrical and molecular states.

Now that the internal and external dynamics have been defined the convergence property is considered. A system is called convergent if it has "a unique, in a certain sense, globally asymptotically stable solution, called the steady-state solution" [30]. The system converges to the unique steady state independent of the initial conditions. The system "forgets" the initialization and all point converge towards the same solution.

Definition 4.2.2. [29] Consider the internal dynamics of subsystem (4.12) where y_i is defined on $(-\infty, +\infty)$ and takes values in a compact set $\mathcal{Y} \subset \mathbb{R}$. The system (4.12) is called *uniformly convergent*, resp. *exponentially convergent* if the following two conditions hold:

1. For all initial conditions $z_i(0)$, the corresponding solutions $z_i(t)$ exist and are bounded for all $t \geq 0$;

2. for all initial conditions $z_i(0)$ there exists a unique solution $\bar{z}_i(t)$, defined for $t \in (-\infty, +\infty)$ which is globally *uniformly asymptotically stable*, resp. *exponentially stable* such that
$$\lim_{t\to\infty} ||z_i(t) - \bar{z}_i(t)|| = 0 \tag{4.14}$$

Note that the internal convergence property again requires the solutions (this time the solutions of a single neuron) to be bounded. In order to validate the convergence of a system, Lemma 4.2.2, which provides a sufficient condition is used.

Lemma 4.2.2. [29] There exists a positive definite matrix P such that the eigenvalues of the matrix
$$Q(z, w) = \left[P \left(\frac{\partial q}{\partial z}(z, w) \right) + \left(\frac{\partial q}{\partial z}(z, w) \right)^T P \right] \tag{4.15}$$
are negative and separated from zero. Here w represents the external signal taken for a compact set $\mathcal{W} \subset \mathbb{R}$. If such a matrix P exists, the system (4.12)(4.13) is *exponentially convergent.*

To summarize, in order for two subsystems to synchronize the subsystems need to have bounded solutions as well as convergent internal dynamics. The bounds of the solutions can be calculated by evaluating the directions of the vector field at the equilibrium points. The convergence of the internal dynamics can by proven by finding a P matrix that satisfies lemma 4.2.2.

Application of theory to the Diekman neuron

Now that all the tools for proving the synchronization theorem have been discussed the electrical subsystem is tested. First, the bounds on the solutions are calculated. Thereafter, the internal convergence of the electrical subsystem is discussed.

Bounded solutions The Diekman differential equations (found in Appendix A) were set to zero and at the zero points the direction of the vector field was calculated. It was found that

Lemma 4.2.3. For the Diekman model there is a set $\Omega \subset \mathbb{R}^{13}$ such that $x(t) \in \Omega$ then $x(t + T) \in \Omega$ for all $T \in \mathbb{R}$

Proof. Appendix C □

Note, that not only the electrical states are bounded but also the molecular states.

Internal convergence The second requirement for the synchronization Theorem 4.2.1 is the exponential convergence of the internal states. Therefore, an attempt is made to prove that the Diekman electrical subsystem is exponentially internally convergent. This will incorporates the many of the previously introduced tools and definitions. The strategy is as follows. First the invertible coordinate change of (4.12),(4.13) is used to split the Diekman electrical subsystem into an internal and an external part. Thereafter, the internal subsystem is split again using lemma 4.2.4 that has yet to be introduced. Then, a matrix P that satisfies the condition of lemma 4.2.2 has to be found for every partitioning of the subsystem. Since this is possible it is concluded that the subsystem is exponentially internally convergent.

Let us start by first applying the invertible coordinate change of (4.12),(4.13) to the Diekman electrical subsystem such that

$$\begin{aligned} y &= x_1 & a &= f_1 \\ z_1 &= x_2 & q_1 &= f_2 \\ z_2 &= x_3 & q_2 &= f_3 \\ z_3 &= x_4 & q_3 &= f_4 \\ z_4 &= x_5 & q_4 &= f_5 \\ z_5 &= x_6 & q_5 &= f_6 \\ z_6 &= x_7 & q_6 &= f_7 \\ z_7 &= x_9 & q_7 &= f_9 \\ z_8 &= x_{10} & q_8 &= f_{10} \\ z_9 &= x_8 & q_9 &= f_8 \end{aligned}$$

Note that the order of the numbering is shifted ($x_{10} = z_8$). This is done so that every internal state only depends on the external subsystem (y) and previous internal states. In this way the cascade like nature of the system is emphasized.

In addition the relationship of the internal dynamics is represented in the block scheme of Figure 4.5.

When looking at Figure 4.5 one can observe the cascade property of the system. This is an important property because if the block $[q_1, .., q_6]$ is convergent it means that block $[q_1, .., q_6]$ has a unique steady state output (regardless of initial conditions) with respect to input y. Therefore, states $z_4, z_5,$ and z_6 are uniquely described by y at steady state. Subsequently, these states (together with y) form the input to the next block. The result is a cascade of convergent states. Therefore, only the individual blocks that are connected in series have to be evaluated. This approach is validated by lemma 4.2.4 for convergence in series connected systems.

Lemma 4.2.4. [30] Consider the system

$$\begin{aligned} \dot{z}_1 &= Q_1(z_1, y) \\ \dot{z}_2 &= Q_2(z_1, z_2, y) \end{aligned} \tag{4.16}$$

Suppose the z_1-subsystem with y as input is convergent, and the z_2-subsystem with (z_1, y) as input is convergent. Then system (4.16) is convergent.

When applying lemma 4.2.4 to the Diekman electrical subsystem (represented in Figure 4.5) one can observe that the convergent system property needs to be evaluated for 4

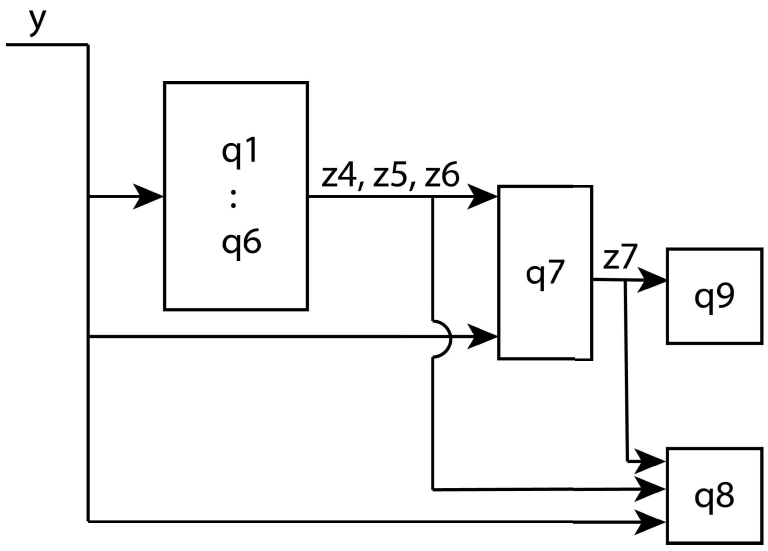

Figure 4.5: Block representation of the internal dynamics of the Diekman electrical subsystem

subsystems ($[q1, .., q_6], [q_7], [q_8], [q_9]$). It is proven that these subsystems are convergent by finding a P that satisfies the condition of lemma 4.2.2 for every block of the subsystem.

The differential equation from Appendix A are used to calculate the jacobian [2] of the first block $[q1, .., q6]$

$$J_{[q_1,..,q_6]}(y) = \begin{pmatrix} -\mathrm{e}^{\frac{y}{160}+\frac{143}{80}} & 0 & 0 & 0 & 0 & 0 \\ 0 & -\frac{1}{\mathrm{e}^{-\frac{10\,y}{71}-\frac{266}{71}}+\frac{51}{100}} & 0 & 0 & 0 & 0 \\ 0 & 0 & -\mathrm{e}^{\frac{y}{68}-\frac{67}{68}} & 0 & 0 & 0 \\ 0 & 0 & 0 & -\frac{1}{\tau_{rl}} & 0 & 0 \\ 0 & 0 & 0 & 0 & -\frac{1}{\tau_{rl}} & 0 \\ 0 & 0 & 0 & 0 & 0 & -\mathrm{e}^{\frac{y}{220}-\frac{111}{55}} \end{pmatrix} \tag{4.17}$$

The jacobian is a variable matrix that only depends on y. Since the jacobian is a diagonal matrix the eigenvalues are on the diagonal. Note that the eigenvalues take only negative values for $y \in \mathbb{R}$. Therefore, with $P = I_6$ the condition in lemma 4.2.2 is satisfied with I_6 representing the six dimensional identity matrix. Therefore, it is concluded that the $[q_1, .., q_6]$ subsystem is convergent.

For the last three subsystems lemma 4.2.2 is to be evaluated for three partial deriva-

[2]The jacobian matrix J is a matrix with dimension $N \times N$ and on the entries the partial derivatives of every function to every state such that for $\dot{X} = F(X, y)$ with $X = [x_1, x_2, ..., x_N]^T$ and $F = [f_1(X, y), f_2(X, y), ..., f_N(X, y)]$ the jacobian matrix is

$$J = \frac{\partial F}{\partial X}(X, y) = \begin{pmatrix} \frac{\partial f_1}{\partial x_1} & \cdots & \frac{\partial f_1}{\partial x_N} \\ \vdots & \ddots & \vdots \\ \frac{\partial f_N}{\partial x_1} & \cdots & \frac{\partial f_N}{\partial x_N} \end{pmatrix}$$

tives. The partial derivatives are:

$$J_{[q_7]}(y, z_4, z7) = -\frac{1}{\text{tauca}_1} - \frac{K_1\, g_{\text{CaL}}\, \text{kca}_1\, z_4\, (E_{\text{Ca}} - y)}{(K_2 + z_7)^2} \tag{4.18}$$

$$J_{[q_8]} = -\frac{1}{\tau_{Ca2}} \tag{4.19}$$

$$J_{[q_9]}(z_7) = -20000\, {z_7}^2 - \frac{7}{625} \tag{4.20}$$

Note that $J_{[q8]}$ is a negative constant constant so $P = 1$ satisfies the condition of lemma 4.2.2. Moreover $J_{[q_9]}(z_7)$ is a negative value for $z_7 \in \mathbb{R}$. Therefore $P = 1$ satisfies the condition of lemma 4.2.2. Finally, using the boundedness property from lemma 4.2.3 and the upper and lower bounds of y, z_4, and z_7 (found in Appendix C) it is found that $J_{[q_7]}(y, z_4, z_7) < 0$ for all $(y, z_4, z_7) \in \Omega$. Therefore using $P = 1$ the condition in lemma 4.2.2 can be fulfilled.

To conclude, all blocks from Figure 4.5 are convergent. Using lemma 4.2.4 about series connection it is concluded that the combined electrical subsystem is therefore internally convergent.

Exponential convergence Previously it was shown using the series connection lemma 4.2.4 that the electrical subsystem is convergent. The series connection lemma is useful, however, it only guarantees convergence instead of exponential convergence. In order to prove that the subsystem is also exponentially convergent, a matrix P that satisfies the inequality of lemma 4.2.2 for the whole electrical subsystem is derived using a MATLAB linear matrix inequality solver.

First, the bounds of the solutions found in Appendix C were substituted in the jacobian of the electrical subsystem. This resulted in 64 static jacobian matrices that span the space in which the dynamic jacobian "lives". Thereafter, considering the series interconnection the structure of matrix P was assumed to be:

$$P = \begin{pmatrix} I_6 & 0 & 0 & 0 \\ 0 & \gamma_1 & 0 & 0 \\ 0 & 0 & \gamma_2 & 0 \\ 0 & 0 & 0 & \gamma_3 \end{pmatrix} \tag{4.21}$$

Finally, a linear matrix inequality solver was used in MATLAB to find the coefficients γ_1, γ_2, and γ_3 that satisfy the inequality of lemma 4.2.2 for every static jacobian matrix.

It was found that:

$$\begin{aligned} \gamma_1 &= 0.1272 \\ \gamma_2 &= 322.46 \\ \gamma_3 &= 3.440 \cdot 10^{-5} \end{aligned} \tag{4.22}$$

results in a matrix P that satisfies the inequality of lemma 4.2.2 for all static jacobian matrices. Therefore, it is concluded that the Diekman electrical subsystem is internally exponentially convergent. Since all criteria of the synchronization theorem have been met, it is concluded that two Diekman electrical subsystems synchronize with sufficient coupling strength.

Summary and conclusion

The goal of this section was to evaluate the hypotheses regarding the electrical subsystem. Using numerical analysis it was found that two coupled electrical subsystem have a lower threshold above which two subsystems synchronize for all initial conditions. Furthermore, it was proven analytically using the synchronization theorem 4.2.1 that there is indeed a lower threshold but no upper threshold. Therefore, both hypotheses are validated.

4.2.5 Molecular subsystems

After the electrical subsystem was evaluated the molecular subsystem is now tested. The goal is to investigate the hypotheses:

1. The molecular subsystem has a lower threshold on the coupling strength.

2. The molecular subsystem has an upper threshold on the coupling strength.

First, a numerical analysis is performed. Thereafter, the previously introduced synchronization theorem 4.2.1 is evaluated for the Diekman neuron including the molecular subsystem.

Recall from section 4.2.4 that the MATCONT approach is only capable of proving the existence of an upper thresholds. Therefore, it is expected to be useful in proving the existence of an upper threshold for the molecular subsystem. In contrast, the analytical approach using the synchronization theorem 4.2.1 is expected to be inconclusive. Proving that lemma 4.2.2 fails does not mean that the synchronization theorem fails as lemma 4.2.2 is merely sufficient (not necessary). Therefore, in this case the analytical approach is believed to yield less useful results.

Numerical analysis

Numerical analysis of the molecular subsystem is challenging for two reasons. First, diffusive coupling as a model for gap junction coupling couples through the membrane voltage which is an electrical state. Therefore, we cannot totally omit the electrical subsystem. Second, as discussed in Chapter 3, simply separating the molecular part and feeding it the x_{10} signal does not result in a model for the molecular state oscillations. Therefore, the molecular subsystem cannot simply be evaluated using numerical analysis. However, the slow dynamics of the Diekman neuron can be analyzed using the smooth switch model introduced in Chapter 3. Since the smooth switch model drastically simplifies the electrical part of the Diekman neuron while it preserves the molecular part, it can shed light on how two molecular subsystems interact when coupled.

In order to do so, first two smooth switch models need to be coupled. Subsequently, the corresponding network system is evaluated. Finally, a lower and an upper threshold for which the synchronized state of the coupled smooth switch model is stable are found using MATCONT.

Smooth switch coupling model First the coupled smooth switch model is derived. Recall that the smooth switch model is a representation of a Diekman neuron in which state x_{13} is fed into a smooth switch. The output of the smooth switch represents the x_{10} state of the original system which is high in case x_{13} is low and x_{10} is low in case x_{13} is high. In this representation the entire electrical subsystem is replaced by a switch.

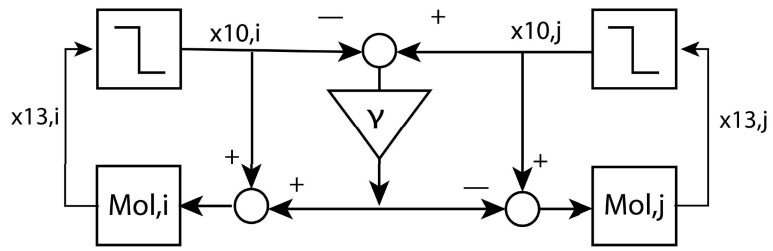

Figure 4.6: Schematic representation of coupled switch models i and j

As demonstrated previously, two coupled electrical subsystem always synchronize for sufficient coupling strength. In case the Diekman electrical system is perfectly synchronized both x_{10} variables are identical. In case the two Diekman electrical subsystems are coupled but not in perfect synchrony the x_{10} states are not equal but "pull" on each other. The extent to which both Diekman x_{10} states influence or pull on each other is determined by the coupling strength.

When taking the average of both x_{10} states the case of instantaneous perfect synchrony of the electrical subsystem is represented. This describes the case of the Diekman coupling strength $\sigma \to \infty$. Recall that this represents the case of Figure 4.3d where the electrical subsystems synchronized almost instantaneously. However, in case it is not infinity a weighted average is used such that the input to smooth switch models i and j is defined as:

$$u_i = (\gamma - 1)x_{10,i} + \gamma x_{10,j}, \tag{4.23}$$

$$u_j = (\gamma - 1)x_{10,j} + \gamma x_{10,i} \tag{4.24}$$

where γ is a coupling strength for the smooth switch model. For $\gamma = 0$ the systems are uncoupled. For $\gamma = 0.5$ the average of both signals are taken. This represents the case for which the Diekman electrical subsystems instantaneously synchronize: $\sigma \to \infty$. In addition figure 4.6 shows a graphical representation of the interaction of two coupled switch models.

Exploration of the coupled smooth switch model Before investigating the hypotheses, the trajectories of the coupled smooth switch model are evaluated. In order to do so, the model was implemented in MATLAB. Figure 4.7 shows the trajectories of the x_{11} states of both systems for coupling strengths 0.03, 0.2, and 0.4. For small coupling strength $\gamma = 0.03$ the coupled smooth switch model do not synchronize. When coupling γ is increased the smooth switch models start to synchronize. For a large coupling strength $\gamma = 0.4$ the models do not synchronize.

Note that the solutions observed in Figure 4.7 represents the solutions of the combined Diekman neurons on the circadian time scale. Compared with the solutions shown in Figure 4.1 similar network solutions can be observed. For low coupling strengths two smooth switch models do not synchronize. For moderate coupling strength the models synchronize. For high coupling strength the smooth switch models do not synchronize and end up in a state that resembles the high coupling non-synchronized state of two coupled Diekman neurons seen in Figures 4.1c and 4.7c. This state is characterized by both neurons or switch models oscillating half a phase apart and by the alternation of a low peak and a high peak.

When analyzing the network solutions it was found that for coupling strengths below a certain threshold at least two solution exist. Therefore, depending on the initial conditions

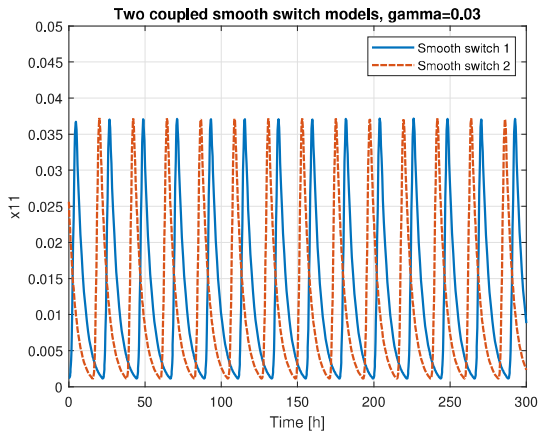

(a) $\gamma = 0.03$

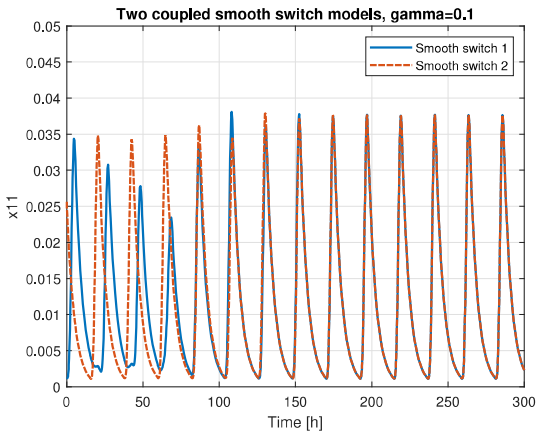

(b) $\gamma = 0.2$

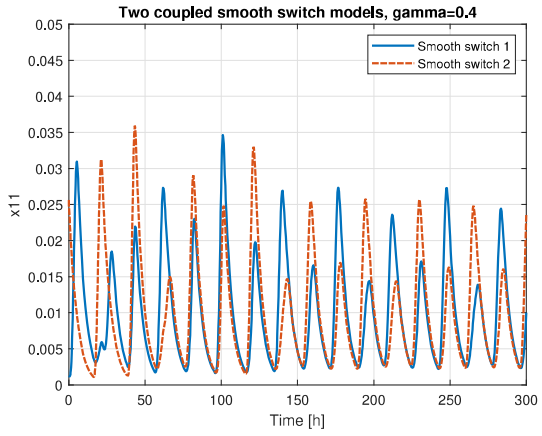

(c) $\gamma = 0.4$

Figure 4.7: Trajectories of x11 for low, middle, and high coupling strength γ for identical initial conditions

the coupled switch model either synchronize or get stuck in a non synchronous attracting steady state. It was found that if the coupling strength is increased across a threshold only the synchronized state was found. Finally, if the coupling strength is increased above a certain threshold the synchronous state becomes unstable and the smooth switch models do not synchronize.

Estimation of the thresholds The main advantage of the switch model is that it can be analyzed effectively in MATCONT. The goal of this analysis is to validate the existence of the thresholds on the coupling strength.

In order to do so, first the coupled smooth switch model is implemented in MATCONT. The initial conditions were set to the synchronized state. The coupling strength σ was chosen as a bifurcation parameter on the range $(0,\ 0.5]$. The multipliers were estimated and shown in Figure 4.8. Note that near $\sigma = 0.27$ a multiplier crosses the threshold of 1. Therefore, it is concluded that the synchronized solution becomes unstable for $\sigma > 0.27$. Moreover, no lower stability threshold was found.

The lower threshold is estimated using MATLAB. The initial conditions were set on the orbits seen in Figure 4.7a. Subsequently, the simulation time was set to 30,000 hours and the coupling strength slowly increased. It was found that the neurons synchronize

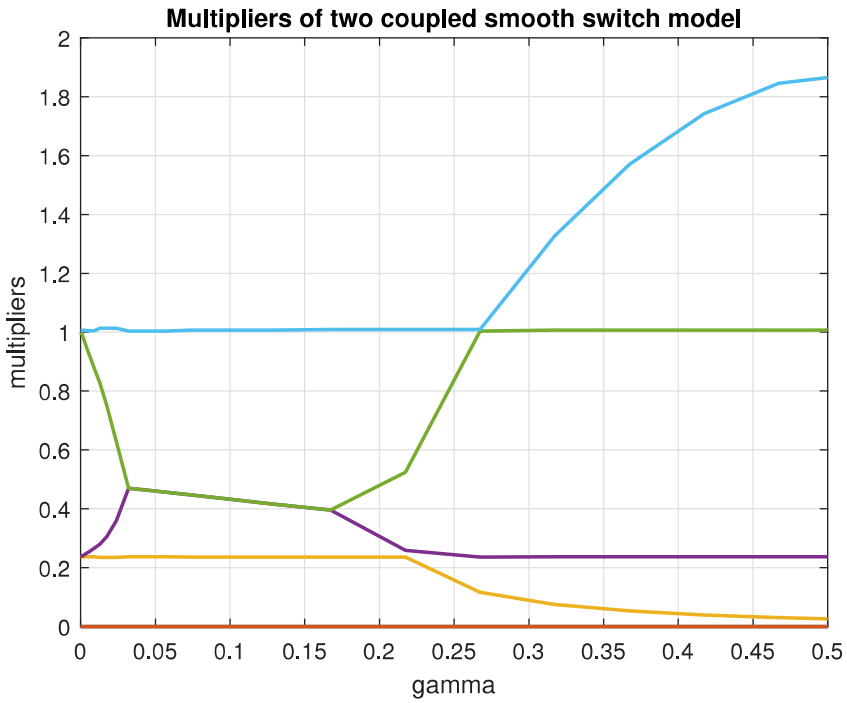

Figure 4.8: Floquet multipliers of two coupled smooth switch models

for $\gamma > 0.04$.

Considering the results, it was concluded that for low coupling strength at least two solutions exists (possibly more). One of these solutions is the synchronized solution. For high coupling strengths the synchronized solution is no longer stable.

Summary and conclusion The smooth switch model was coupled by taking the weighted average of the x_{10} inputs of the switch models. In this way, a system was created that models two slow molecular subsystems that are coupled by diffusive coupling. Using MATLAB and MATCONT, a lower threshold and an upper threshold were found for the coupled smooth switch model for which the synchronized steady state is globally stable. Therefore, it was concluded that the molecular subsystem in a coupled Diekman neuron poses an lower threshold as well as an upper threshold on the coupling strength for which the synchronized state is globally stable. Thereby, the fifth and sixth hypotheses are considered validated.

Analytical approach

The intention of this section is to analyze the synchronization property of the molecular subsystem using an analytical approach. Using a bifurcation analysis it was found previously that the molecular subsystem creates a lower threshold and an upper threshold. The objective of this section is to find out how this relates to the synchronization theorem 4.2.1.

The stability of the synchronous solution of a double Diekman neuron network has an upper threshold. Therefore, the synchronization theorem 4.2.1 does not hold for a Diekman neuron. Previously, it was proven that the theorem holds for the electrical subsystem. Therefore, it was hypothesized that the synchronization theorem 4.2.1 does

not hold when the molecular subsystem is added to the electrical model (to form a Diekman neuron). The goal of this section is to prove that the synchronization theorem is not satisfied when the molecular subsystem is included in the neuron dynamics. Moreover, it is demonstrated why the synchronization theorem fails.

Synchronization theorem Since there exist an upper threshold on the stability of the synchronized state, it is known that the synchronization theorem fails for the full Diekman neuron. Recall that the synchronization theorem has two requirements:

1. The solutions of the individual neurons are bounded
2. The internal states are exponentially convergent

Lemma 4.2.3 demonstrates that the solutions of the entire Diekman model are bounded. Therefore, the first requirement is satisfied. Consequently, the second requirement must be unsatisfied. Therefore, it is concluded that the Diekman neuron is not internally convergent.

Moreover, it was shown that the electrical subsystem is internally exponentially convergent. Since the molecular subsystem is connected to the electrical subsystem in series, the molecular subsystem can be evaluated individually (lemma 4.2.4). Consequently, it is hypothesized that the molecular subsystem is not convergent.

Simulations of convergence property In order to investigate the convergence property of the molecular subsystem, a simulation was conducted. The goal is to demonstrate numerically that the molecular subsystem is not convergent. This is done by searching for sets of initial conditions that result in a different steady state solution.

Recall that a convergent system has a unique steady state relation to its input regardless of initial conditions. Since the Diekman neuron is a nonlinear model, the steady state cannot be calculated. However, the steady state can be estimated numerically. The goal is to excite various identical systems with an identical input system but with a set of varying initial conditions. For a convergent system all trajectories end up in the same steady state. However, if the system is not convergent the steady state solutions are not identical. Note that this approach is not guaranteed to be conclusive.

An arbitrary number of twenty Diekman molecular subsystem with different initial conditions were given an identical electrical input signal. Since the molecular subsystems only oscillate on the circadian time scale the simulation was conducted on the slow time scale. The twenty subsystem received an identical x_{10} input signal. Since the x_{10} electrical input signal does not oscillate on the circadian time scale (for constant input x_{13}) an auxiliary molecular model was introduced. A graphical representation of the setup can be seen in Figure 4.9a. The initial conditions of the 20 molecular subsystems were chosen randomly within Ω (see Appendix C).

The trajectories of the states are shown in 4.9b. After the transients dissolve two distinct steady state trajectories can be seen. Depending on the initial conditions the subsystems either converge to one or the other. Therefore, it is concluded that the molecular subsystem in not convergent.

Analytical analysis of the convergence property In addition to the numerical result that the molecular subsystem is not convergent, an analytical approach regarding the convergence is provided. The goal is to prove that the sufficient test of lemma

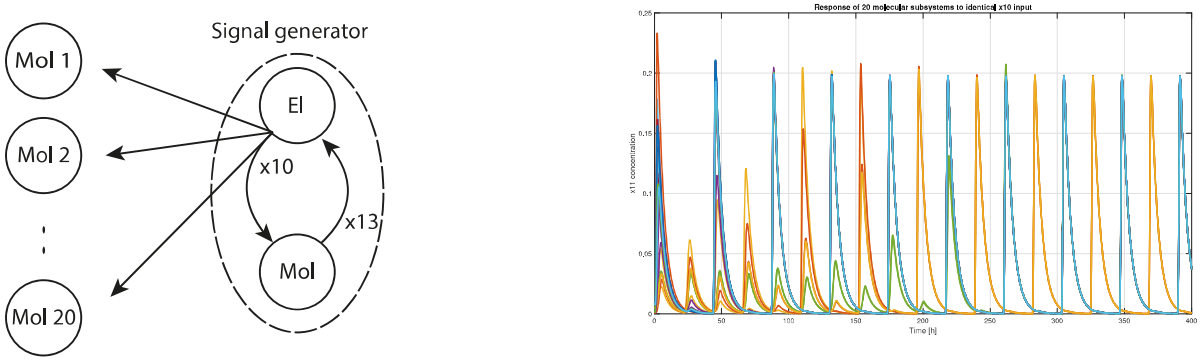

(a) An oscillating electrical x10 signal is feed to 20 molecular subsystems.

(b) Trajectories of the x_{11} states of the molecular subsystem with an identical x10 input signal but 20 different sets of initial conditions

Figure 4.9: Cell to molecular system. Left most molecular system is given 20 random initial conditions within bounds. All trajectories grow towards one limit cycle with a delay/advance of half a period

4.2.2 fails for the molecular subsystem. In order to do so, the same strategy as for the electrical subsystem is used: extend the invertable coordinate change, construct the jacobian, evaluate the matrix P that satisfies lemma 4.2.2.

First, the coordinate change of (4.12)(4.13) is extended to the molecular system:

$$\begin{aligned} x_{11} &= z_{10}(z_8, z_{10}, z_{12}) \\ x_{12} &= z_{11}(z_{10}, z_{11}) \\ x_{13} &= z_{12}(z_{11}, z_{12}) \end{aligned} \tag{4.25}$$

Note that the molecular subsystem can be evaluated individually because it is connected in series to the electrical subsystem (lemma 4.2.4).

The jacobian of the molecular subsystem

$$J_{[z_{10},..,z_{12}]}(z_8, z_{12}) = \begin{pmatrix} -a & 0 & -a \cdot R(z_8, z_{12}) \\ a & -a & 0 \\ 0 & a & -a \end{pmatrix} \text{ with } R(z_8, z_{12}) = \frac{\text{CRE}(z_8)}{2.5 \cdot 10^{11}(z_{12} + 0.001)^5} \tag{4.26}$$

was created. There is a special conditions for the eigenvalues of $J(z_8, z_{12})$ for which it can be proven that a matrix P satisfying lemma 4.2.2 does not exists. If an eigenvalue of $J(z_8, z_{12})$ has a positive real part the matrix P does not exist. This is an specification from an Ostrowski-Schneider inertia theorem [31].

When using the bounds of $z_8, z_9 \in \Omega$ (found in Appendix C) the eigenvalues of the jacobian $J(z_8, z_{12})$ take values with positive real part for z_8 and z_{12} in a subset of the space Ω. For example using $z_8 = z_{12} = 0.001 \in \Omega$ results in $Re(\lambda) \approx -3.8,\ 0.42,\ 0.42$

To conclude, the occurrence of eigenvalues (of J) with positive real part proves that the matrix P does not exists. This demonstrates that lemma 4.2.2 cannot be satisfied for the molecular subsystem.

Conclusion Using numerical analysis it was concluded that the molecular subsystem is not convergent. This means that two molecular subsystems might react differently to

the same electrical input. In case two electrical subsystems are perfectly synchronized the molecular subsystems may end up in different network solutions. Therefore, the molecular states do not necessarily synchronize. This is what appear to happen when the coupling strength is too large. In that case the electrical subsystems synchronize while the molecular subsystems respond with a different steady state solution.

Summary and conclusion

The goal of this section was to investigate the hypotheses

1. The molecular subsystem has a lower threshold on the coupling strength.

2. The molecular subsystem has an upper threshold on the coupling strength.

In order to represent the molecular system the smooth switch model was used. Using the result that the electrical subsystems synchronize a weighted average of the x_{10} inputs (depending on the coupling strength) was taken.

A bifurcation analysis in MATCONT indicated that the solutions of the smooth switch models indeed pose a lower threshold and an upper threshold on the coupling strength for which the synchronized state is globally stable. Therefore, the hypotheses are considered validated.

Thereafter, the synchronization theorem 4.2.1 was evaluated for the Diekman neuron. Using the synchronization theorem it was hypothesized that the synchronization theorem of the combined Diekman neuron fails because the molecular subsystem is not convergent. Simulations demonstrated that the molecular subsystem has a output response that depends on its initial conditions. Therefore, it was concluded that the molecular subsystem is not convergent. Besides, it was proven analytically that the sufficient test for convergence of lemma 4.2.2 fails for the molecular subsystem.

4.2.6 Summary and conclusion

The intention of this section was to investigate diffusive coupling for two coupled neurons. The objective was to investigate the first research question "Can two neurons synchronize when coupled by gap junction coupling". In order to do so, six hypotheses were formed regarding gap junction coupling in a double neuron network. It was found that for low coupling strength multiple solutions exist. Both the synchronized steady state as well as other states are stable. For coupling strengths above a certain threshold two neurons synchronize. For even larger coupling strength two neurons do not synchronize.

Using the synchronization theorem, it was concluded that two coupled electrical subsystems synchronize (for all initial conditions) when a lower threshold is crossed. It was concluded that there is no upper threshold after which two electrical subsystems desynchronize. Subsequently, using the insight that two electrical subsystem synchronize (when a certain threshold is crossed), two smooth switch models were coupled. Using a bifurcation analysis on the smooth switch model, it was concluded that the molecular subsystem poses an upper threshold on the coupling strength for which the synchronized state is stable.

To conclude, two Diekman neurons coupled by diffusive coupling can synchronize (for all initial conditions) for a certain range of coupling strengths. Therefore, it was concluded that two SCN neuron coupled can synchronize when coupled only by gap junctions. Thereby, the first research question is considered answered.

4.3 Neuromodulator coupling

In Chapter 2, two important means of coupling are discussed. These are coupling by gap junctions and coupling by neuromodulator diffusion. This section focuses on neuromodulator diffusion. The goal is to evaluate the second research question: "Can two SCN neurons synchronize when only coupled by neuromodulator diffusion?" In order to do so, the Gonze model [25] for neuromodulator diffusion is used.

First, in section 4.3.1 the neuromodulator coupling model is introduced and implemented in the Diekman model. Thereafter, in section 4.3.2 the case of a single Diekman neuron with neuromodulator action is evaluated. Finally, in section 4.3.3 the synchronizing property of two coupled neurons is evaluated.

4.3.1 Gonze model

The Gonze model is a coupled Goodwin model [22] that was introduced in 2005. It couples Goodwin oscillators using a general excitatory neuromodulator, which is designed to represent basic VIP coupling. It is a powerful model because it is relatively simple and describes the most essential parts of neuromodulator coupling.[25][32]

The Gonze model couples Goodwin oscillators in a mean field network. It means that the input to every cell is the average of all outputs. The differential equations of the Gonze model are

$$\frac{dX_i}{dt} = v_1 \frac{K_1^n}{K_1^n + Z_i^n} - v_2 \frac{X_i}{K_2 + X_i} + f(F), \quad \text{with} \quad f(F) = v_s \frac{\mu F}{k_r + \mu F} \tag{4.27}$$

$$\frac{dY_i}{dt} = k_3 X_i - v_4 \frac{Y_i}{K_4 + Y_i} \tag{4.28}$$

$$\frac{dZ_i}{dt} = k_5 Y_i - v_6 \frac{Z_i}{K_6 + Z_i} \tag{4.29}$$

$$\frac{dV_i}{dt} = k_7 X_i - v_8 \frac{V_i}{K_8 + V_i} \tag{4.30}$$

$$F = \frac{1}{N} \sum_{i=1}^{N} V_i \tag{4.31}$$

where X, Y, Z are the familiar Goodwin states in nanomol. The state V represents the dynamics of the neuromodulator and K_j and v_j are constants. The concentration of V is induced by the activation of X. The state V (and X, Y, Z) degrade in a nonlinear manner. Subsequently, the average of every neuron V state is taken and fed back into the first differential equation. The function $f(F)$ describes how a neuron perceives a concentration of the neuromodulator. Since the number of receptors on the membrane is limited, a saturation is used. At peak saturation a maximum of v_s reached, and k_r is the amount of neuromodulator at mid saturation. The value μ represents the variable coupling strength.

Implementation in a Diekman neuron

Since the Diekman model also uses a Goodwin-like molecular subsystem, the implementation of Gonze coupling can be done relatively easily. As the Diekman model uses only

linear degradation terms the nonlinear degradation from the Gonze model was replaced by a linear one such that the Diekman molecular model now look like

$$\dot{x}_{11} = a\left(CRE(x_{10})\left(\frac{1}{1000 \cdot x_{13}+1}\right)^{n} - x_{11} + f(V_{mean})\right) \tag{4.32}$$

$$\dot{x}_{12} = a(x_{11} - x_{12}) \tag{4.33}$$

$$\dot{x}_{13} = a(x_{12} - x_{13}) \tag{4.34}$$

$$\dot{V} = \tau(x_{11} - v_d V) \tag{4.35}$$

Here, the function $f(V_{mean})$ describes how a neuron perceives a high neuromodulator concentration similar to the Gonze model:

$$f(V) = v_s \cdot \frac{\mu V_{mean}}{k_r + \mu V_{mean}} \tag{4.36}$$

where v_s is a constant describing the sensitivity of a neuron to the neuromodulator. The average is again defined as

$$V_{mean} = \frac{1}{N}\sum_{i=1}^{N} V_i \tag{4.37}$$

Parameterset of the Gonze model The parameters of the Gonze model cannot be directly translated to the Diekman neuron since the dynamics of the Goodwin systems are slightly different. However the Gonze model provided an indication. The ratio between the constants of the Gonze model were analyzed. The result is a set of parameters for the Diekman model: $v_s = 1$ nM/h, $\tau = a$ ms^{-1}, $k_r = 1$ nM, $v_d = 3$ nM/h. In the following this set is referred to as the *default parameter set* for neuromodulator coupling. Note that μ, the coupling strength will be varied.

4.3.2 Single cell neuromodulator

One of the interesting implications of the model is that it couples a neuron to itself. In this case a neuron receives an input that is identical to its own neuromodulator output. This case is worth investigating since it represents the case of a neuron in a synchronized network. The goal is to determine how the neuromodulator coupling strength affects the the self-modulated neuron and thereby affects the synchronized state.

In the single neuron representation the neuromodulator concentration is only dependent on $x_{11,i}$ and time. The dynamics for the neuromodulator state can be rewritten as:

$$\frac{dV_{mean}}{dt} = \tau\left(x_{11} - v_d V_{mean}\right), \quad \text{if } N = 1 \tag{4.38}$$

This is an isolated neurons that receives its own neuromodulator output as an input. This will be referred to as a *self modulated neuron*. Before coupling multiple neurons a self modulated neuron is evaluated. The goal is to investigate how the (neuromodulator) coupling strength μ affects a single Diekman neuron.

Trajectories

First the trajectories of a self modulated neuron are compared to a original Diekman neuron. Figure 4.10 shows the development of the state x_{11} of one self modulated neuron

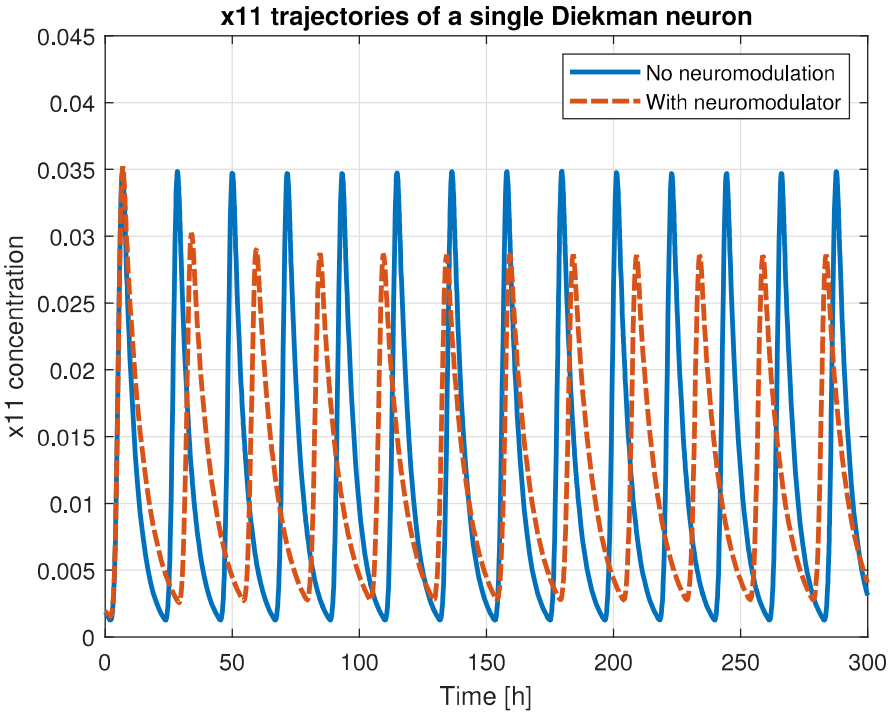

Figure 4.10: Original vs. self modulated neuron

(using the default parameter set) and one original Diekman neuron on the circadian time scale (with identical initial conditions). It can be noted that the period of the self modulated neuron is larger than the original Diekman neuron. In fact, this is a well-known result of VIP coupling observed in biological experiments [33]. Moreover, the amplitude of the self modulated signal is lower than the original model.

Additional exploratory simulation indicated that the size of the amplitude depends on the coupling strength μ. With increasing μ the amplitude decreases. When a certain threshold is crossed a stable equilibrium can be found. Therefore, it was hypothesized that the self modulated neuron undergoes a Hopf bifurcation when the coupling strength crosses a certain threshold.

Thresholds on the coupling strength The hypothesis is tested using a bifurcation analysis in MATCONT. In order to do so, the smooth switch model was used (instead of the Diekman neuron) because it of the single time scale property. Note that the smooth switch model is very useful for neuromodulator coupling. Neuromodulator coupling is slow and unlike diffusive coupling the input and output for neuromodulator coupling are located in the molecular subsystem. Therefore, the neuromodulator smooth switch network is assumed to represent the neuromodulator Diekman network well.

The value of $f(V)$ was taken as a bifurcation parameter. A Hopf bifurcation was found at $f(V) = 0.0071$. For $f(V) > 0.0071$ a stable equilibrium emerges at $x_{11,0} = x_{12,0} = x_{13,0} = 0.0085$. Note that the equilibrium of the smooth switch model is uniquely described by $f(V)$. Therefore, it was concluded that the equilibrium changes stability at $x_0 = 0.0085$.

This equilibrium is further inspected analytically. The goal is to come up with a condition on the coupling strength (and parameters) for which the neuron oscillates on the circadian time scale. In order to do so, first, the equilibrium is substituted in the

state equations. Secondly, the equilibrium depending on the parameters is calculated. Finally, a condition for which the equilibrium crosses the $x_0 = 0.0085$ point is found.

The self modulated smooth switch model is represented by

$$\begin{aligned} \dot{x}_{11} &= a(h(x_{13}) - x_{11} + f(V)), \quad \text{with} \quad f(V) = \frac{\mu V}{k_r + \mu V} \\ \dot{x}_{12} &= a(x_{11} - x_{12}) \\ \dot{x}_{13} &= a(x_{12} - x_{13}) \\ \dot{V} &= \tau(x_{11} - v_d \cdot V) \end{aligned} \tag{4.39}$$

Substituting the equilibrium $x_{11,0} = x_{12,0} = x_{13,0} = x_0$:

$$\begin{aligned} x_{11,0} &= h(x_0) + \frac{\mu V_0}{k_r + \mu V_0} \approx \frac{\mu V_0}{k_r + \mu V_0}, \\ x_{12,0} &= x_0, \\ x_{13,0} &= x_0, \\ V_0 &= \frac{x_0}{v_d} \end{aligned} \tag{4.40}$$

Recall that the function $h(x_{13})$ is monotonically decreasing (Chapter 3). For large values of x_{13} it is practically zero. Since we are interested in the equilibrium near the bifurcation we can use the fact that $h(x_{13,Hopf}) \approx 0$. Substituting final row in the first row of Equation (4.40)

$$\begin{aligned} x_0 &\approx v_s \frac{x_0 \cdot \mu / v_d}{k_r + x_0 \cdot \mu / v_d} \\ x_0 &\approx v_s - k_r \frac{v_d}{\mu} \end{aligned} \tag{4.41}$$

which describes the equilibrium (in the region $h(x_{13,Hopf}) \approx 0$) near the bifurcation. In order for the neuron not to bifurcate to a stable equilibrium, the condition

$$v_s - k_r \frac{v_d}{\mu} < 0.0085, \quad \text{or} \tag{4.42}$$

$$\mu < \frac{k_r \cdot v_d}{v_s + 0.0085} \tag{4.43}$$

has to be satisfied. The Gonze parameters are usually larger much values than $x_0 = 0.0085$ so the condition can be approximated to $\mu \cdot v_s < k_r \cdot v_d$. Using the default parameter set, it is concluded that the constant steady state is reached for $\mu > 3$.

The previous results only hold for the smooth switch model. Convenient as it may be, this toy model does not represent an SCN neuron. Therefore, an attempt is made to translate the results from the smooth switch model to the Diekman model. Since the self-modulated smooth switch model is believed to be a accurate representation of the self-modulated Diekman neuron, it is hypothesized that the $\mu > 3$ threshold holds for the Diekman neuron.

In an attempt to validate the hypothesis several simulations were conducted. In every simulation the neuron was simulated until steady state was reached. In case the solution was oscillatory the coupling strength μ was slightly increased. The threshold was found to be $\mu \approx 3.1$ (± 0.1). Therefore, the hypothesis was considered validated.

It is hard to overestimate the importance of the oscillation condition of Equation (4.43). It does not only provide a condition on an oscillating self modulated neuron but also on a synchronized network of arbitrary size. Consider a network of two coupled neurons. In the synchronized network the state V_i of neuron i is equal to state V_j of neuron j. The input V_{mean} to both neurons is the average of both states V_i and V_j. Since both states are equal the average is equal as well such that $V_{mean} = V_i = V_j$. So, every neuron receives its own V state as an input. Therefore, in the synchronized state the coupling disappears and both neurons can be represented as a self modulated neuron. Consequently the inequality (4.43) provides a condition for which the synchronized state of a network with arbitrary size is oscillatory.

To summarize, the self modulated neuron is a representation of a single Diekman neuron with neuromodulator action. It also represents the case of a network of neurons in complete synchrony. When using the default parameter set it was concluded that the self modulated neuron is oscillatory for $\mu < 3$.

4.3.3 Two coupled neurons

In the previous, a condition on the coupling strength for which the synchronous state is oscillatory was derived (Inequality (4.43)). However, a condition for which coupling strength actually synchronizes two neurons has not been derived yet. The goal of this section is to find out if there is a range of coupling strengths that can synchronize two neurons. In order to do so, first some initial simulations are done. Thereafter, a bifurcation analysis is conducted.

Two neurons were coupled using the default parameter set. Figure 4.11 shows the trajectories of the eleventh state (x_{11}) on the circadian time scale. The neurons synchronize with passing time. Note that the neurons synchronize fast at first but as the error decreases it takes significantly longer to synchronize further.

In order to investigate the range of coupling strengths that synchronize two neuron a bifurcation analysis was conducted in MATCONT. The modulator coupled smooth switch model was used in combination with the default parameter set. The coupling strength μ was used as a bifurcation parameter and the stability of the error dynamics was analyzed. The neurons were initiated in the synchronized state and μ was varied on the domain $\mu \in [0,\ 3]$.

On the domain $\mu \in [0,\ 3]$ the error dynamics did not undergo a bifurcation and remained at the stable equilibrium (at zero). Therefore, it was concluded that the entire range of the coupling strength can (locally) synchronize two neurons. Moreover, for coupling strengths $\mu < 0.12$ a region containing multiple solutions was found. Depending on the initial conditions the solutions end up in either a synchronized state or a non-synchronized attracting state. Therefore, it was concluded that the synchronous state is globally stable for $\mu \in [0.12,\ 3]$

The previous results found using MATCONT only hold for the smooth switch model. Therefore, an attempt is made to translate the results from the smooth switch model to the Diekman model. Since the self-modulated smooth switch model is believed to be a accurate representation of the self-modulated Diekman neuron, it is hypothesized that the synchronous solutions of two coupled Diekman neurons are locally stable for the entire range of $\mu \in [0,\ 3]$, and globally stable for the for $\mu \in [0.12,\ 3]$.

In an attempt to validate the hypothesis, several simulations were conducted in MAT-

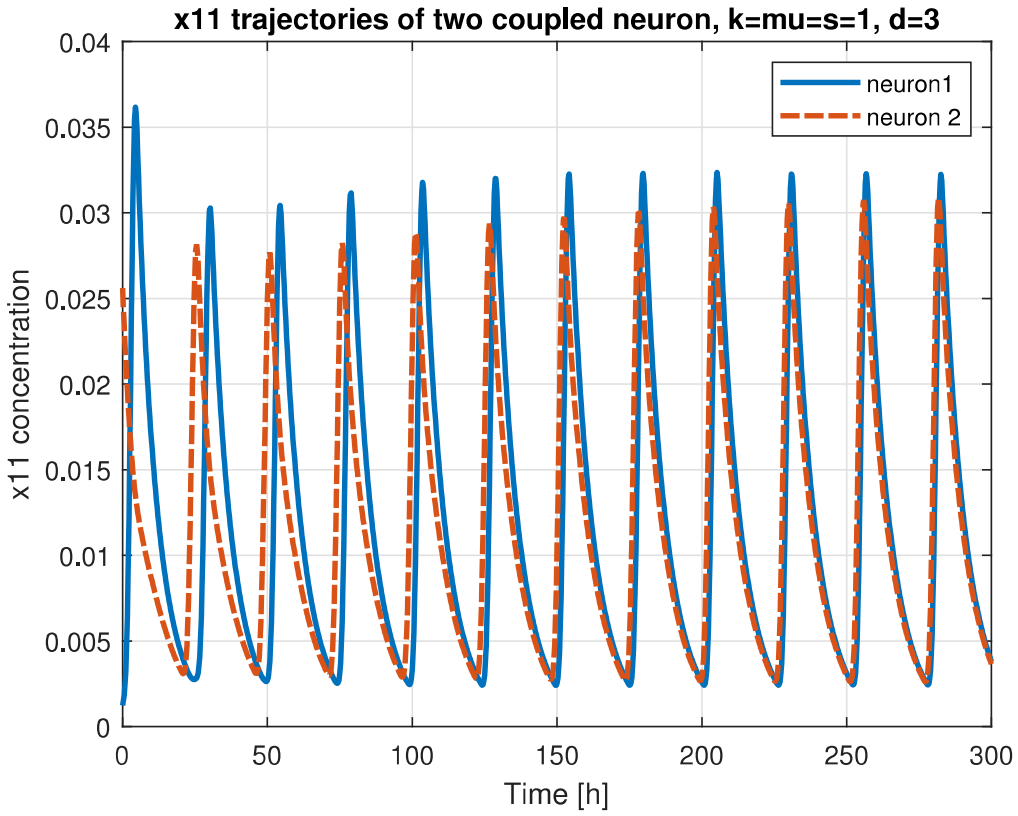

Figure 4.11: Two neurons coupled by neuromodulator action with default parameter set

LAB. In every simulation the neurons were initiated at a non synchronous attracting state and simulated for 30,000 hours. The coupling strength μ was increased and the network solution analyzed. It was estimated that the non synchronous states are stable for $\mu < 0.006$. Therefore, the hypothesis was considered falsified. However, there exists a threshold for which synchronized states become globally stable.

The results are summarized in the graph of Figure 4.12. The graph shows the type of solution depending on the coupling strength and independent on initial conditions.

To summarize, the self modulated neuron representation was scaled to a two neuron network. Using the default parameter set, a bifurcation analysis was conducted. It was found that the synchronized state is oscillatory and locally stable for all $\mu \in [0, 3]$ and globally stable for all $\mu \in [0.006, 3]$. Therefore, it was concluded that neuromodulator coupling with sufficient coupling strength can synchronize two neurons independent of initial conditions.

4.3.4 Conclusion

This section evaluated the synchronizing properties of neuromodulator coupling. This was done by coupling Diekman neurons through a Gonze-like coupling model. The parameters from the Gonze model were translated to the Diekman neuron resulting in a set of parameters call the default parameter set. Thereafter, the newly created Diekman neuron with neuromodulator coupling was evaluated. First a single self-modulated neuron was analyzed, in which it was found that the coupling can result in a non-oscillatory response. A condition on the parameter set and the coupling strength was derived for

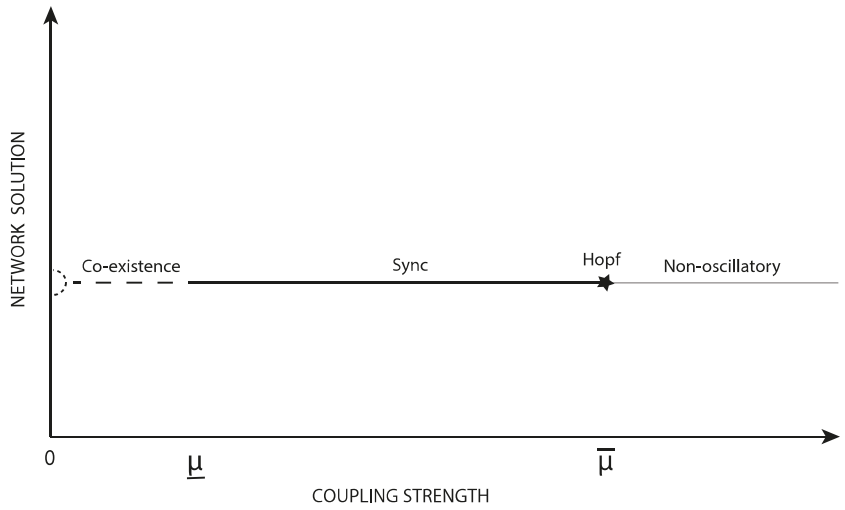

Figure 4.12: The ensemble steady state solution depending on the coupling strength μ

which that the neuron oscillates. It was found that the default parameter set satisfied this condition for $0 < \mu < 3$. Thereafter, two neurons were coupled and the network solutions analyzed. In order to do so, a MATCONT bifurcation analysis was conducted. It was found that for the two neurons coupled by neuromodulator action with sufficient coupling strength synchronize independent of initial conditions.

Therefore, it was concluded that two neurons coupled by neuromodulator synchronize under certain conditions. Therefore the research question "Can two neurons synchronize when only coupled by neuromodulator coupling" was considered answered.

4.4 Combination of gap junction and neuromodulator diffusion

Previously diffusive coupling and neuromodulator diffusion were discussed individually. It was shown that both diffusive coupling and neuromodulator coupling can synchronize two Diekman neurons. However, in biology, neurons are not necessarily limited to one or the other coupling, but may couple in both ways. Therefore the combination between diffusive coupling and neuromodulator coupling is investigated. The goal is to find out how the combination of diffusive coupling and neuromodulator coupling affects the thresholds on the coupling strengths for which the synchronous steady state is globally stable. In addition, also the performance of the combined coupled coupling was discussed.

4.4.1 Combination of the thresholds of the coupling strengths

For both diffusive and neuromodulator coupling a lower threshold was found. Since both types of coupling have a lower threshold, it is hypothesized that the combination also results in a region resulting in co-existent solutions for low values of the coupling strengths. For diffusive coupling with high coupling strengths the electrical subsystems of two neurons synchronize while the molecular subsystems do not synchronize. Since neuromodulator action couples the molecular states directly, it is hypothesized that by adding neuromodulator coupling the upper threshold is shifted such that higher coupling strengths σ still allow for a synchronized solution. For neuromodulator coupling an

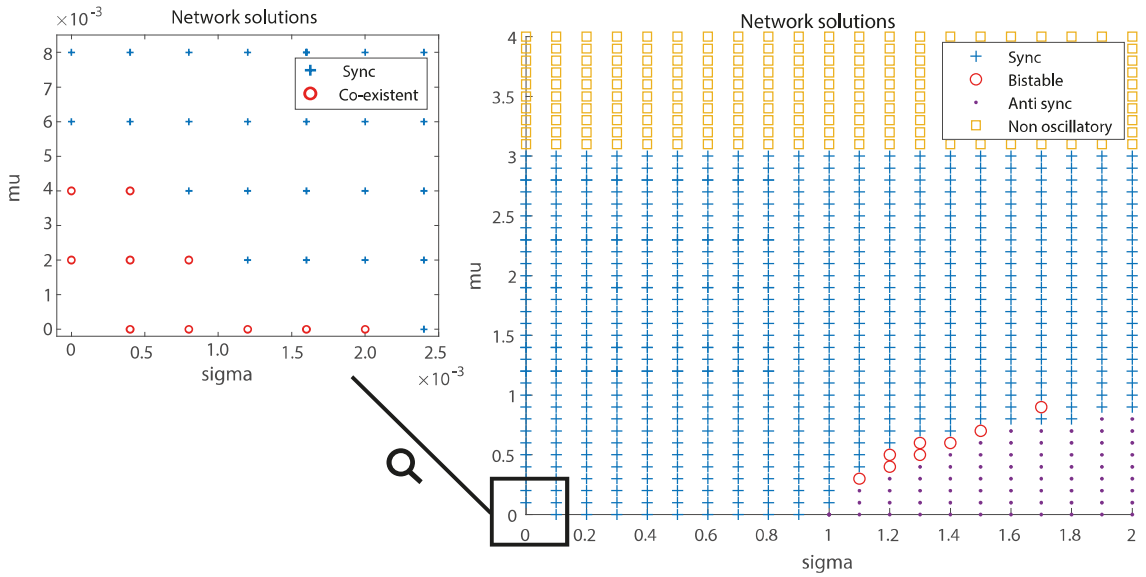

Figure 4.13: Type of network solution depending on the coupling strength.

upper threshold was found after which the response is no longer oscillatory. Since this bifurcation is invariant for σ it is hypothesized that the upper threshold on μ does not change.

In order to test these hypotheses, a numerical experiment was conducted. In short, the experiment consists of coupling two neurons, varying the coupling strengths, and analyze the steady state solutions for different initial conditions. The goal is to find the steady state solutions depending on the two coupling strengths and independent of initial conditions. The result are shown in Figure 4.13.

Figure 4.13 contains two scatter plots with on the horizontal axis the diffusive coupling strength (on the domain $[0,\ 2]$) and on the vertical axis the neuromodulator coupling strength (on the domain $[0,\ 4]$). Four different network solutions are displayed in the plot: sync, co-existent/bistable, non oscillatory (sync), and anti sync. The scatter plot on the left on Figure 4.13 zooms in on the region around the origin.

The area in blue '+' represents a synchronized solution. The red '$\circ$' represents a co-existence of solutions depending on the initial conditions. The purple '$\cdot$' represents the anti sync solutions which represent the non-synchronized solutions resulting from diffusive coupling strength above the $\overline{\sigma}$ threshold. These solutions are characterized by signals with an alternating low and high peak and two neurons oscillating at half a phase delay. The yellow '$\square$' represent non oscillatory solutions resulting from neuromodulator coupling strengths above the $\overline{\mu}$ threshold.

Let us have a look at some solutions in time while considering the line $\sigma = 1.3$. For low μ the solution the steady state solutions end in anti synchrony as can be seen in Figure 4.14a. When μ is increased to $\mu = 0.5$ (and $\sigma = 1.3$) the solutions become bistable. In this case both the synchronized solution and the anti synchronized solution are stable. For an initial phase difference of 2 hour the solution ends up in anti synchrony as seen in Figure 4.14b. However, for an initial phase difference of 30 minutes two neurons synchronize as can be seen in Figure 4.14c. For $\mu = 1.5$ (and $\sigma = 1.3$) the solutions synchronize independent of the initial conditions as can be seen in Figure 4.14d. For $\mu = 3.2$ (and $\sigma = 1.3$) the solution is non oscillatory as seen in Figure 4.14e.

The lower co-existence area seen in the left scatter plot of Figure 4.13 contain non

synchronous solutions and the synchronized steady state solution. For $\sigma = 0.0004$, $\mu = 0.002$ the solution is either synchronous, as seen in the plots of Figure 4.15a or not synchronized, as seen in the plots of Figure 4.15b.

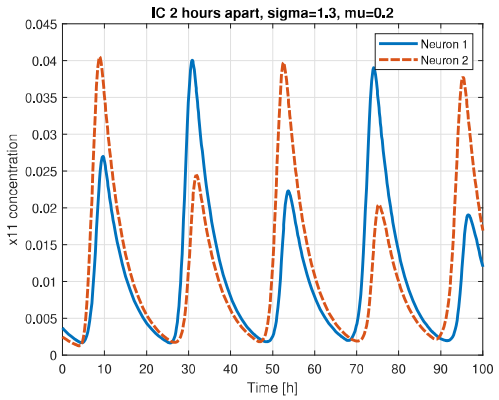

(a) Anti synchronized solution for $\sigma = 1.3$, $\mu = 0.2$

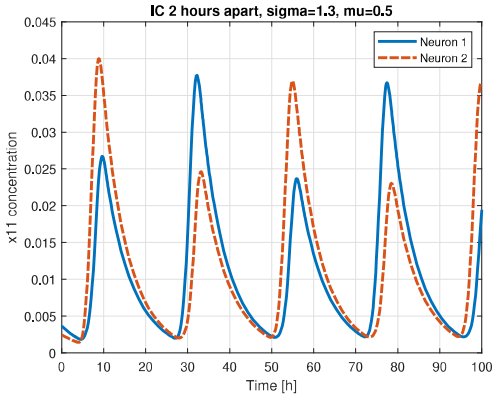

(b) Bistable for $\sigma = 1.3$, $\mu = 0.5$. Anti synchronization for initial phase difference of 2 hours.

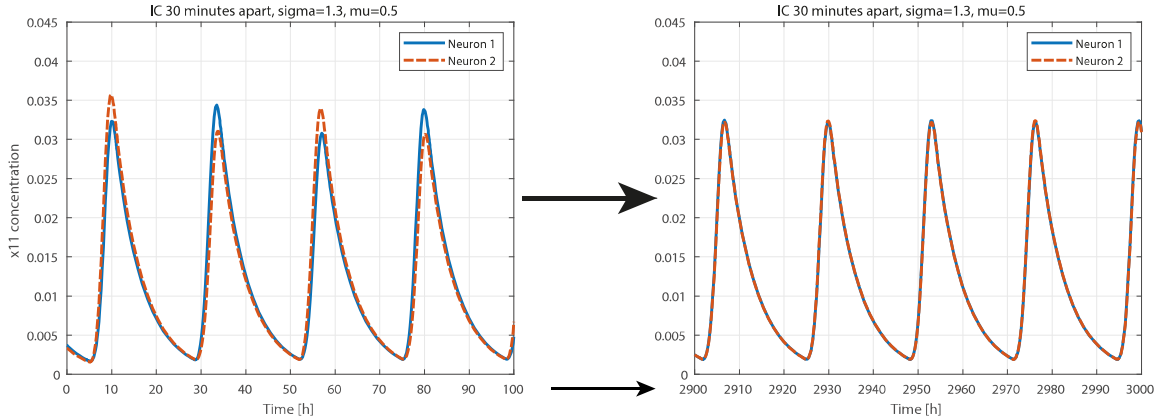

(c) Bistable for $\sigma = 1.3$, $\mu = 0.5$. Synchronization for initial phase difference 30 minutes. Left plot shows the first 100 hours of the simulation. The plot on the right shows the final 100 hours of the simulation.

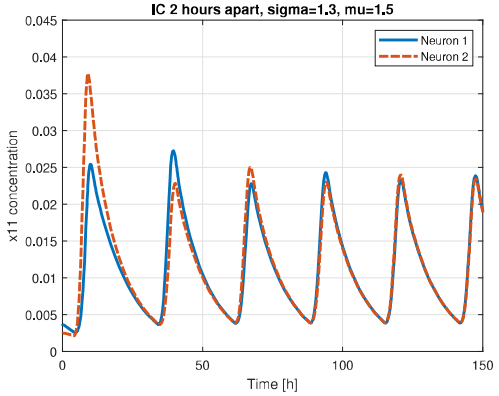

(d) Synchronous solution for $\sigma = 1.3$, $\mu = 1.5$

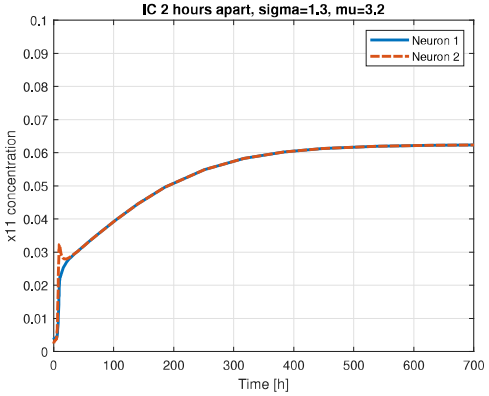

(e) Non oscillatory solution for $\sigma = 1.3$, $\mu = 3.2$

Figure 4.14: Solutions in time on the line $\sigma = 1.3$.

Considering the results it is concluded that the upper threshold on μ for which the

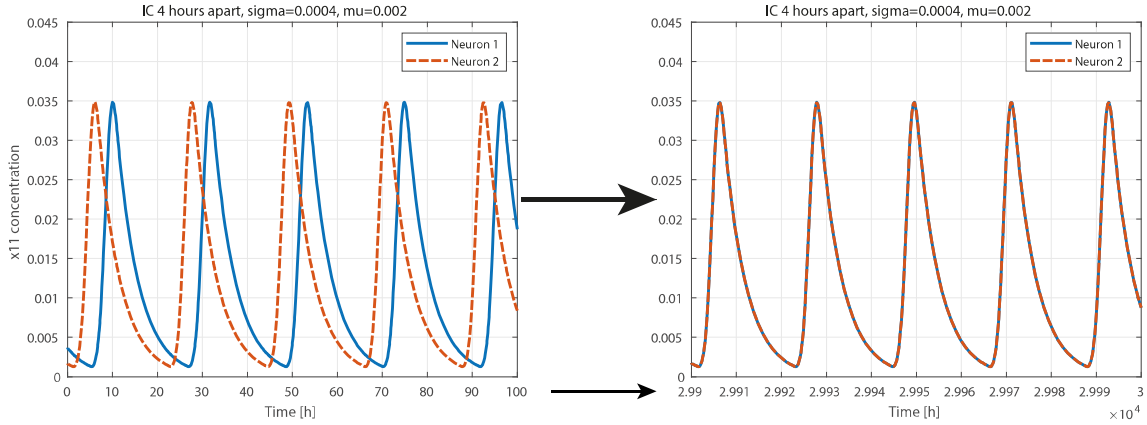

(a) Synchronized solution for initial conditions 4 hours apart. Left plot shows the first 100 hours of the simulation. The plot on the right shows the final 100 hours of the simulation

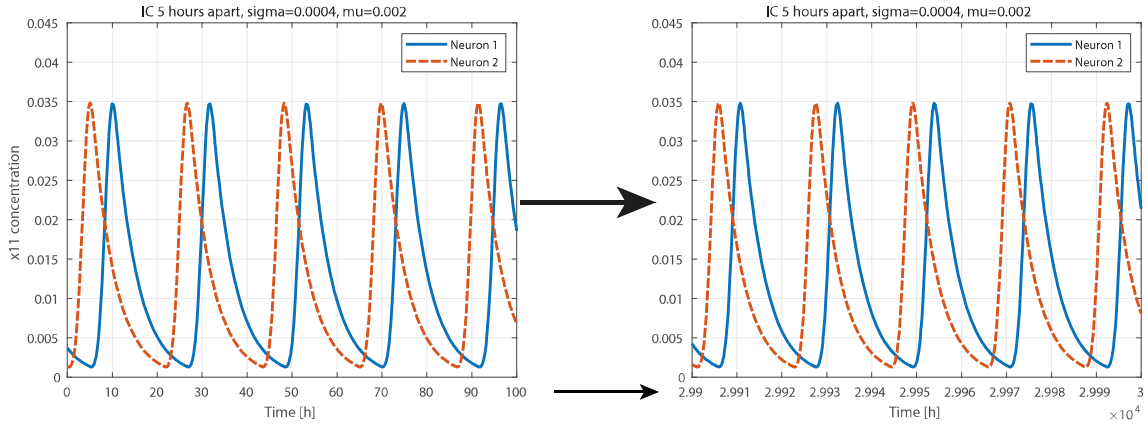

(b) non synchronous attracting solution for initial conditions 5 hour apart. Left plot shows the first 100 hours of the simulation. The plot on the right shows the final 100 hours of the simulation

Figure 4.15: Depending on the initial conditions the solutions of $\sigma = 0.0004$, $\mu = 0.002$ either synchronize or not.

solution is oscillatory does not change. Moreover, it is concluded that by adding neuromodulator coupling to a diffusely coupled network the upper threshold is indeed shifted such that higher coupling strengths σ still allow for a synchronized solution. The previous experiment was conducted on the domain $\sigma \in [0,\ 2]$. However, the tilting slope of the anti sync area in Figure 4.13 suggests that there is a coupling strength μ that guarantees a synchronous solution independent of the value of σ. Therefore, the experiment of Figure 4.13 was repeated with σ on a logistic scale on the domain $[1,\ 10^{10}]$. It was found that for $\mu > 0.93$ all solutions are synchronized.

To summarize, adding neuromodulator coupling to a diffusely coupled network of Diekman neurons increases the range of coupling strengths that synchronizes the network. Moreover, there is a neuromodulator coupling strength that guarantees a synchronous solution (independent of coupling strength σ and initial conditions).

4.4.2 Performance of neuromodulator coupling compared to diffusive coupling

In the following section the performance of the combination of both coupling mechanisms is discussed. The performance is measured as the time required for two neurons to reach (near) synchrony from an initial time lag.

Definition 4.4.1. Consider two Diekman neurons with synchrony outputs w_i and w_j. The initial time lag is defined as the time T_0 such that

$$\begin{aligned} &w_i(0), \\ &w_j(0) = w_i(0 + T_0) \end{aligned} \tag{4.44}$$

Note that $T_0 = 0$ represents initializing in a synchronized state

Definition 4.4.2. Consider two Diekman neurons with synchrony outputs w_i and w_j. Given that two neurons synchronize, the performance is the time t required to reach an error equivalent to a time lag δ such that

$$||w_i(t) - w_j(t)|| < ||w_i(t) - w_i(t + \delta)||, \text{ with } \ w_j(0) = w_i(0 + T_0) \tag{4.45}$$

where T_0 is the initial time lag.

Definition 4.4.2 is satisfied if the absolute error between the two sets of synchrony outputs becomes smaller that a certain threshold error. The threshold error is defined as the absolute error of a neuron and the same neuron shifted in time by a time δ.

First, an exploratory simulation is conducted. The goal is to form a hypotheses on how the combination of diffusive coupling and neuromodulator coupling affects the time it takes to reach synchrony with respect to the individual coupling mechanisms. Subsequently, some simulations that compare diffusive coupling and neuromodulator coupling are conducted. Thereafter, an analytical comparison is made by examining the Diekman differential equations. Finally, the combination of diffusive coupling and neuromodulator coupling is discussed.

Exploratory simulations

First two sets of initial conditions were chosen to accommodate a simulation in MATLAB. The sets are chosen such that the uncoupled systems are initiated with a significant time

lag (seven hours). Subsequently, a set of coupling parameters was chosen for which the systems synchronize.

The trajectories for both neurons were estimated using MATLAB for a simulation time of 2,000 hours. In the first experiment only neuromodulator coupling was used. The trajectories, absolute error, and the time lag of the state x_{11} are shown in Figure 4.16b. The time lag falls exponentially towards zero. When the error is large the decrease in error is large, however, when the error becomes small the error is hardly reduced any further. For the second simulation only diffusive coupling is applied. The trajectories, absolute error, and the development of the time lag, shown in Figure 4.16c hardly converge for as long as the time lag is over six hours. However, after the threshold (of approximately 6 hours difference) is reached both neurons synchronize rapidly and perfectly. Finally both neurons were coupled by neuromodulation and diffusive coupling. The trajectories shown in Figure 4.16d converge fast. In the first stage, the time lag rapidly drops to six hours. Once there, the states quickly lock resulting in a (near) zero error.

Considering the results, it hypothesized that neuromodulator coupling can synchronize effectively when the errors are high while diffusive coupling can synchronize effectively when the time lag is low.

Numerical approach

In order to test the hypothesis, an experiment is conducted in MATLAB. Two Diekman neurons were coupled with either diffusive coupling or neuromodulator coupling. The initial conditions were set near the periodical orbit with nearly half a phase as initial time lag. The coupling strengths were varied and the development of the time lag was recorded. The time lag was measured as the difference in peak times of the x_{11} states. Furthermore, it was assumed that initiating the two neurons with a high time lag also represents the case of small initial time lags as high time lags automatically decay to smaller time lags. It is therefore assumed that the time lag curve is shifted in time when initiated at different initial time lags.

First, diffusive coupling was evaluated. The coupling strength σ was varied on the range $[0.1,\ 0.4]$ in 60 evenly spaced intervals. The range $[0.1,\ 0.4]$ was chosen such that the neurons synchronize fast but not too fast to create the time lag curve (within 4 x_{11} peak times which result in just 4 data points). Figure 4.17a shows the development of the time lag for five coupling strengths. It can be observed that the time lag curve consists of two parts. First, a slow decay can be observed for all coupling strengths. Thereafter an "elbow" followed by a steep drop can be seen. Higher coupling strengths σ result in faster decays.

Finally, neuromodulator coupling is evaluated. The initial conditions are set near the periodical orbit with nearly half a phase as initial time lag. The neuromodulator coupling strength was varied on the domain $[0.1,\ 3]$ in 60 evenly spaced intervals. Figure 4.17b shows the development of the time lag for five different coupling strengths. For all coupling strengths it can be observed that the decay in time lag is initially strong. However, as time passes the time lag curve flattens. Higher coupling strengths result in sharper decays.

When comparing Figures 4.17a and 4.17b it can be observed that the time lag curve for diffusive coupling is initially flat but rapidly falls as the time lag becomes smaller. For neuromodulator coupling the decay in time lag is initially large but becomes significantly smaller as time passes.

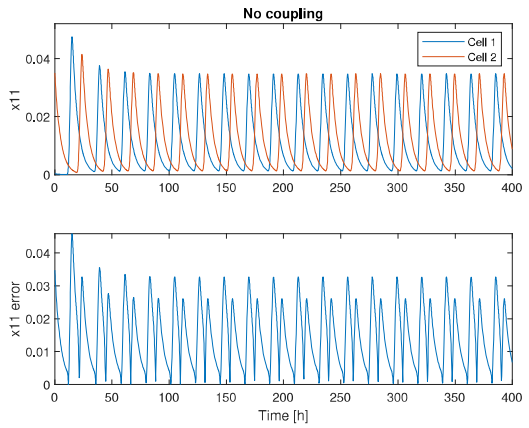

(a) No coupling

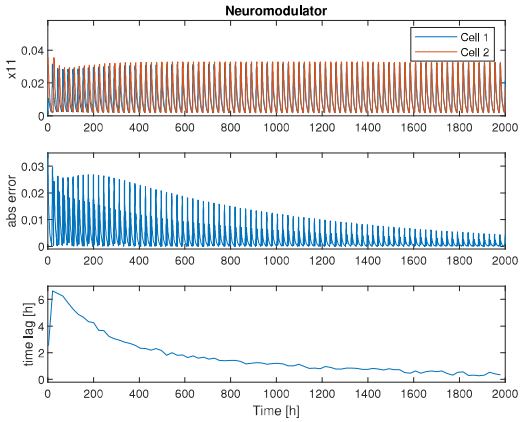

(b) Neuromodulator coupling with default set and $\mu = 0.5$

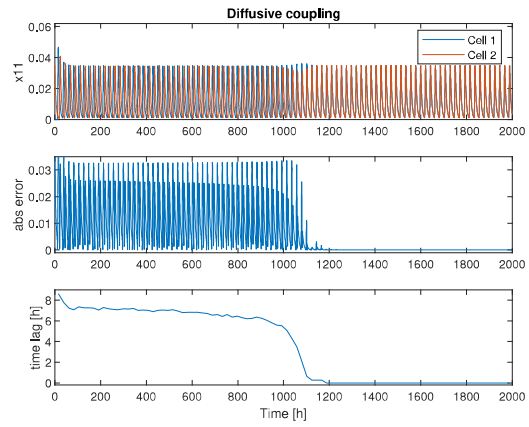

(c) Diffusive coupling with $\sigma = 0.1$

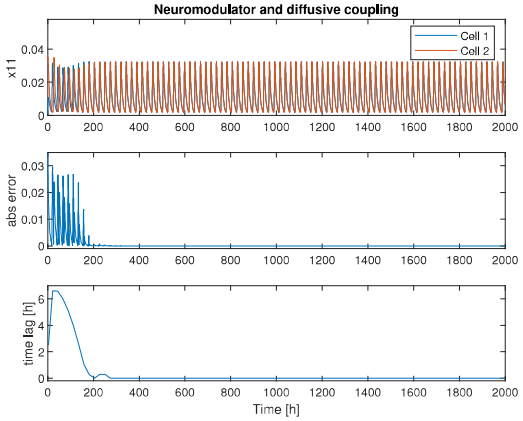

(d) Diffusive and neuromodulator coupling with default parameter set, $\mu = 0.5$, and $\sigma = 0.1$

Figure 4.16: Trajectories of x11 for two systems with no coupling, neuromodulator coupling, gap junction, neuromodulator and gap junction coupling for identical initial conditions. The initial conditions are placed with an approximately time lag of seven hours. The absolute error is the absolute difference in x_{11} states.

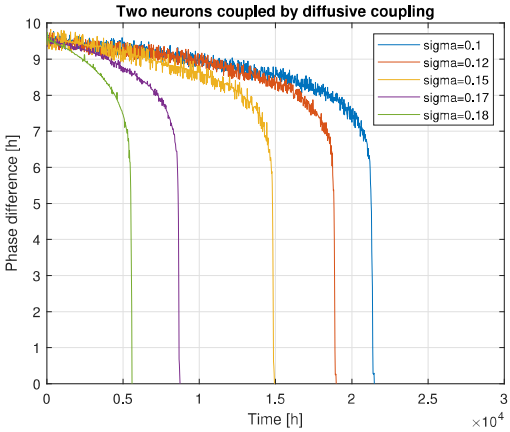

(a) Dependence of diffusive coupling strength on the development of the phase error.

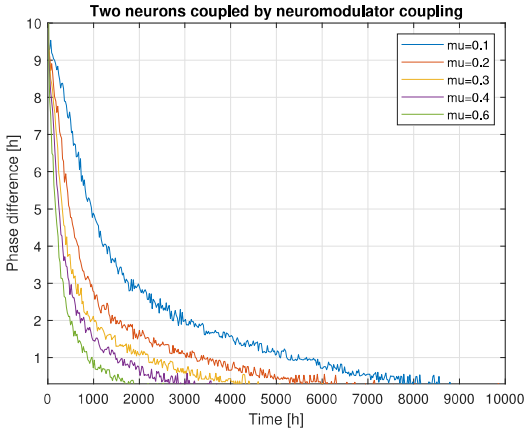

(b) Dependence of neuromodulator coupling strength on the development of the phase error.

Figure 4.17: Development of the phase error for different diffusive and modulator coupling strengths. Initial phase error of approximately 9.5 hours.

One of the limitations of the previous experiment is the small range of coupling strengths that was used. For high coupling strengths synchronization simply occurs too fast to estimate the time lag curve. Therefore, it is challenging to predict the development of the phase error curves for strongly coupled neurons.

Considering the results it is concluded that diffusive coupling is effective in synchronizing smaller time lags. In order to synchronize rapidly, the errors should be no further apart that six or seven hours. On the other hand, neuromodulator coupling is effective when the time lags are large. However, when the errors are becoming small, neuromodulator coupling becomes less effective.

Analytical approach

In addition to the numerical analysis, an analytic approach is used. In order to do so, the differential equation of x_{11} is evaluated. Recall that:

$$\dot{x}_{11} = a(CRE(x_{10})Ebox(x_{13})^4 - x_{11} + f(V)), \text{ with} \tag{4.46}$$

$$Ebox = \frac{1}{1000 \cdot x_{13} + 1}, \tag{4.47}$$

$$CRE = \max(0, 10^6\ x_{10} - 75) \tag{4.48}$$

It can be observed that the neuromodulator action $f(V)$ acts regardless of the state of the neuron. Therefore, large errors decrease significantly faster regardless of the state of the neuron. However, diffusive coupling enters the molecular subsystem through state x_{10}. Note that only when $Ebox(x_{13})^4$ is high the neuron is actually sensitive to the $CRE(x_{10})$ input. Therefore, effective coupling of the molecular model is only possible in case $Ebox(x_{13})^4$ is high (x_{13} is low). In order to validate this hypothesis a MATLAB simulation is conducted. The goal is to find the time span for which $Ebox(x_{13})^4$ is high and compare it to the six hours time span previously estimated.

A single neuron was simulated in MATLAB on its periodical orbit and the $Ebox(x_{13})^4$ function was plotted in Figure 4.18. For most of the circadian cycle the sensitivity is low.

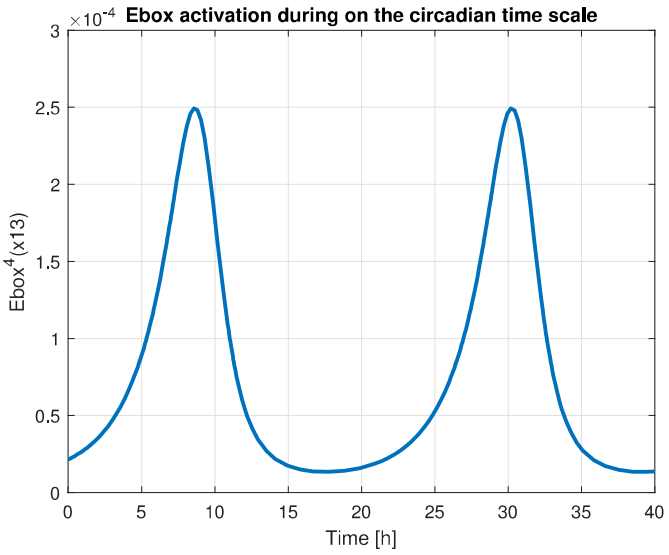

Figure 4.18: Sensitivity to x10

Only for a range of six or seven hours the $Ebox(x_{13})^4$ function peaks. Therefore, the hypothesis is considered validated. Consequently, it is concluded that only during the six or seven hour window of peak Ebox activity two neurons can synchronize their molecular states effectively (through diffusive coupling).

Combined performance

Previously, diffusive coupling and neuromodulator coupling were compared. The goal of this section is to compare the individual coupling mechanisms with the combination of neuromodulator coupling and diffusive coupling.

The exploratory simulations indicated that the combination can enhance the performance (shorten the time required to reach near synchrony). However, only one set of coupling strengths was tested. Therefore, a wider range of coupling strengths will be evaluated. The goal is to investigate the influence of the coupling strengths on the time needed to synchronize.

In order to do so, a MATLAB experiment was conducted. Two neurons were initiated near their periodic orbit with a 9.5 hour phase difference. The neurons were coupled both with diffusive coupling and neuromodulator coupling. The coupling strengths were varied and the absolute errors between the states were calculated. Finally, the performance with $\delta = 10$ minutes (for Definition 4.4.2) was calculated. The results can be seen in Figure 4.19.

Figure 4.19 shows a scatter plot with on the horizontal axis the diffusive coupling strength σ and on the vertical axis the neuromodulator coupling strength μ. The size of the circles in the plot indicate the time required to reach a state near synchrony. Unsurprisingly, on the vertical axis it can be seen that low coupling strength μ take significantly more time to synchronize that higher coupling strength μ. On the horizontal axis a similar result can be seen for diffusive coupling. The white area in the lower right corner of the plot contains the coupling strengths that do not result in a synchronous solution. For the same reason the point $[\mu, \sigma] = [0, 0]$ is not included in the plot. The combination of diffusive and neuromodulator coupling decreases the time to synchronized especially for low coupling strengths (μ and σ). When the coupling strengths are higher

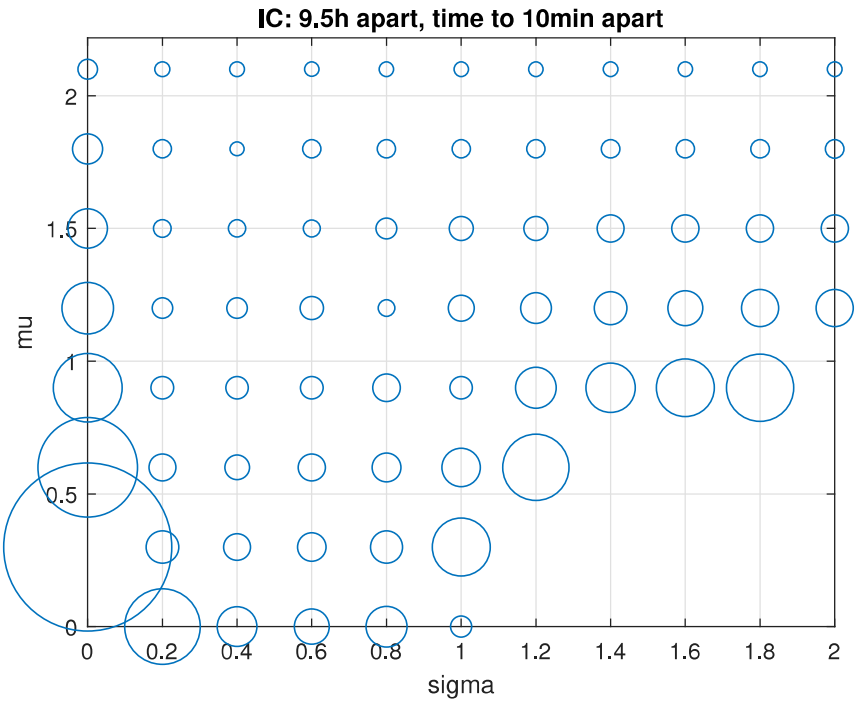

Figure 4.19: The time required to reach near synchrony depending on the coupling strengths μ and σ. The size of the circle represents the performance of the μ, σ pair.

the combination becomes less relevant.

To summarize, it was observed that the combination between diffusive coupling and neuromodulator reduces that time required to synchronize, especially for low coupling strengths. Therefore, it is expected that the combination of diffusive coupling and neuromodulator coupling is beneficial in rapid synchronization of two neurons.

Conclusion

To conclude, neuromodulator coupling can synchronize two neurons with large (initial) time lags fast while diffusive coupling is better at synchronizing two neurons with small time lags. The combination of neuromodulator coupling and diffusive coupling can reduce time lags faster that the individual part, highlighting the importance of the combination rather than the individual parts. However, more research is needed on the performance of the combinedly coupled neurons.

4.4.3 Conclusion

This section combined diffusive coupling with neuromodulator coupling. It was shown that the upper threshold of the coupling strength for diffusive coupling can be scaled with sufficient neuromodulator action. The neuromodulator thresholds remained unaltered. It was therefore concluded that neuromodulator action broadens the range of diffusive coupling strengths that guarantees synchrony. Moreover, there is a neuromodulator coupling strength that always results in a synchronous solution regardless of the applied diffusive coupling strength. Consequently, the third research question: "Does the combination of neuromodulator coupling and gap junction coupling enhance synchronization between

two SCN neurons?" was answered. Moreover, not only the range for globally stable synchronous solutions was increased. Also the performance of the coupling is improved when neuromodulator coupling and diffusive coupling are combined. Neuromodulator coupling synchronized best when the time lag is large while diffusive coupling synchronizes best when the time lag is lower. The combination of the two allows for rapid synchronization of a larger range of errors that the individual mechanisms.

4.5 Conclusion

This chapter investigated if two coupled SCN neurons can synchronize. This was done by analyzing two Diekman neurons coupled by diffusive coupling and neuromodulator coupling. First, diffusive coupling was discussed whereafter neuromodulator coupling was considered. Finally, the combination between diffusive coupling and neuromodulator diffusion was considered.

It was proven analytically that for diffusive coupling two coupled electrical Diekman subsystem synchronize provided the coupling strength is sufficiently high. However, the combined Diekman neuron (electrical and molecular) does not necessarily synchronize since the molecular subsystem is not convergent. This results non synchronous solutions for coupling strengths above a certain threshold. However, since there exists a range for the coupling strength for which the synchronous steady state is globally stable, it was concluded that two SCN neurons can synchronize when only coupled with gap junctions. Therefore, the first research question was considered answered.

Thereafter, neuromodulator coupling was evaluated. In order to do so, the Gonze coupling model was added to the Diekman neuron. It was shown that for a sufficiently high coupling strength two Diekman neurons synchronize. However, there is an upper threshold above which the solution becomes non oscillatory on the circadian time scale. Since there exists a range of coupling strengths that can synchronize two Diekman neurons, it was concluded that using only neuromodulator diffusion two SCN neurons can synchronize. Therefore, the second research question was answered.

Finally the combination of neuromodulator coupling and diffusive coupling was discussed. It was shown that the lower and upper thresholds of the coupling strength for diffusive coupling can be scaled with sufficient neuromodulator action. It was therefore concluded that neuromodulator action broadens the range of diffusive coupling strengths that guarantees a synchronous solution. Moreover, it was demonstrated that neuromodulator coupling is very effective when the difference between two neurons are large. However, when the differences between neurons become smaller neuromodulator coupling is less effective. In contrast, diffusive coupling is only effective when the differences are small. The combination of the coupling mechanisms allows for rapid synchronization for a larger range of differences than the individual mechanisms. In all, it can be concluded that the combination of neuromodulator coupling and diffusive coupling is more effective at synchronizing two neurons than the individual coupling mechanisms. Therefore the third research question: "Does the combination of neuromodulator coupling and gap junction coupling enhance synchronization between two SCN neurons?" was answered.

Chapter 5

Coupled network

Previously, a single Diekman neuron and two coupled Diekman neurons were discussed. Two neurons were coupled by means of diffusive coupling en neuromodulator coupling. These coupling methods are models for gap junction coupling and diffusion of neuromodulators. However, as discussed in Chapter 2, the SCN is a network of coupled neurons. The network of the SCN is of great importance in creating a reliable output. This chapter aims to investigate how different networks affect the ability of a network of Diekman neurons to synchronize. This corresponds with addressing the final three research questions.

The exact biological network structure is unknown. However, as was discussed in Chapter 2, gap junction coupling is believed to couple locally in a distributed network. For the sake of simplicity, regular nearest neighbour networks will be used. Neuromodulator coupling is represented to couple globally in an all-to-all network as discussed in Chapter 2. Therefore this research is focused on nearest neighbour networks and all-to-all network.

The organization of this chapter is as follows. Firstly, a general network representation is discussed. Here, some useful terminology and definitions are introduced. Thereafter, diffusive coupling in general networks is addressed. Using the feedback gain, the importance of the eigenratio of the Laplacian for diffusive coupling is demonstrated. Subsequently, the eigenratio for several nearest neighbour networks is calculated. Then, neuromodulator coupling in all-to-all networks is discussed. Finally, the combination between gap junction coupling and neuromodulator coupling is addressed.

Network representation In order to scale the two coupled neuron case to a network, a few definitions need to be provided. The neurons i and j of the network are coupled if there exists a link between them. A link between two neurons i and j is called an edge (i, j) with $\mathcal{E}$ representing the set of all edges in the network. In this report, only undirected edges are used meaning that if $(i, j) \in \mathcal{E}$, then $(j, i) \in \mathcal{E}$. The graph (or network) is called simple if the nodes do not have internal loops $(i, i) \notin \mathcal{E}$ and any two nodes are connected by at most one edge. The graph is called connected if there exists a path between any two nodes i and j [34].

For a better insight in set $\mathcal{E}$, a graph is often represented in a graphical way. Figure 5.1 shows a connected graph with two nodes. Here, and throughout the rapport, the black dot represents a node and an arrow represents an edge.

An adjacency matrix A is a one-hot representation of the set $\mathcal{E}$ [34][35]. It is an $N \times N$ matrix with N being the total number of nodes in the network. The value of the ij-th entry of A is 1 if and only if there is an edge connection nodes i and j. Everywhere else it is zero.

Figure 5.1: Two coupled nodes

Synchonization in a network Previously, synchronization for two coupled neurons was discussed. However, when increasing the network size a new type of synchronization has to be defined.

Consider for example a network of four coupled neurons. In case all neurons are synchronized the network is said to be completely synchronized with definition 5.0.1. In case two or more neurons synchronize but not all neurons synchronize, the network system is said to be partially synchronized. The synchronized neurons combined are called a cluster.

Definition 5.0.1. Consider a network of N coupled neurons with w_i the synchrony output (definition 4.1.1) of the i-th neuron. The network system is said to completely synchronize if:

$$w_i(t) \to w_s(t) \text{ as } t \to \infty \text{ for all} i \in [1, 2, .., N] \tag{5.1}$$

where $x_s(t)$ represents the completely synchronized solution.

To summarize, the SCN is a network of coupled neurons. The neurons are coupled through their inputs and outputs. A link between two neurons is called an edge, and the set of all edges can be represented in the adjacency matrix. Through this network neurons potentially synchronize. A network for which every neuron is synchronized is called a completely synchronized network.

5.1 Diffusive coupling in a network

In this section the double diffusely coupled neuron case is extended to a network of arbitrary size. The goal is to answer the fourth research question: "Can a network of SCN neurons synchronize when coupled only by gap junction coupling?".

In order to do so, first a mathematical representation of a network of neurons coupled by diffusive coupling is described. This representation uses a coupling matrix called the Laplacian. Thereafter, the relationship between the Laplacian and the thresholds on the coupling strength is derived. Thereafter, the general relationship is specified for several nearest neighbour networks. Finally, a condition on the network for which the network completely synchronizes is derived.

5.1.1 Network system representation

Like in the case of a single Diekman neuron a state space representation of the entire network can be derived. The goal is to expand the state space representation of a single neuron to the state space representation of the network system. This is useful since it allows us to represent large networks in a compact notation.

Consider a network of N identical Diekman neurons. Recall the dynamics of the i-th neuron:

$$\dot{x_i} = f(x_i) + Bu_i \tag{5.2}$$
$$y_i = Cx_i \tag{5.3}$$

Recall that $x_i \in \mathbb{R}^n$ represents the statevector of the i-th Diekman neuron with n represents the number of states. The vector $f(x_i)$ contains n functions translating the state values x_i of the i-th subsystem to the rate of change $\dot{x}_i$ of the i-th subsystem. The input $u_i \in \mathbb{R}^m$ describes the input of the i-th subsystem with m being the number of inputs. The output $y_i \in \mathbb{R}^p$ represents output of the i-th neuron with p being the number of outputs. $B \in \mathbb{R}^{n\times m}$ represents the control matrix which determines how the system input affects the state change. The output matrix $C \in \mathbb{R}^{p\times m}$ determines the relationship between the system states and the system output. The neurons are identical hence f, B, and C do not depend on i.

The dynamics of a single neuron can be extended to a network system such that:

$$\begin{aligned} \dot{x} &= F(x) + (I_N \otimes B)u \\ y &= (I_N \otimes C)x \end{aligned} \tag{5.4}$$

Here x represents the network state vector with $x = [x_1^T\ x_2^T\ ...\ x_N^T]^T$ with x_i the state vector of the i-th subsystem. $F(x) = [f^T(x_1)\ f^T(x_2)\ ...\ f^T(x_N)]^T$ is a vector containing continuous functions describing the state changes of the individual neurons. I_N represents the identity matrix with dimensions $N \times N$. The $\otimes$ symbol represents the Kronecker product[1]. Basically this notation is a concatenation of all individual neuron dynamics. This notation can always be used even if the network is unconnected. The coupling is described by the way in which the network system output vector y is translated into the network system input vector u. For diffusive coupling this is done by an elegant coupling matrix that will be described shortly.

Recall that for diffusive coupling the total input received by the i-th neuron is the sum of individual inputs. The number of individual inputs is equal to the number of edges of the neuron. In case a neuron is coupled to four other neurons then the total input is the sum of four inputs. The input of neuron i can therefore be written as:

$$u_i = \sum_{j\in\mathcal{E}_i} \sigma(y_j - y_i) \tag{5.5}$$

where j represents all neurons in the set of edges of neuron i. Using the adjacency matrix, the input for the entire network can be written as:

$$u = \sigma(Ay - Dy) \tag{5.6}$$

where u is the full input vector of the network system, and D is a diagonal matrix with entries equal to the number of edges of the corresponding node. Matrix D is known as

[1]Given matrix A with dimensions $q \times r$ and B with $s \times t$ than $A \otimes B$ is the $qs \times rt$ matrix

$$\begin{pmatrix} a_{11}B & \cdots & a_{1r}B \\ \vdots & \ddots & \vdots \\ a_{q1}B & \cdots & a_{qr}B \end{pmatrix}$$

the degree matrix of the network [34]. Note that the entries of matrix D are equal to the row sums of the adjacency matrix. The adjacency matrix and the degree matrix can be combined into the Laplacian matrix [34][36]:

$$L = D - A \tag{5.7}$$

The result is the network system input vector

$$u = -\sigma L \otimes y \tag{5.8}$$

Since the Laplacian matrix is diagonally dominant[2] and all diagonal terms are real non-negative entries, matrix L is positive semi-definite. Combined with the insight that the rank of L is $N-1$ (with N the number of nodes), it is concluded that the eigenvalues of L are $0 = \lambda_1 \leq \lambda_2 \leq ... \leq \lambda_N$.

Now that the input (5.8) has been defined it can be added to the network system description (5.4) such that it is represented as an input-output system with output-feedback such that:

$$\begin{aligned} \dot{x} &= F(x) + (I_N \otimes B)u \\ y &= (I_N \otimes C)x \\ u &= -\sigma L \otimes y \end{aligned} \tag{5.9}$$

To summarize, the network model as represented in (5.9) is a concatenation of individual dynamics and a coupling. The entire network is represented as the Laplacian matrix, and the coupling is represented as a feedback gain.

5.1.2 Exploratory simulations and hypotheses

In order to evaluate the dependence of the network on the synchronization property of the network, a number of simulations were conducted. The objective of the simulations is to explore the relationship between the coupling strength and the network solution. The goal is to form a conjecture regarding the thresholds for which the synchronous state is globally stable.

Four Diekman neurons were coupled in a 2 nearest neighbour network as seen in Figure 5.2a. The coupling strength was varied while the initial conditions were kept constant. The simulation time has set such that the steady state was reached. The coupling strengths were set to $\sigma = 0.002$, $\sigma = 0.4$, $\sigma = 0.8$.

Figure 5.2 shows the trajectories of the state x_{11} for the four neurons. For a low coupling strength the network does not necessarily completely synchronizes. Instead, two clusters form. For a coupling strength of $\sigma = 0.4$ the network completely synchronizes while for a coupling strength of $\sigma = 0.8$ the network does not synchronizes.

The network solutions found in the four neuron network are similar to the solutions found for the two neuron network. Once again it appears that there is region containing multiple solutions for low coupling strengths, a region where the synchronized state is stable, and a region where the synchronous solution is not stable. However, in the four neuron network a coupling strength of $\sigma = 0.8$ already results in non synchronous solutions. Recall, that for the double neuron network the synchronized state becomes

[2]Matrix $A = a(i,j)$ is diagonally dominent if $a(i,i) \geq \sum_{j \neq i} |a(i,j)|$ for all i

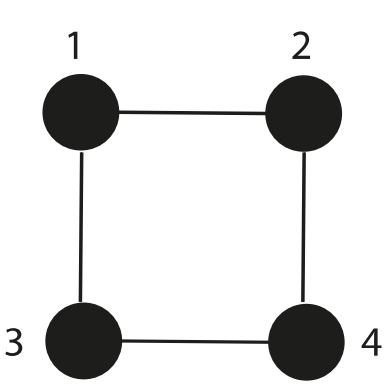

(a) Network layout

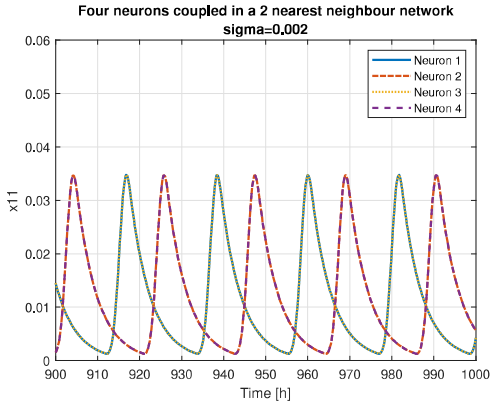

(b) Partial synchrony for $\sigma = 0.002$

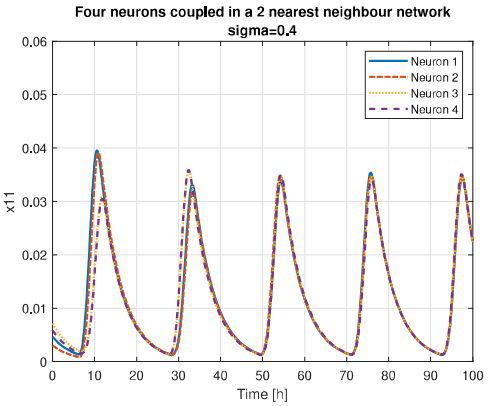

(c) Complete synchronous state $\sigma = 0.4$

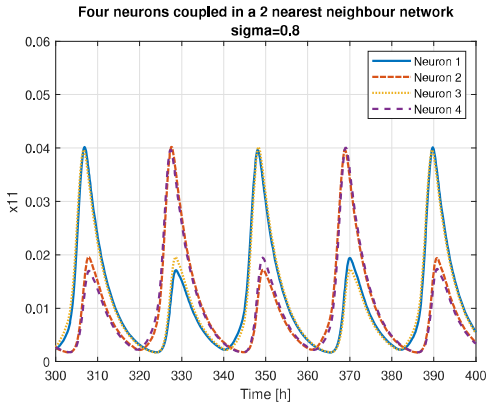

(d) No synchrony for $\sigma = 0.8$

Figure 5.2: Steady state oscillations of state x11 for four neurons coupled in a 2 nearest neighbour network.

unstable when $\sigma > 1$. Therefore, it was concluded that the network shifts the thresholds on the coupling strength.

Before further investigating the dependency of the thresholds on the network, the thresholds are estimated. The goal is to find the range of coupling strengths for which the synchronous state is stable. Since a (numerical) bifurcation analysis is very challenging for the Diekman model, MATLAB simulations are used instead. For every simulation the network was initiated in one of the network solution. The simulation time was set to 5,000 hours to allow the network to reach steady state.

First, the prevelent non-synchronized low coupling strength solution seen in Figure 5.2c was evaluated. It was found that this state is unstable for $\sigma > 0.002$ (± 0.0005). Thereafter, the synchronous network solution was tested. It was found that for $\sigma < 0.51$ (± 0.01) the synchronous state is stable. Finally, the steady state seen in Figure 5.2d was evaluated. It was found that this steady state becomes unstable for $\sigma < 0.51$ (± 0.01).

The simulations indicate that the four neuron network has similar solutions as the double neuron network. However, the range of coupling strengths for every solution is scaled. The lower threshold appear to be equal to the threshold found for the double neuron network, as discussed in Chapter 4. The upper threshold was estimated to be half of the threshold of the double neuron network found in Chapter 4.

Eigenvectors of the Laplacian

In section 5.1.1, it was demonstrated that the entire network structure can be written as a Laplacian feedback gain. Moreover, it was shown that the network, and thus the Laplacian scales the thresholds on the coupling strength for which the synchronous state is gloabally stable. The goal of this section is to form a hypotheses on how the Laplacian scales the thresholds. In order to do so, the feedback gain for section 5.1.1 is reevaluated.

Substitute (5.8) into (5.4) such that

$$\dot{x} = F(x) - \sigma(I_N \otimes B)L(I_N \otimes C)x \tag{5.10}$$

As discussed in Chapter 4 the coupling disappears when the system is synchronized. Therefore the matrix $(I_N \otimes B)L(I_N \otimes C)x$ becomes zero when the network is synchronized. Therefore, it is concluded that the synchronized state is the eigenvector corresponding to the zero eigenvalue of L. This will be demonstrated with an example.

Recall the four neuron two nearest neighbour network of Figure 5.2a. For this network the Laplacian is:

$$L = \begin{pmatrix} 2 & -1 & 0 & -1 \\ -1 & 2 & -1 & 0 \\ 0 & -1 & 2 & -1 \\ -1 & 0 & -1 & 2 \end{pmatrix} \tag{5.11}$$

with eigenvalues λ_i and eigenvectors v_i

$$\lambda_1 = 0,\ v_1 = \begin{pmatrix} 1 \\ 1 \\ 1 \\ 1 \end{pmatrix},\ \lambda_{2,3} = 2,\ v_2 = \begin{pmatrix} 1 \\ 0 \\ -1 \\ 0 \end{pmatrix},\ v_3 = \begin{pmatrix} 0 \\ 1 \\ 0 \\ -1 \end{pmatrix},\ \lambda_4 = 4,\ v_4 = \begin{pmatrix} -1 \\ 1 \\ -1 \\ 1 \end{pmatrix} \tag{5.12}$$

When all outputs are identical as for the first eigenvector the feedback gain is zero. This corresponds to the synchronized state. The network solutions of Figure 5.2d can also be recognized. This state is characterized by the cluster with two states near synchrony and the other two states in anti synchrony. This state might be represented by the eigenvector corresponding to eigenvalue 4. In this case the loop gain is scaled by 4. Compared to the double neuron network the thresholds appears to be scales by a factor 2. This makes sense since the largest eigenvalue of the double neuron network is $\lambda_N = 2$.

The lower threshold of the four neuron network appears to be equal to the double neuron network. When examine the eigenvalues it is found that the smallest non-zero eigenvalues of both networks are equal (both $\lambda_2 = 2$). This indicates that the lower threshold scales with the lower threshold.

Considering the eigenvectors and eigenvalues of the Laplacian it is hypothesized that:
1) The upper threshold scales with the largest eigenvalue of the Laplacian.
2) The lower threshold scales with the smallest nonzero eigenvalue of the Laplacian.

To summarize, when coupling multiple neurons in a network the thresholds for which the complete synchronous state is globally stable appears to be scales with respect to the double neuron network. In order to investigate the scaling property, two hypotheses were constructed.

Network	Estimate upper threshold	$\overline{\sigma}_1/\lambda_N$
2N1NN	1.00 ± 0.02	1.00
4N2NN	0.50 ± 0.02	0.50
4N3NN	0.50 ± 0.02	0.50
6N2NN	0.50 ± 0.02	0.50
6N4NN	0.33 ± 0.02	0.33
6N5NN	0.33 ± 0.02	0.33

Table 5.1: Numerically estimated upper synchronization threshold for several networks compared to the scaled threshold. The network aNbNN is a network with a neurons connected to b nearest neighbours. Naturally $a = b + 1$ represents an all-to-all network.

5.1.3 Eigenvalues scale thresholds

The relationship between the eigenvalues and the thresholds is investigated numerically using MATLAB simulation. The goal of the simulation is to estimate the thresholds of various all-to-all network and nearest neighbour networks. Subsequently, the expected thresholds are calculated by scaling them with the eigenvalues of the Laplacian. Finally, a comparison was made between the estimated and scale threshold.

Six all-to-all and nearest neighbour networks were created. The networks are described in the first column of Table 5.1. In order to inspect the upper threshold, the neurons in the networks were initiated in synchrony. The simulation time was set to 5,000 hours in order for the states to converge to their final state. The final states were evaluated and the coupling strength either increased or decreased. The second column of Table 5.1 shows the estimated thresholds.

In Chapter 4, the upper limit for the two neuron case was estimated to be $\overline{\sigma} \approx 1$. The largest (and only) nonzero eigenvalue of a two neuron network is $\lambda_N = 2$. The upper threshold for the two neuron case was already scaled by a factor two (compared to the unscaled threshold). Therefore, the upper condition for the synchronous state of an arbitrary network can be redefined as $\sigma < \overline{\sigma}_1/\lambda_N$ where $\overline{\sigma}_1 = 2$ represents the unscaled upper threshold. The 1 subscript in $\overline{\sigma}_1$ represents the unscaled value.

The largest eigenvalue of all six networks was calculated using MATLAB. Subsequently, the upper threshold was scaled per network and listed in the third column of Table 5.1.

In Table 5.1, it can be observed that the threshold for which the synchronized network solution is stable is determined by the network. When comparing with the scaled thresholds, it was concluded that the thresholds can be predicted by scaling the threshold of the double neuron network with the largest eigenvalue of the Laplacian. Therefore, the first hypothesis "The upper threshold scales with the largest eigenvalue of the Laplacian" was considered validated.

In order to inspect the lower threshold, the same six networks were used. The neurons in the networks were initiated near a non-synchronized attracting state. Subsequently, after 30,000 hours of simulation time the states were evaluated. The simulation time was set considerably higher since for low coupling strengths neurons need more time to reach their steady state. At the end of every simulation the final state was evaluated and the coupling strength was either increased or decreased. The thresholds found are listed in the second column of Table 5.2.

Network	Estimate lower threshold	$\overline{\sigma}_1/\lambda_2$
2N1NN	0.0024 ± 0.0002	0.0024
4N2NN	0.0022 ± 0.0002	0.0024
4N3NN	0.0012 ± 0.0002	0.0012
6N2NN	0.0048 ± 0.0002	0.0048
6N4NN	0.0012 ± 0.0002	0.0012
6N5NN	0.0010 ± 0.0002	0.0008

Table 5.2: Numerically estimated lower synchronization threshold for several networks compared to the scaled threshold. The network aNbNN is a network with a neurons connected to b nearest neighbours. Naturally $a = b + 1$ represents an all-to-all network.

In the two coupled neuron case the lower threshold was found to be $\underline{\sigma} \approx 0.0024$. Therefore, in a network of arbitrary size the lower threshold is $\sigma > \underline{\sigma}_1/\lambda_2$ where $\underline{\sigma}_1 = 0.0048$ which represents the unscaled lower threshold. The 1 subscript in $\underline{\sigma}_1$ represents the unscaled value.

The smallest eigenvalue of the six networks was calculated using MATLAB. Subsequently, the lower threshold was scaled per network and listed in the third column of Table 5.2.

In Table 5.2 it can be observed that the lower threshold is determined by the network. When comparing the estimated threshold with the scaled thresholds, it was concluded that the thresholds can be predicted by scaling the threshold of the double neuron network with the smallest non-zero eigenvalue of the Laplacian. Therefore, the second hypothesis "The lower threshold scales with the smallest non-zero eigenvalue of the Laplacian" was considered validated.

To summarize, the thresholds on the coupling strength for several networks were estimated. Subsequently, the thresholds found for the double neuron network were scaled by the eigenvalues of the Laplacian. It was concluded that the upper threshold scales with the largest eigenvalue of the Laplacian while the lower threshold scales with the smallest non-zero eigenvalue. Therefore, the hypotheses posed in section 5.1.2 were considered validated.

5.1.4 Diffusive coupling in nearest neighbour networks

Previously the importance of the eigenvalues of the Laplacian was demonstrated. It was shown that the thresholds can be predicted by the scaling the thresholds of the double neuron network by the eigenvalues of the Laplacian. Therefore, when evaluating the synchronization property of any network, only the smallest and largest eigenvalue of the Laplacian have to be evaluated. This section analyses the smallest non-zero and largest eigenvalue of a general nearest neighbour network. The goal is to derive a condition on the network for which the neurons completely synchronize independent of initial conditions.

Eigenratio

One the most important properties of the eigenvalues of the Laplacian is the eigenratio. When λ_N is low and λ_2 is high the range for values of the coupling strength is high. However, when λ_N is high and λ_2 is low the range for values of the coupling strength for

which the system synchronizes becomes small. In fact if $\frac{\lambda_2}{\lambda_N} > \frac{\sigma_1}{\sigma_1}$ then there is no area for which the neurons in the network completely synchronizes (for all initial conditions). This fraction $R = \frac{\lambda_2}{\lambda_N}$ is called the eigenratio of the Laplacian. It has a range of (0,1] (for a connected graph). If the eigenratio is 1 (all-to-all network) both the lower and upper thresholds are scaled proportionally. However, if the eigenratio is smaller than one, the thresholds are not proportionally scaled. Moreover, there is an eigenratio for which no coupling strength can completely synchronize the network.

Laplacian spectrum

In order to predict if there is a coupling strength that can completely synchronize the network independent of initial conditions, the eigenratio of the network has to be determined. In order to do so, the set of eigenvalues, called the spectrum of a matrix is calculated. This is do for any nearest neighbour network (with even number of neighbours). The calculations can be found in Appendix D. The result is the following function

$$\lambda_u = k - 2 \sum_{j=1}^{k/2} \cos\left(\frac{2\pi u j}{N}\right), \quad \text{if } k = 2 \cdot p, \quad \text{with } p \in \mathbb{R} \tag{5.13}$$

describing the eigenvalues of the Laplacian. Here $u = [1, 2, .., N]$ represents the number of the eigenvalue and N the number of nodes in the network. The number of neighbours is represented by k.

In order to illustrate the spectrum that Equation (5.13) generates, an example is provided. A 41 node nearest neighbour network was created. The number of neighbours was initiate at $k = 2$ and increased to $k = N - 1$. The eigenvalues were calculated using Equation (5.13) and shown in Figure 5.3a per number of neighbours. Note that the scale is divided by k in order to fit the figure.

Note that all sets of eigenvalues contain one zero eigenvalue as is characteristic for the Laplacian spectrum. In Figure 5.3a it can be seen that for $k = 2$ the eigenvalues are centered around k. When the number of neighbours increases the eigenvalues tend to grow towards the value N. When $k = N - 1$ (an all-to-all network) all eigenvalues take the value N except for a single zero eigenvalue. In addition, Figure 5.3b shows the development of just the smallest and the largest eigenvalue. Note that at $k = N - 1$ the eigenratio is one and decreases with decreasing k.

Eigenratio and node degree

As discussed previously, a sufficiently high eigenratio is needed to guarantee the existence of a coupling strength that completely synchronizes a network. The goal of this section is to find out what properties of a nearest neighbour network result in a high eigenratio.

Equation (5.13) (and Figure 5.3) suggest that the eigenratio of a nearest neighbour network is a measure of the connectivity of a network. For eigenratio with a value 1 the network is highly connected in an all-to-all network. An eigenratio close to zero indicates a poorly connected network. Using this insight, one could argue that the eigenratio of a nearest neighbour network might be predictable considering the connectivity of the network.

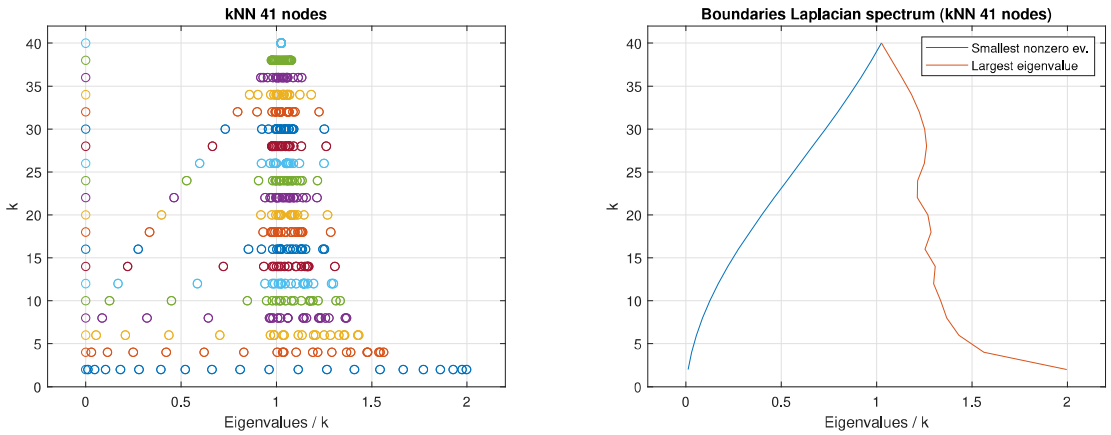

(a) All eigenvalues per k.

(b) Smallest and largest nonzero eigenvalues.

Figure 5.3: Spectrum of a 41 node kNN Laplacian.

In order to represent the connectivity of a network, the node density is used. The node density D_i is the number of edges of a node i divided by the total possible number of edges for that node such that

$$D_i = \frac{k}{N-1} \tag{5.14}$$

Since all nodes in a kNN network have the same number of edges and the same potential number of edges, $D = D_i$. A density $D = 1$ represents the all-to-all network. A density $D \to 0$ represents a network with a high number of nodes and a low number of links. It is hypothesized that the density of a network is proportional to the eigenratio of its Laplacian.

In order to test the hypothesis, three kNN networks were created. The number of neighbours k was varied while the number of nodes was constant at 11, 21, and 41. For every k both the node degree and the eigenratio of the network was calculated. The results were plotted in Figure 5.4.

It can be observed that the eigenratio R is low with low density and high for high densities. Moreover, the node density is a relatively network size (N) invariant measure. When the number of nodes increases (11,21,41) the relationship to the eigenratio stays more or less the same.

Therefore, it is concluded that the density of a nearest neighbour network is proportional to the eigenratio of its Laplacian. Recall that for an eigenratio $R < \frac{\sigma_1}{\bar{\sigma}_1}$ there is no coupling strength that can synchronize a network of diffusely coupled Diekman neurons. Using the thresholds found in Chapter 4 and Figure 5.4, it was found that $R < \frac{\sigma_1}{\bar{\sigma}_1}$ can be approximated by a nearest neighbour network with density $D < 0.04$. Therefore, it was concluded that Diekman neurons in a diffusely coupled nearest neighbour network need to couple to at least 4% of the total number of neurons (in the network) in order for a completely synchronous solution to be globally stable.

5.1.5 Summary and conclusion

The objective of this section was to investigate the fourth research question: "Can a network of SCN neurons synchronize when coupled only by gap junction coupling?". In order to do so, nearest neighbour networks of diffusely coupled Diekman neurons

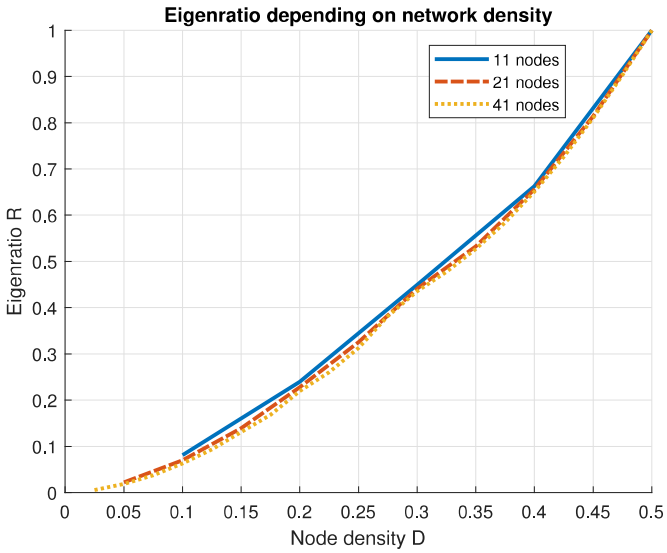

Figure 5.4: The eigenratio as a function of the network density for nearest neighbour networks.

were evaluated. Two hypotheses regarding the scaling of the thresholds on the coupling strength were formed. It was found that the lower threshold on the coupling strength for which the synchronous state is globally stable scales with the smallest nonzero eigenvalue of the Laplacian. Furthermore, the upper threshold on the coupling strength for which the synchronous state is stable scales with the largest eigenvalue of the Laplacian. The fraction between the smallest nonzero and largest eigenvalue is called the eigenratio. For an eigenratio below a certain threshold there is no coupling strength that completely synchronizes a network. Furthermore, it was found that there is a relation between the node density of a nearest neighbour network and its eigenratio. It was found that poorly connected networks (networks with a low density) have a low eigenratio while highly connected networks have a high eigenratio. Consequently, in order to guarantee complete synchrony, a network of Diekman neurons requires a minimum number of connections per neuron. Or, given a constant number of connections per neuron, there is a maximum number of Diekman neurons that can synchronize.

Considering these results, it is concluded that a network of SCN neurons does not necessarily synchronize when coupled only by gap junctions coupling. The lack of global connections has a limiting factor on the synchronizing ability of the network. Therefore, it is believed that gap junctions create local synchronized clusters. Large SCN wide synchronization is deemed unlikely. Thereby, the fourth research question is considered answered.

5.2 Neuromodulator coupling

This section discusses neuromodulator coupling in a network setting. The goal is to evaluate the fifth research question: "Can a network of SCN neurons synchronize when coupled only by neuromodulator coupling?"

In order to do so, first, the network representation and the coupling matrix are discussed. Thereafter, some hypotheses are formed and tested regarding the thresholds of a network.

5.2.1 Network representation

The case of a network of Diekman neuron coupled by neuromodulator coupling can be represented by a state space notation. The goal of this section is to extend the single neuron state space notation of Chapter 4 to a state space notation representing the entire network. As for diffusive coupling in section 5.1.1, the network is can be represented by:

$$\begin{aligned} \dot{x} &= F(x) + (I_N \otimes B)G(u) \\ y &= (I_N \otimes C)x \\ u &= \frac{\mu}{N} Jy \end{aligned} \tag{5.15}$$

Here x represents the network state vector with $x = [x_1\ x_2\ ...\ x_N]^T$ with x_i the state vector of the i-th subsystem. Recall from Chapter 4 that for neuromodulator coupling every neuron was given an additional state V such that the statevector becomes $x_i = [x_{i,1}, .., x_{i,13}, V_i]^T$. $F(x) = [f(x_1)\ f(x_2)\ ...\ f(x_N)]^T$ is a vector containing continuous functions describing the state changes of the individual neurons. I_N represents the identity matrix with dimensions $N \times N$. The $\otimes$ symbol represents the Kronecker product. Vectors B and C are chosen such that the $G(u_i)$ is added to the 11-th state of neuron i and the output $y_i = V_i$. The coupling matrix J is an N times N matrix with all entries equal to 1. Note that the input is equal to taking the average of all outputs. The function G represents the saturation function

$$G(u) = v_s \cdot I_N \cdot \frac{u}{k_r \cdot I_N + u} \tag{5.16}$$

5.2.2 Neuromodulator thresholds in a network

Neuromodulator coupling, as represented by (5.15) has several interesting properties. First of all, the input to any neuron is equivalent to the input to any other neuron. Moreover, the input to the neuron does not scale as the network grows. Therefore it is hypothesized that the (lower) threshold for synchronization and the (upper) threshold are invariant with respect to the network size.

In order to test this hypothesis a simulation in MATLAB was conducted. A network containing 2, 4, 8, and 16 Diekman neurons were initiated with a phase difference of 5 hours. For every network the lower threshold on the coupling strength was estimated (with an 0.01 precision). The same threshold (± 0.01) was found for all four networks. Thereafter, the upper threshold was evaluated similarly. The same threshold (3.0 ± 0.1) was found for all four networks.

Considering the results, it is concluded that the thresholds of the neuromodulator coupling strength are invariant to the network size.

5.3 Neuromodulator with diffusive coupling

Previously it was shown that there is a finite network size for which a network of Diekman neurons coupled by only diffusive coupling cannot completely synchronize the network. In this section neuromodulator is added. The goal is to evaluate the final research question: "Does the combination of neuromodulator coupling and gap junction coupling enhance synchronization in a network of SCN neurons?".

First, in section 5.3.1, a network representation of the dual coupled system is provided. Subsequently, in section 5.3.2, some simulations are conducted in order to form a hypothesis regarding the combination of diffusive coupling and neuromodulator coupling. Thereafter, in section 5.3.3, an analytical approach is used to analyze the coupling matrices.

5.3.1 Network representation

The combined coupling can be represented in a network state space representation such that

$$\begin{aligned} \dot{x} &= F(x) + (I_N \otimes B_{el})u_{el} + (I_N \otimes B_{nm})G(u_{nm}) \\ G(u_{nm}) &= v_s \cdot I_N \cdot \frac{u_{nm}}{k_r \cdot I_N + u_{nm}} \\ y_{el} &= (I_N \otimes C_{el})\ x \\ u_{el} &= -\sigma\ L\ y_{el} \\ y_{nm} &= (I_N \otimes C_{nm})\ x \\ u_{nm} &= \frac{\mu}{N} J\ y_{nm} \end{aligned} \tag{5.17}$$

Here x represents the network state vector with $x = [x_1\ x_2\ ...\ x_N]^T$ with x_i the state vector of the i-th subsystem such that $x_i = [x_{i,1}, .., x_{i,13}, V_i]^T$. $F(x) = [f(x_1)\ f(x_2)\ ...\ f(x_N)]^T$ is a vector containing continuous functions describing the state changes of the individual neurons. I_N represents the identity matrix with dimensions $N \times N$. The $\otimes$ symbol represents the Kronecker product. Vector B_{el} is chosen such that the input $u_{i,el}$ of neuron i is added to the first state. Vector C_{el} is chosen such that the first state of neuron i is taken as an output ($y_{el,i} = x_{i,1}$). The coupling matrix L represents the Laplacian of the network and σ represents the diffusive coupling strength. Vectors B_{nm} and C_{nm} are chosen such that the $G(u_i)$ is added to the 11-th state of neuron i and the output $y_{nm,i} = V_i$. The coupling matrix J is an N times N matrix with all entries equal to 1. The μ represents the neuromodulator coupling strength. The function G represents the neuromodulator saturation function.

5.3.2 Exploratory simulations

First, a simulation is conducted to form a hypothesis on how adding neuromodulator action might influence the system. The goal of the experiment is to evaluate the network solutions on a range of coupling. In short, the experiment consists of coupling four neurons in a two nearest neighbour network. The coupling strengths are varied and the steady state solutions for different initial conditions are analyzed. The result are shown in Figure 5.5.

Figure 5.5 shows the network solutions for the four neuron network. The horizontal axis represents the diffusive coupling strength (on the domain [0, 2]), and the vertical axis represents the neuromodulator coupling strength (on the domain [0, 4]). Four different network solutions are found in the plot: sync, co-existent/bistable, non-oscillatory (sync), and anti sync. The scatter plot on the left on Figure 5.5 zooms in on the region around the origin.

When comparing Figure 5.5 to Figure 4.13 of section 4.4, several interesting properties of the network can be observed. As discussed previously, the diffusive coupling upper

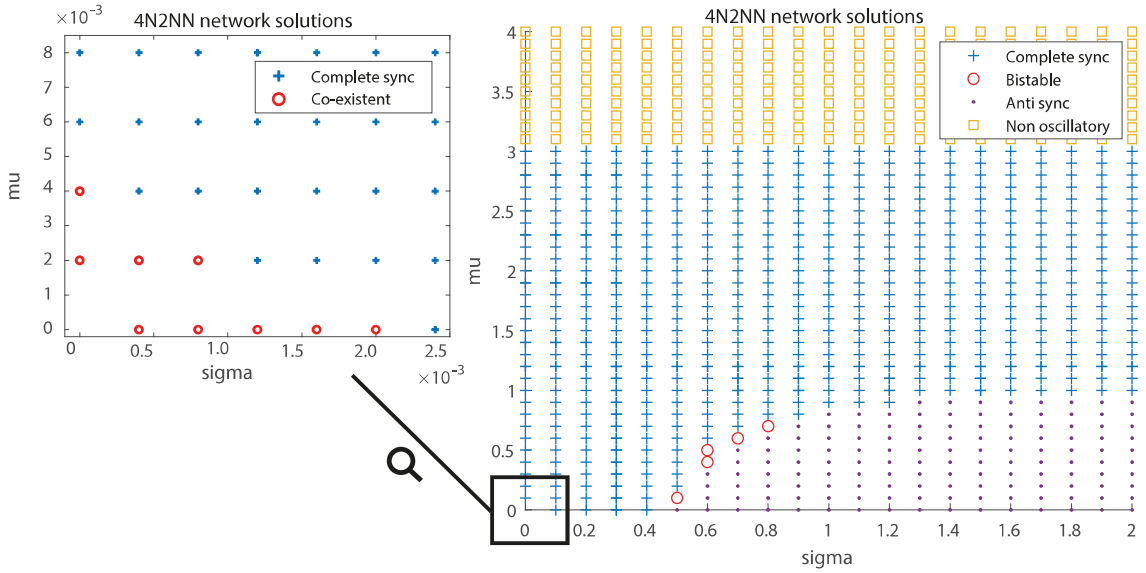

Figure 5.5: Type of network solution for a 4 neuron 2 neighbour network depending on the coupling strength.

threshold is scaled to $\overline{\sigma} = \overline{\sigma}_1/\lambda_N \approx 0.5$. The lower threshold is not scaled with respect to the double neuron case. Therefore, the horizontal axis of Figure 5.5 is scaled compared to the axis of Figure 4.13.

As discussed in section 5.2, the thresholds on the neuromodulator coupling strength do not scale with the network. Therefore, the vertical axis of Figure 5.5 remains unchanged. In section 4.4, it was found that there is a μ that can synchronize both neurons (of a double neuron network) regardless of the diffusive coupling strength or initial conditions. When evaluating Figure 5.5 it appears that this is also the case for the four neuron two nearest neighbour network.

In order to test this, the experiment of Figure 5.5 was repeated with σ on a logistic scale on the domain $[1,\ 10^{10}]$. It was found that for $\mu > 0.93$ all solutions are synchronized. Therefore, it was concluded that for the four neuron two nearest neighbour network $\mu > 0.93$ unconditionally synchronizes the network.

Considering these results, it was hypothesized that there is a threshold on the neuromodulator coupling strength that synchronizes any network of Diekman neurons (coupled by diffusive coupling in nearest neighbour fashion and neuromodulator coupling in a mean field representation) independent of the diffusive coupling strength and initial conditions.

5.3.3 Simultaneous diagonalization

In order to test this hypotheses, an analysis of the coupling matrices is performed. The goal is to prove that, with sufficient neuromodulator coupling strength any network synchronizes. In order to do so, an eigenvector decomposition on the coupling matrices is performed.

Recall the coupling matrices J and L. The coupling matrices commute since

$$J = \vec{1}\,\vec{1}^{\,T} \text{ and } \sum_{j=1}^{n} L_{i,j} = 0\ \forall i, \quad \text{therefore} \quad LJ = JL = \vec{0}\,\vec{0}^{\,T} \tag{5.18}$$

where $\vec{1}$ represents the one vector and $\vec{0}$ represents the zero vector of appropriate dimensions. Since the coupling matrices commute, the same matrix can be used to diagonalizes both coupling matrices. Consequently, a decomposition along the eigenvectors of the coupling matrices can be made which allows us to predict the local stability of the synchronized state, given the knowledge of the double neuron network. More specifically, if a double neuron network (coupled diffusely in an nearest neighbour network and via neuromodulator in a all-to-all network) synchronizes for a certain μ, any network synchronizes for that μ.

Given the previous result and the existence of a neuromodulator coupling strength μ that synchronizes a double neuron network (independent of the diffusive coupling strength σ and initial conditions), it is concluded that this neuromodulator coupling strength μ synchronizes any network of Diekman neurons (coupled via nearest neighbour and all-to-all). Therefore, the hypothesis was considered validated.

5.3.4 Conclusion

This section discussed the combination of neuromodulator and diffusive coupling in a network. In doing so, the thresholds on the coupling strengths for larger networks were evaluated. It was shown that the thresholds of diffusive coupling scale while the thresholds of neuromodulation remain unaltered. The result is a certain threshold on the neuromodulator coupling strength for which any size network synchronizes. Therefore, it is concluded that that any Diekman neuron network coupled by diffusive coupling and neuromodulator coupling synchronizes if the neuromodulator coupling strength is sufficiently high. Therefore, the sixth research question "Does the combination of neuromodulator coupling and gap junction coupling enhance synchronization in a network of SCN neurons?" is considered answered.

5.4 Summary and conclusion

The goal of this chapter was to extend the double neuron diffusive coupling case to a network setting. This was done by evaluating the synchronization property of diffusive coupling in a nearest neighbour network and neuromodulator coupling in a mean field representation.

For diffusive coupling, it was found that the upper limit for synchrony scales with the largest eigenvalue of the Laplacian. Subsequently, the lower threshold scales with smallest nonzero eigenvalue. The ratio between the smallest nonzero and largest eigenvalue is called the eigenratio. When the eigenratio of a network drops below a certain threshold, the network does not completely synchronize for all initial conditions.

In order for the eigenratio not to cross the threshold, the network needs to be sufficiently well-connected. However, as the number of gap junctions is limited, larger networks are not able to completely synchronize. It is therefore concluded that gap junction coupling alone does not necessarily synchronize (larger) networks of SCN neurons.

On the other hand, neuromodulator is able to synchronize larger networks of Diekman neurons. The mean field representation ensures that the thresholds are unscaled. Therefore, it is concluded that neuromodulator diffusion can synchronize networks of SCN neurons of arbitrary size.

Moreover, the combination of neuromodulator and diffusive coupling was evaluated. It was found that a network coupled by both diffusive coupling and neuromodulator

coupling always completely synchronizes provided the neuromodulator coupling strength is sufficiently high. Therefore, it was concluded that the adding neuromodulator diffusive strongly enhances the synchronizing properties of a network of SCN neurons coupled by diffusive coupling.

Chapter 6

Discussion

The goal of this research was to investigate the synchronizing properties of a network of SCN neuron by means of gap junction coupling and neuromodulator diffusion. This was done using a modelling approach. To aid the research, a research question was formed: "How do gap junction and neuromodulator coupling synchronize the gene expression of a network of SCN neurons?"
To answer the research question, six sub question were posed:

1. Can two SCN neurons synchronize when they are only coupled by gap junction coupling?
2. Can two SCN neurons synchronize when coupled only by neuromodulator coupling?
3. Does the combination of neuromodulator coupling and gap junction coupling enhance synchronization between two SCN neurons?
4. Can a network of SCN neurons synchronize when coupled only by gap junction coupling?
5. Can a network of SCN neurons synchronize when coupled only by neuromodulator coupling?
6. Does the combination of neuromodulator coupling and gap junction coupling enhance synchronization in a network of SCN neurons?

In the following section 6.1 a summary and the general conclusions of the research are provided. Thereafter, in section 6.2, some limitations of the research are discussed. Finally, in section 6.3, some recommendations for further research are provided.

6.1 Summary and conclusion

In Chapter 4, two coupled Diekman neurons were investigated. First, in section 4.2, diffusive coupling between two Diekman neurons was investigated. It was found that the electrical subsystem of two Diekman neurons synchronize, provided the coupling strength is high enough. However, the molecular subsystem imposes an upper threshold on the coupling strength for which the synchronous state becomes unstable. Therefore, two Diekman neurons coupled by diffusive coupling can only synchronize when the coupling

strength is in a certain range. Therefore, it was concluded that two SCN neurons can synchronize when coupled by gap junction coupling.

In section 4.3, the Gonze model was used to couple two Diekman neurons. It was found that two Diekman neurons synchronize for a sufficiently high coupling strength (independent of initial conditions). Moreover, if the coupling strength is too high, the neurons do not oscillate on the circadian time scale. Therefore, it was concluded that two SCN neurons coupled by neuromodulator coupling can synchronize.

Thereafter, in section 4.4, the combination of diffusive coupling and neuromodulator coupling was investigated. It was found that with a sufficiently high neuromodulator coupling strength two neurons synchronize for all diffusive coupling strengths. Therefore, it was concluded that neuromodulator coupling (with sufficiently high coupling strength) can guarantee a synchronous output when added to two gap junction coupled neurons. Moreover, it was found that neuromodulator coupling is effective for synchronizing neurons with a large phase difference while diffusive coupling synchronizes best when the phase difference is small. Therefore, it was concluded that the combination of neuromodulator diffusion and gap junction coupling also enhances the performance of the synchronization property.

In Chapter 5, the synchronization property of a network of Diekman neurons was investigated. First, in section 5.1, several Diekman neurons were coupled in a nearest neighbour network by diffusive coupling. It was found that the network properties scale the thresholds on the coupling strength. It was found that large networks are only able to completely synchronize if the number of connections is also large. Since the number of connections for gap junction coupling is assumed to be limited, it is concluded that gap junction coupling is not able to synchronize a network of SCN neurons larger than a certain size.

In section 5.2, neuromodulator coupling in all-to-all networks of Diekman neurons was evaluated. It was demonstrated that the thresholds for neuromodulator coupling are network invariant (at least for all-to-all networks). Therefore, it was concluded that neuromodulator diffusion synchronizes networks of SCN neurons of arbitrary size.

Thereafter, in section 5.3, the combination of diffusive coupling and neuromodulator coupling was investigated. It was found that even though gap junction coupling cannot synchronize large networks the combination of neuromodulator and gap junction can synchronize networks of arbitrary size. Therefore, it was concluded that the combination of neuromodulator and gap junction coupling can synchronize networks of SCN neurons of arbitrary size.

Finally, the main research question is evaluated. "How do gap junctions and neuromodulator coupling synchronize the gene expression of a network of SCN neurons?"
Gap junction coupling is a form of coupling that synchronizes neurons fast and precisely. It is able to synchronize both the daily cycle as well as individual action potentials. However, when synchronizing the daily cycle, it is only effective when phase differences are small. Furthermore, when coupled in a large network it is not able to completely synchronize the network. On the other hand, neuromodulator coupling is in many ways the opposite. It is slow, not precise and only effective when the phase differences are large. However, when coupled in a large network neuromodulator coupling is able to completely synchronize a network of SCN neurons. Therefore, the combination between these two types of coupling is very important in the establishment of network with versatile synchronization properties.

6.2 Limitations

Considering the methodology of the research, a couple of limitations need to be addressed. First of all, are results are of a mathematical nature. Therefore, the conclusions are limited with regard to the biological system. It may be the case that gap junction coupling in the SCN is of a different nature than represented by diffusive coupling. Moreover, the Diekman neuron is a single neuron model. Scaling the Diekman neuron to a network does not necessarily represent a network of SCN neurons. As a result of the scaling of the Diekman neuron, unwanted or improbable properties might surface.

Furthermore, validation of the mathematical results is very challenging as many of the biological states are unobservable. Therefore, it is challenging to interpret or validate the mathematical results.

6.3 Recommendations and further research

Regarding further research, several recommendations need to be addressed. First of all, this research was limited to coupling by means of gap junctions and neuromodulator coupling. However, in order to better represent the connections between two neurons, synaptic coupling also needs to be considered. This type of coupling could be interesting when added to the other coupling mechanisms.

Moreover, this research was focused on the Diekman single neuron model. In scaling the Diekman single neuron model to a network setting, the non convergence property of the molecular subsystem played a key role. However, whether this peculiarity is a property of the Diekman model or that of an SCN neuron in general is unclear. Therefore, the results from this research using the Diekman neuron model need to be validated using different mathematical SCN neuron models.

Besides, this research focused on a networks of SCN neurons instead of the actual SCN network. The SCN is a network with high heterogeneity between the neurons. Not only is every neuron slightly different than the other neurons, also on the level of the SCN there are multiple areas consisting of different neurons [37]. These areas differ by the kind of neuromodulator they are able to secrete or observe as well as the number of electrical connections. Therefore, further research is needed to evaluated how the conclusion hold up in a heterogeneous SCN network.

Moreover, the all-to-all and nearest neighbour networks represented here are only simplification of real SCN networks. The nearest neighbour networks were used to represent a local network while the all-to-all networks were used to represent a globally connected network. However, in biology, neurons are very unlikely to couple in a (perfect) nearest neighbour or all-to-all network. Therefore, more research is needed on the effect of network impurities on the synchronizing ability of the neurons.

Appendix A

Diekman equations and parameter set

This appendix contains the entire set of differential equations of the Diekman model. Two separate representations of the model are provided. First, a more intuitive representation containing many algebraic equations is given. This is a representation is especially useful for those with a proper understanding of the biological system. Thereafter, a state space representation without any algebraic equations is given. This representation is particularly useful for those with a background in systems theory. Finally, the parameter set of the Diekman model is provided as well.

Intuitive representation

$$\dot{x}_1 = \frac{\sum I_c}{C_m}$$

$$\sum I_c = I_{Na} + I_K + I_{CaL} + I_{CaNonL} + I_{KCa} + I_{Kleak} + I_{Naleak}$$

$$\begin{aligned}
I_{Na} &= \bar{g}_{Na}\, x_2^3\, x_3\, (x_1 - E_{Na}) \\
I_K &= \bar{g}_K\, x_4^4\, (x_1 - E_K) \\
I_{CaL} &= \bar{g}_{CaL}\, x_5\, \frac{K_1}{K_2 + x_9} (x_1 - E_{Ca}) \\
I_{CaNonL} &= \bar{g}_{CaNonL}\, x_6\, x_7\, (x_1 - E_{Ca}) \\
I_{KCa} &= \bar{g}_{KCa} x_8^2\, (x_1 - E_K) \\
I_{Kleak} &= \bar{g}_{Kleak} (x_1 - E_K) \\
I_{Naleak} &= \bar{g}_{Naleak} (x_1 - E_{Na})
\end{aligned}$$

$$\dot{x}_i = \frac{x_{i,\infty} - x_i}{\tau_i}, \quad i = 2, 3, ..., 8$$

$$
\begin{aligned}
x_{2,\infty} &= \frac{1}{1+\exp(-(x_1+35.2)/8.1)},\\
x_{3,\infty} &= \frac{1}{1+\exp((V+62)/2)},\\
x_{4,\infty} &= \frac{1}{1+\exp((x_1-14)/-17))^{0.25}},\\
x_{5,\infty} &= \frac{1}{1+\exp(-(x_1+36)/5.1)},\\
x_{6,\infty} &= \frac{1}{1+\exp(-(x_1+21.6)/6.7)},\\
x_{7,\infty} &= \frac{1}{1+\exp((x_1+260)/65)},\\
x_{8,\infty} &= \frac{10^7 x_9^2}{10^7 x_9^2+5.6}
\end{aligned}
$$

$$
\begin{aligned}
\tau_2 &= \exp(-(x_1+286)/160),\\
\tau_3 &= 0.51+\exp(-(V+26.6)/7.1),\\
\tau_4 &= \exp(-(x_1-67)/68),\\
\tau_5 = \tau_6 &= 3.1,\\
\tau_7 &= \exp(-(x_1-444)/220),\\
\tau_8 &= 500/(10^7 x_9^2+5.6)
\end{aligned}
$$

$$
\dot{x}_i = -k_i(I_{CaL}+I_{CaNonL}) - \frac{x_i}{\tau_i} + b_i, \quad i = 9, 10
$$

$$
\begin{aligned}
\dot{x}_{11} &= a\left(CRE(x_{10})Ebox(x_{13})^n - x_{11}\right),\\
\dot{x}_{12} &= a(x_{11}-x_{12}),\\
\dot{x}_{13} &= a(x_{12}-x_{13}),\\
CRE(x_{10}) &= \max(0, 10^6\cdot x_{10}-75),\\
Ebox(x_{13}) &= \left(\frac{k_i}{k_i+x_{13}}\right)
\end{aligned}
$$

State space representation

$$
\begin{aligned}
\dot{x} &= f(x)+Bu,\\
y &= Cx
\end{aligned}
$$

$$f_1(x_1, x_2, x_3, x_4, x_5, x_6, x_7, x_8, x_9, x_{13})$$
$$f_2(x_1, x_2)$$
$$f_3(x_1, x_3)$$
$$f_4(x_1, x_4)$$
$$f_5(x_1, x_5)$$
$$f_6(x_1, x_6)$$
$$f_7(x_1, x_7)$$
$$f_8(x_8, x_9)$$
$$f_9(x_1, x_5, x_6, x_7, x_9)$$
$$f_{10}(x_1, x_5, x_6, x_7, x_9, x_{10})$$
$$f_{11}(x_{10}, x_{11}, x_{13})$$
$$f_{12}(x_{11}, x_{12})$$
$$f_{13}(x_{12}, x_{13})$$

$$\begin{aligned} C_m \cdot f_1 =& g_{\text{Naleak}} \left(E_{\text{Na}} - x_1(t)\right) + \frac{E_K - x_1(t)}{5 \left(\mathrm{e}^{\frac{217}{1000\left(x_{13}(t) + \frac{1}{1000}\right)} - \frac{217}{10}} + 1\right)} + g_K \, x_4(t)^4 \left(E_K - x_1(t)\right) \\ &+ x_8(t)^2 \left(\frac{198}{\mathrm{e}^{\frac{217}{1000\left(x_{13}(t) + \frac{1}{1000}\right)} - \frac{217}{10}} + 1} + 2\right) \left(E_K - x_1(t)\right) + g_{\text{CaNonL}} \, x_6(t) \, x_7(t) \left(E_{\text{Ca}} - x_1(t)\right) \\ &+ g_{\text{Na}} \, x_2(t)^3 \, x_3(t) \left(E_{\text{Na}} - x_1(t)\right) + \frac{K_1 \, g_{\text{CaL}} \, x_5(t) \left(E_{\text{Ca}} - x_1(t)\right)}{K_2 + x_9(t)} \end{aligned}$$

$$f_{2,3,\ldots,13} = \left(\begin{array}{c} -\mathrm{e}^{\frac{x_1(t)}{160}+\frac{143}{80}} \left(x_2(t) - \frac{1}{\mathrm{e}^{-\frac{10\,x_1(t)}{81}-\frac{352}{81}}+1} \right) \\ -\frac{x_3(t)-\frac{1}{\mathrm{e}^{\frac{x_1(t)}{2}+31}+1}}{\mathrm{e}^{-\frac{10\,x_1(t)}{71}-\frac{266}{71}}+\frac{51}{100}} \\ -\mathrm{e}^{\frac{x_1(t)}{68}-\frac{67}{68}} \left(x_4(t) - \frac{1}{\left(\mathrm{e}^{\frac{14}{17}-\frac{x_1(t)}{17}}+1\right)^{1/4}} \right) \\ -\frac{x_5(t)-\frac{1}{\mathrm{e}^{-\frac{10\,x_1(t)}{51}-\frac{120}{17}}+1}}{\mathrm{taurl}} \\ -\frac{x_6(t)-\frac{1}{\mathrm{e}^{-\frac{10\,x_1(t)}{67}-\frac{216}{67}}+1}}{\mathrm{taurnl}} \\ -\mathrm{e}^{\frac{x_1(t)}{220}-\frac{111}{55}} \left(x_7(t) - \frac{1}{\mathrm{e}^{\frac{x_1(t)}{65}+4}+1} \right) \\ -\left(20000\,x_9(t)^2+\frac{7}{625}\right) \left(x_8(t) - \frac{10^7\,x_9(t)^2}{10^7\,x_9(t)^2+\frac{28}{5}} \right) \\ \mathrm{bca}_9 - \frac{x_9(t)}{\tau_9} + \mathrm{kca}_9 \left(g_{\mathrm{CaNonL}}\,x_6(t)\;x_7(t)\;(E_{\mathrm{Ca}}-x_1(t)) + \frac{K_1}{K_2+x_9(t)}\,g_{\mathrm{CaL}}\,x_5(t)\;(E_{\mathrm{Ca}}-x_1(t)) \right) \\ \mathrm{bca}_{10} - \frac{x_{10}(t)}{\tau_{10}} + \mathrm{kca}_{10} \left(g_{\mathrm{CaNonL}}\,x_6(t)\;x_7(t)\;(E_{\mathrm{Ca}}-x_1(t)) + \frac{K_1}{K_2+x_9(t)}\,g_{\mathrm{CaL}}\,x_5(t)\;(E_{\mathrm{Ca}}-x_1(t)) \right) \\ -a \left(x_{11}(t) - \left(\frac{1}{1000\left(x_{13}(t)+\frac{1}{1000}\right)} \right)^n \max\left(0, 10^6\,x_{10}(t) - 75\right) \right) \\ a\;(x_{11}(t) - x_{12}(t)) \\ a\;(x_{12}(t) - x_{13}(t)) \end{array} \right)$$

Table A.1: Parameter set of the Diekman model

Parameter symbol	Value	Unit	Description
C_m	5.7	pF	membrane capacitance per unit area
g_{Na}	229	nS	Na+ conductance per unit area
g_{Naleak}	0.0576	nS	Na+ leak conductance per unit area
g_K	3	nS	K^+ conductance per unit area
g_{Kleak}	0.0333	nS	K^+ leak conductance per unit area
g_{CaL}	6	nS	Ca^{2+} conductance per unit area for L-type channel
g_{CaNonL}	20	nS	Ca^{2+} conductance per unit area for non L-type channel
g_{KCa}	100	nS	Ca^{2+} activated K+ current
E_{Na}	45	mV	equilibrium potential for Na+
E_K	-97	mV	equilibrium potential for K+
E_{Ca}	54	mV	equilibrium potential for Ca^{2+}
K_1	$3.93 \cdot 10^{-5}$	mM	mRNA concentration of a general clock gene
K_2	$6.55 \cdot 10^{-4}$	mM	Protein
kca_9	$1.65 \cdot 10^{-4}$	mM/fC	calcium near membrane current to concentration conversion factor
kca_{10}	$8.59 \cdot 10^{-9}$	mM/fC	calcium in cytosol current to concentration conversion factor
τ_9	0.1	ms	calcium near membrane clearance time constant
τ_{10}	$1.65 \cdot 10^3$	ms	calcium in cytosol clearance time constant
bca_9	$5.425 \cdot 10^{-4}$	mM/ms	basal calcium near membrane concentration
bca_{10}	$3.1 \cdot 10^{-8}$	mM/ms	basal calcium in cytosol concentration
τ_{rL}	3.1	ms	time constant for the rl gate
τ_{rnL}	3.1	ms	time constant for the rnl gate
a	$5.6 \cdot 10^{-8}$	ms^{-1}	time constant molecular subsystem

Appendix B

Stability analysis of the molecular subsystem

This Appendix demonstrates the stability of the unique and stable equilibrium for a constant CRE input. This is done by 1) calculating the equilibrium, 2) deriving the jacobian, 3) evaluating the eigenvalues of the jacobian at the equilibrium.

Differnetial equations

$$\begin{pmatrix} \dot{x}_{11} \\ \dot{x}_{12} \\ \dot{x}_{13} \end{pmatrix} = \begin{pmatrix} a\left(CRE \cdot \left(\frac{1}{1000 \cdot x_{13}+1}\right)^n - x_{11}\right) \\ a\,(x_{11} - x_{12}) \\ a\,(x_{12} - x_{13}) \end{pmatrix} \tag{B.1}$$

Equilibrium The equilibrium of the Diekman molecular subsystem is calculated by substituting $\dot{x}_{11,ss} = \dot{x}_{12,ss} = \dot{x}_{13,ss} = 0$ in the differential equation. For the second and thrid molecular differential equation this results in $x_{11ss} = x_{12ss}, x_{12ss} = x_{13ss}$ such that $x_0 = x_{11ss} = x_{12ss} = x_{13ss}$. Rewriting the first differential equations (3.10) yields

$$\dot{x} = CRE \cdot (\frac{0.001}{0.001 + x_0})^n - x_0 = 0 \tag{B.2}$$

$$CRE_0 = x_0(1000 \cdot x_0 + 1)^n, \;\; CRE, x_0, n > 0 \tag{B.3}$$

$$\tag{B.4}$$

Equation B.4 shows that the equilibrium of the molecular system can uniquely be described by the input constant CRE. The equilibrium does not have a saturation and for arbitrarily high CRE the equilibrium becomes arbitrarily high. Also note that $CRE = x_0(1000 \cdot x_0 + 1)^n$ has only one solution for $x > 0$. Therefore the equilibrium is unique for $x > 0$.

Jacobian of molecular subsystem The jacobian matrix was formulated as:

$$J_{mol} = \begin{pmatrix} -a & 0 & -aR \\ a & -a & 0 \\ 0 & a & -a \end{pmatrix} \text{ with } R = \frac{CRE}{0.001^n \cdot n \cdot x(\frac{1}{0.001+x})^{1+n}} \tag{B.5}$$

When the equilibrium $CRE_0 = x_0(1000 \cdot x_0 + 1)^n$ is substituted the R function becomes

$$R = 0.001^n \cdot n \cdot x_0 \cdot (1 + 1000x_0)^n \cdot \left(\frac{1}{0.001 + x_0}\right)^{1+n} \tag{B.6}$$

When assuming $x, n > 0$ Equation (B.6) can be simplified drastically to

$$R = \frac{nx_0}{x_0 + 0.001} \tag{B.7}$$

Evaluating the eigenvalues of the jacobian For positive x this fraction (B.7) is bounded between 0 and n. The equilibrium point is locally stable if and only if the real parts of all the eigenvalues of the jacobian matrix evaluated at the equilibrium are negative. To test this, the Routh-Hurwitz criterion was used [38]. The Routh-Hurwitz criterion applied to a cubic equation

$$\lambda^3 + a_2\lambda^2 + a_1\lambda + a_0 = 0 \tag{B.8}$$

is satisfied if $a_2, a_0 > 0$ and $a_2 \cdot a_1 > a_0$ [38]. The characteristic equation of the jacobian matrix is given by to the characteristic equation, which is

$$(\lambda - 1)^3 - R = 0 \tag{B.9}$$

$$\lambda^3 + 3\lambda^2 + 3\lambda + 1 + R = 0 \tag{B.10}$$

Clearly, the Routh-Hurwitz criterion is satisfied in case $R + 1 < 9$. So $R > 8$ in order for the jacobian to have eigenvalues in the open right half plane. When we combine this with the result of (B.7) it is clear that the Hurwitz's criterium cannot be satisfied for $n < 8$. Therefore the trajectories of the Diekman model (with $n = 4$) are attracted to a stable equilibrium.

Appendix C

Bounded solutions

The solutions of the Diekman model are bounded. In order to prove this every differential equation (of the model) is considered. It is shown that at every equilibrium the vector field is directed inwards.

The analysis starts by taking a look at the system's gating variables. The dynamics of the gating variables $x_{2,3,...,8}$ are described by:

$$\frac{dx_i}{dt} = \frac{x_{i\infty} - x_i}{\tau_i}, \quad i = 2, 3, ..., 8 \tag{C.1}$$

where, $0 < x_{i\infty} < 1$ and $\tau_i > 0$ such that $\frac{dx_i}{dt} > 0$ for $x_i = 0$ and $\frac{dx_i}{dt} < 0$ for $x_i = 1$. Consequently, when $0 < x_i(t_0) < 1$ the solutions will never leave this space such that $0 < x_i(t) < 1$. Now let's look at the differential equation describing the membrane voltage. It is given by:

$$\begin{aligned} C\frac{dx_1}{dt} &= -I_{Na} - I_K - I_{CaL} - I_{CaNonL} - I_{KCa} - I_{K-leak} - I_{Na-leak} + u \\ &= -g_{Na}x_2^3x_3(x_1 - E_{Na}) - g_K x_4^4(x_1 - E_K) - g_{CaL}x_5 f_L(x_1 - E_{Ca}) \\ &- g_{CaNonL}x_6x_7(x_1 - E_{Ca}) - g_{KCa}(x_{13})x_8^2(x_1 - E_k) - g_{K-leak}(x_{13})(x_1 - E_k) \\ &- g_{Na-leak}(x_1 - E_{Na}) + u \end{aligned} \tag{C.2}$$

where $g_{Na}, g_K, g_{CaL}, g_{CaNonL}, g_{Na-leak}, C \in \mathbb{R}$ are positive constants and $E_{Na}, E_K, E_{Ca}, I \in \mathbb{R}$. Conductances $g_{KCa}(x_{13})$ and $g_{K-leak}(x_{13})$ are also positive with boundaries $2 < g_{KCa}(x_{13}) < 200, 0 < g_{K-leak}(x_{13}) < 0.2$. Moreover f_L is defined as $f_L = \frac{K_1}{K_2 + x_9}$, where $K_1 > 0$ and $K_2 > 0$ such that $0 < f_L < \frac{K1}{K2}$. The reversal potentials are given as $E_{Ca} > E_{Na} > 0$ and $E_K < 0$. At $x_1 = E_K$ equation (C.2) can be simplified to:

$$\begin{aligned} \dot{x}_1 = &- g_{Na}x_2^3x_3(E_K - E_{Na}) - g_{CaL}x_5 f_L(E_K - E_{Ca}) \\ &- g_{CaNonL}x_6x_7(E_K - E_{Ca}) - g_{Na-leak}(E_K - E_{Na}) \end{aligned} \tag{C.3}$$

where $(E_K - E_{Na}) < 0$ and $(E_K - E_{Ca}) < 0$. Since all conductances $g > 0$ and all gating variables $x_{1,2,...,8} > 0$ the right-hand side of (C.3) is a sum of positive terms. Therefore $\dot{x}_1$ is always larger than zero for $x_1 = E_K$. Moreover, in case $x_1 = E_{Ca}$ Equation C.2 can be rewritten as:

$$\begin{aligned} \dot{x}_1 = &- g_{Na}x_2^3x_3(E_{Ca} - E_{Na}) - g_K x_4^4(E_{Ca} - E_K) - g_{KCa}(x_{13})x_8^2(E_{Ca} - E_k) \\ &- g_{K-leak}(x_{13})(E_{Ca} - E_k) - g_{Na-leak}(E_{Ca} - E_{Na}) \end{aligned} \tag{C.4}$$

where $(E_{Ca} - E_{Na}) > 0$ and $(E_{Ca} - E_K) > 0$. Since all conductances g are positive and all gating variables $x_{2,3,\ldots,8}$ are nonnegative the right-hand side of (C.4) is a sum of negative terms. Therefore $\dot{x}_1$ is always smaller than zero for $x_1 = E_{Ca}$. When x_1 takes the value of E_K $\dot{x}_1$ is positive and x_1 increases. When x_1 takes the value E_{Ca} $\dot{x}_1$ is negative and x_1 decreases. So when x_1 is in this boundary, it will never get out. So when $x_1(t) \in \mathbb{R} : E_K \leq x(t) \leq E_{Ca}$ than $x_1(t+T) \in \mathbb{R} : E_K \leq x(t+T) \leq E_{Ca}$ with $T \in \mathbb{R}$. In fact, when solving the the equation $\dot{x}_1 = 0$ the bound around x_1 can be taken a little tighter.

Subsequently it can be shown that x_9 and x_{10} are also bounded for bounded x_1. Note that x_9 and x_{10} represent the intercellular calcium concentrations. Therefore they are only defined for $x_9, x_{10} > 0$. The states are described by

$$\frac{dx_i}{dt} = -k_i(I_{CaL} + I_{CaNonL}) - \frac{x_i}{\tau_i} + b_i, \quad i = 9, 10 \tag{C.5}$$

$$= -k_i(g_{CaL}x_5 f_L(x_1 - E_{Ca}) + g_{CaNonL}x_6 x_7(x_1 - E_{Ca})) - \frac{x_i}{\tau_i} + b_i \tag{C.6}$$

where k_i, τ_i and b_i are positive constants. The gating variables $x_{2,3,\ldots,8}$ occupy values between zero and one (for initial conditions between zero and one). Since $x_1 \leq E_{Ca}$ the first term of the right-hand side of (C.5) is always nonnegative. Therefore $\dot{x}_9$ and $\dot{x}_{10}$ are always nonnegative for $x_9, x_{10} \geq \tau_i b_i$. So for $x_9, x_{10} \geq \tau_i b_i$, the states will never drop below $\tau_i b_i$. When we substitute the lower bound of $x_1 = E_K$ the maximum functions of $\dot{x}_9$ and $\dot{x}_{10}$ are given by

$$\frac{dx_i}{dt} \leq -k_i(g_{CaL}\frac{K_1}{K_2}(E_K - E_{Ca}) + g_{CaNonL}(E_K - E_{Ca})) + b_i - \frac{x_i}{\tau_i} \tag{C.7}$$

When setting to zero and solving this equation one can find the upper bounds

$$x_i \leq -k_i \cdot \tau_i(g_{CaL}\frac{K_1}{K_2}(E_K - E_{Ca}) + g_{CaNonL}(E_K - E_{Ca})) + \tau_i b_i, \quad i = 9, 10 \tag{C.8}$$

Therefore states x_9 and x_{10} are also bounded for bounded x_1 and bounded gating variables $x_{2,3,\ldots,8}$.

For completeness let's evaluate the bounds for for the final three differential equations. x_{11} represents the mRNA concentration defined as:

$$\frac{dx_{11}}{dt} = a(CRE(x_{10}) \cdot E_{box}(x_{13})^n - x_{11}) \tag{C.9}$$

where $0 < E_{box}(x_{13}) < 1$ for $x_{13} > 0$ and a and n are positive constants. Since the altered version of $CRE(x_{10}) = \max(0, 10^6 \cdot x_{10} - 75)$ only takes nonnegative values the lower bound of x_{11} is zero. The upper bound of x_{11} is given by substituting the upper bound of $CRE(x_{10})$ and $E_{box(x_{13})}$ in Equation (C.9). The upper bound becomes

$$x_{11} \leq (10^6 \cdot (-k_{10} \cdot \tau_{10}(g_{CaL}\frac{K_1}{K_2}(E_K - E_{Ca}) + g_{CaNonL}(E_K - E_{Ca})) + \tau_{10}b_{10}) - 75) - x_{11}) \tag{C.10}$$

When we substitute the lower bound of x_{11} in the 12th differential equation we get

$$\frac{dx_{12}}{dt} = -ax_{12} \tag{C.11}$$

which is converges to zero. So the lower bound of x_{12} is zero. The upper bound of x_{12} is equal to the upper bound of x_{11} described by

$$x_{12} \leq (10^6 \cdot (-k_{10} \cdot \tau_{10}(g_{CaL}\frac{K_1}{K_2}(E_K - E_{Ca}) + g_{CaNonL}(E_K - E_{Ca})) + \tau_{10}b_{10}) - 75) - x_{11}) \tag{C.12}$$

Subsequently, the lower bound of x_{13} is zero and the upper bound is equal to the upper bounds of x_{11} and x_{12}.

To summarize, the space Ω is defined as:

$$\begin{aligned}
E_K \leq & x_1 \leq E_{Ca} \\
0 \leq & x_2 \leq 1 \\
0 \leq & x_3 \leq 1 \\
0 \leq & x_4 \leq 1 \\
0 \leq & x_5 \leq 1 \\
0 \leq & x_6 \leq 1 \\
0 \leq & x_7 \leq 1 \\
0 \leq & x_8 \leq 1 \\
\tau_9 b_9 \leq & x_9 \leq (-k_9 \cdot \tau_9(g_{CaL}\frac{K_1}{K_2}(E_K - E_{Ca}) + g_{CaNonL}(E_K - E_{Ca})) + \tau_9 b_9) \\
\tau_{10} b_{10} \leq & x_{10} \leq (-k_{10} \cdot \tau_{10}(g_{CaL}\frac{K_1}{K_2}(E_K - E_{Ca}) + g_{CaNonL}(E_K - E_{Ca})) + \tau_{10} b_{10}) \\
0 \leq & x_{11} \leq (10^6 \cdot (-k_{10} \cdot \tau_{10}(g_{CaL}\frac{K_1}{K_2}(E_K - E_{Ca}) + g_{CaNonL}(E_K - E_{Ca})) + \tau_{10} b_{10}) - 75)) \\
0 \leq & x_{12} \leq (10^6 \cdot (-k_{10} \cdot \tau_{10}(g_{CaL}\frac{K_1}{K_2}(E_K - E_{Ca}) + g_{CaNonL}(E_K - E_{Ca})) + \tau_{10} b_{10}) - 75)) \\
0 \leq & x_{13} \leq (10^6 \cdot (-k_{10} \cdot \tau_{10}(g_{CaL}\frac{K_1}{K_2}(E_K - E_{Ca}) + g_{CaNonL}(E_K - E_{Ca})) + \tau_{10} b_{10}) - 75))
\end{aligned} \tag{C.13}$$

In the previous we have seen that there is a space $\Omega \subset \mathbb{R}^{13}$ such that $x(t) \in \Omega$ than $x(t+T) \in \Omega$ with $T \in \mathbb{R}$. This means that if the system is initiated within B than it will never leave Ω. The space Ω is a 13 dimensional space spanned by the previously estimated bounds of the states.

Appendix D

Laplacian spectrum

The goal of this appendix is to calculate the spectrum a a nearest neighbour matrix. First, a notion about circulant matrices will be considered. Thereafter, the spectrum of (some) nearest neighbour networks is calculated.

D.1 Circulant matrices

A circulant matrix is a special kind of matrix. It is characterized by a high order of repetition. Every row in the matrix is the same as the previous row but shifted to the right by one position. Equation D.1 gives a example of an $n \times n$ circulant matrix C. Note that every row is shifted by one to represent the next row. This shift is called a circular shift. This can be done until the final row of the matrix is reached. However, when the final row is shifted the first row of the matrix appears. One can say the matrix is circular in some sense.

$$C = \begin{pmatrix} c_0 & c_1 & c_2 & \cdots & c_{n-2} & c_{n-1} \\ c_{n-1} & c_0 & \ddots & & & c_{n-2} \\ c_{n-2} & \ddots & \ddots & \ddots & & \vdots \\ \vdots & & \ddots & \ddots & \ddots & c_{n-2} \\ c_2 & & & & c_0 & c_1 \\ c_1 & c_2 & \cdots & c_{n-2} & c_{n-1} & c_0 \end{pmatrix} \tag{D.1}$$

The repetitive structure of a circulant matrix C can be captured in a matrix polynomial $p(C)$. The polynomial is build out of special permutation matrices. A permutation matrix is any matrix that has a single one entry in every row and the rest zeros. An example of a special permutation matrix is

$$M = \begin{pmatrix} 0 & 1 & 0 & \cdots & 0 \\ \vdots & 0 & 1 & 0 & 0 \\ \vdots & & \ddots & \ddots & \vdots \\ 0 & & & \ddots & 1 \\ 1 & 0 & \cdots & \cdots & 0 \end{pmatrix} \tag{D.2}$$

This permutation matrix itself is circulant. In fact it is the identity matrix subjected to one circulant shift. Moreover, it is equal to the one nearest neighbour adjacency matrix.

This will be further discussed later. Any circulant matrix can be represented as the sum of powers of the permutation matrix [39]. When taking the power of the permutation matrix every one entry moves one position to the right. Obviously, the powers of the permutation matrix are again circulant.

Lemma D.1.1. [39] Any circulant matrix C can be written as a matrix polynomial $P(C)$ such that

$$p(C) = c_0 I + c_1 M + c_2 M^2 + ... + c_{N-1} M^{N-2} = \sum_{j=0}^{N-1} c_j M^{j-1} \tag{D.3}$$

where M is the permutation matrix

When evaluating the eigenvectors of a circulant matrix it is useful to consider the eigenvectors of the permutation matrix. Since any circulant matrix is the sum of powers of permutation matrices the eigenvectors of a circulant matrix can be distilled from the eigenvectors of the permutation matrix. The permutation matrix has a special characteristic equation. In order to invesigate this the determinant of $(\lambda I - M)$ is taken.

$$\det(\lambda I - M) = \begin{vmatrix} \lambda & -1 & 0 & \cdots & 0 \\ 0 & \lambda & -1 & \ddots & \vdots \\ \vdots & \ddots & \ddots & \ddots & \\ 0 & & \ddots & \ddots & -1 \\ -1 & 0 & \ddots & 0 & \lambda \end{vmatrix}^{N\times N} = \lambda \begin{vmatrix} \lambda & -1 & 0 & \cdots & 0 \\ 0 & \lambda & -1 & \ddots & \vdots \\ \vdots & \ddots & \ddots & \ddots & \\ 0 & & \ddots & \ddots & -1 \\ 0 & 0 & \ddots & 0 & \lambda \end{vmatrix}^{(N-1)\times(N-1)}$$

$$(-1)^N \begin{vmatrix} -1 & 0 & \cdots & \cdots & 0 \\ \lambda & -1 & \ddots & & \vdots \\ 0 & \ddots & \ddots & \ddots & \vdots \\ \vdots & & \ddots & -1 & 0 \\ 0 & \cdots & 0 & \lambda & -1 \end{vmatrix}^{(N-1)\times(N-1)} \tag{D.4}$$

The determinant of $(\lambda I - M)$ is expanded to two determinants (D.4). The first determinant is a triangular. Consequently, the determinant is equal to the product of the diagonal entries i.e. the eigenvalues. The second determinant has values -1 on the diagonal and the eigenvalues on the sub-diagonal. It is also triangular. Consequently, the determinant is equal to the product of all diagonal entries. Therefore the characteristic equation of matrix M for arbitrary dimensions is

$$\det(\lambda I - M) = \lambda^N - 1 \tag{D.5}$$

The permutation matrix therefore has the eigenvalue $\lambda^N = 1$. These eigenvalues are called *roots of unity* [39]. They lay on the unit circle such that

$$\lambda = \cos\left(\frac{2\pi u}{N}\right) + i\sin\left(\frac{2\pi u}{N}\right) = e^{\frac{2i\pi u}{N}}, \quad \text{with } u = \{1, 2, .., N\} \tag{D.6}$$

Lemma D.1.2. [39] Let λ be an eigenvalue of any matrix permutation matrix (not just M) than λ^n is an eigenvalue of M^n with the same corresponding eigenvector ($v \neq 0$).

Proof. Let M be a permutation matrix with eigenvalue λ with corresponding eigenvector v than

$$\begin{aligned} Mv &= \lambda v \\ M^n v &= M^{n-1}(\lambda v) \\ M^n v &= \lambda(M^{n-1} v) \\ M^n v &= \lambda^n v \end{aligned}$$

□

Lemma D.1.3. Let $p(C) = c_0 I + c_1 M + c_2 M^2 + ... + c_{N-1} M^{N-1}$. Suppose λ is an eigenvalue of M with corresponding eigenvector v. Then $p(\lambda)$ is an eigenvalue of $p(C)$ with the same eigenvector v

Proof. Suppose λ is an eigenvalue of M with corresponding eigenvector v. Than using lemma D.1.2

$$\begin{aligned} p(C) &= c_0 I + c_1 M + c_2 M^2 + ... + c_{n-1} M^{n-1} \\ p(C)\, v &= \left(c_0 I + c_1 M + c_2 M^2 + ... + c_{n-1} M^{n-1}\right)\, v \\ p(C)\, v &= \left(c_0 I + c_1 \lambda + c_2 \lambda^2 + ... + c_{n-1} \lambda^{n-1}\right)\, v \\ p(C) &= p(\lambda) \end{aligned}$$

□

By using lemma D.1.3 the eigenvalues of any circulant matrix can be written as the sum of powers of the roots of unity. Next sections apply this concept to the all-to-all network and some nearest neighbour networks.

D.2 Nearest neighbour networks

A nearest neighbour network is characterized by the number of nodes N and the number of neighbours k.

Using lemma D.1.1 the Laplacian matrix for even k can be written as a matrix polynomial such that

$$L_N = kI_N + (-1)\sum_{j=1}^{k/2}\left(M^j + M^{N-j}\right), \quad \text{given that } \; k = 2 \cdot p, \quad \text{and } p \in \mathbb{R}$$

Using lemma D.1.3 the eigenvalues of the Laplacian are

$$\lambda_u = k + (-1)\sum_{j=1}^{k/2}\left(\lambda_{M,u}^j + \lambda_{M,u}^{N-j}\right), \quad \text{with } u = \{1, 2, ..., N\}$$

Substitute the standard eigenvalues of the permutation matrix

$$\lambda_u = k + (-1)\sum_{j=1}^{k/2}\left(e^{\frac{2i\pi u}{N}j} + e^{2i\pi u\frac{N-j}{N}}\right)$$

The Euler equation is used to separate the complex exponential into a real and an imaginary part. The imaginary part drops from the equation such that

$$\lambda_u = k - \sum_{j=1}^{k/2}\left(cos(\frac{2\pi uj}{N}) + cos(2\pi(1-\frac{j}{N})u)\right)$$

Note that the second term in the summation is equal to the first (with a period shift) such that

$$\lambda_u = k - 2\sum_{j=1}^{k/2}\cos\left(\frac{2\pi uj}{N}\right), \quad u = \{1, 2, ..., N\} \tag{D.7}$$

Bibliography

[1] Nikolay B Milev and Akhilesh B Reddy. Circadian redox oscillations and metabolism. *Trends in Endocrinology & Metabolism*, 26(8):430–437, 2015.

[2] Robert Y Moore. The suprachiasmatic nucleus and the circadian timing system. In *Progress in molecular biology and translational science*, volume 119, pages 1–28. Elsevier, 2013.

[3] Jyoti Madhusoodanan. Circadian rhythms influence treatment effects. *The Scientist*, 4, 2017.

[4] DB Boivin and P Boudreau. Impacts of shift work on sleep and circadian rhythms. *Pathologie Biologie*, 62(5):292–301, 2014.

[5] Oscar Heerkens Thijssen. *Neuronal coupling the suprachiasmaticnucleus*. TU Delft, 2019.

[6] Harvey Lodish, Arnold Berk, S Lawrence Zipursky, Paul Matsudaira, David Baltimore, James Darnell, et al. *Molecular cell biology*, volume 3. WH Freeman New York, 1995.

[7] Vallath Reghunandanan and Rajalaxmy Reghunandanan. Neurotransmitters of the suprachiasmatic nuclei. *Journal of Circadian Rhythms*, 4(1):2, 2006.

[8] Steven M Reppert and David R Weaver. Molecular analysis of mammalian circadian rhythms. *Annual review of physiology*, 63(1):647–676, 2001.

[9] Steven R. Bolsover. *Cell Biology : A Short Course.*, volume 2nd ed. Wiley-Liss, 2004.

[10] Eric E Zhang, Andrew C Liu, Tsuyoshi Hirota, Loren J Miraglia, Genevieve Welch, Pagkapol Y Pongsawakul, Xianzhong Liu, Ann Atwood, Jon W Huss III, Jeff Janes, et al. A genome-wide rnai screen for modifiers of the circadian clock in human cells. *Cell*, 139(1):199–210, 2009.

[11] Caroline H Ko and Joseph S Takahashi. Molecular components of the mammalian circadian clock. *Human molecular genetics*, 15(suppl_2):R271–R277, 2006.

[12] Jennifer A Mohawk and Joseph S Takahashi. Cell autonomy and synchrony of suprachiasmatic nucleus circadian oscillators. *Trends in neurosciences*, 34(7):349–358, 2011.

[13] David K Welsh, Joseph S Takahashi, and Steve A Kay. Suprachiasmatic nucleus: cell autonomy and network properties. *Annual review of physiology*, 72:551–577, 2010.

[14] Christina Vasalou and Michael A Henson. A multiscale model to investigate circadian rhythmicity of pacemaker neurons in the suprachiasmatic nucleus. *PLoS computational biology*, 6(3):e1000706, 2010.

[15] Sandra J Kuhlman and Douglas G McMahon. Rhythmic regulation of membrane potential and potassium current persists in scn neurons in the absence of environmental input. *European Journal of Neuroscience*, 20(4):1113–1117, 2004.

[16] Mino DC Belle, Casey O Diekman, Daniel B Forger, and Hugh D Piggins. Daily electrical silencing in the mammalian circadian clock. *Science*, 326(5950):281–284, 2009.

[17] Sara J Aton and Erik D Herzog. Come together, right... now: synchronization of rhythms in a mammalian circadian clock. *Neuron*, 48(4):531–534, 2005.

[18] Michael A Long, Michael J Jutras, Barry W Connors, and Rebecca D Burwell. Electrical synapses coordinate activity in the suprachiasmatic nucleus. *Nature neuroscience*, 8(1):61, 2005.

[19] Erik D Herzog, Sara J Aton, Rika Numano, Yoshiyuki Sakaki, and Hajime Tei. Temporal precision in the mammalian circadian system: a reliable clock from less reliable neurons. *Journal of biological rhythms*, 19(1):35–46, 2004.

[20] Per Brodal. *The central nervous system: structure and function*. Oxford University Press, 2004.

[21] Alan L Hodgkin and Andrew F Huxley. A quantitative description of membrane current and its application to conduction and excitation in nerve. *The Journal of physiology*, 117(4):500–544, 1952.

[22] Brian C Goodwin. Oscillatory behavior in enzymatic control processes. *Advances in enzyme regulation*, 3:425–437, 1965.

[23] Casey O Diekman, Mino DC Belle, Robert P Irwin, Charles N Allen, Hugh D Piggins, and Daniel B Forger. Causes and consequences of hyperexcitation in central clock neurons. *PLoS computational biology*, 9(8):e1003196, 2013.

[24] Ferdinand Verhulst. *Methods and applications of singular perturbations: boundary layers and multiple timescale dynamics*, volume 50. Springer Science & Business Media, 2005.

[25] Didier Gonze, Samuel Bernard, Christian Waltermann, Achim Kramer, and Hanspeter Herzel. Spontaneous synchronization of coupled circadian oscillators. *Biophysical journal*, 89(1):120–129, 2005.

[26] H.K. Khalil. *Nonlinear Control*. Always Learning. Pearson Education Limited, 2014.

[27] Christof Koch. *Biophysics of computation: information processing in single neurons*. Oxford university press, 2004.

[28] B Malcolm Brown, Michael SP Eastham, and Karl Michael Schmidt. *Periodic differential operators*, volume 228. Springer Science & Business Media, 2012.

[29] Erik Steur, Ivan Tyukin, and Henk Nijmeijer. Semi-passivity and synchronization of diffusively coupled neuronal oscillators. *Physica D: Nonlinear Phenomena*, 238(21):2119–2128, 2009.

[30] Alexey Victorovich Pavlov, Nathan van de Wouw, and Henk Nijmeijer. *Uniform output regulation of nonlinear systems: a convergent dynamics approach*. Springer Science & Business Media, 2006.

[31] Alexander Ostrowski and Hans Schneider. Some theorems on the inertia of general matrices. *J. Math. Anal. Appl*, 4(1):72–84, 1962.

[32] Mino DC Belle and Casey O Diekman. Neuronal oscillations on an ultra-slow timescale: daily rhythms in electrical activity and gene expression in the mammalian master circadian clockwork. *European Journal of Neuroscience*, 2018.

[33] Harry Pantazopoulos, Hamid Dolatshad, and Fred C Davis. Chronic stimulation of the hypothalamic vasoactive intestinal peptide receptor lengthens circadian period in mice and hamsters. *American Journal of Physiology-Regulatory, Integrative and Comparative Physiology*, 299(1):R379–R385, 2010.

[34] Chris Godsil and Gordon F Royle. *Algebraic graph theory*, volume 207. Springer Science & Business Media, 2013.

[35] Alex Arenas, Albert Díaz-Guilera, Jurgen Kurths, Yamir Moreno, and Changsong Zhou. Synchronization in complex networks. *Physics reports*, 469(3):93–153, 2008.

[36] Reinhard Diestel. *Graphentheory*. Springer, 2000.

[37] Nicholas C Foley, Tina Y Tong, Duncan Foley, Joseph LeSauter, David K Welsh, and Rae Silver. Characterization of orderly spatiotemporal patterns of clock gene activation in mammalian suprachiasmatic nucleus. *European Journal of Neuroscience*, 33(10):1851–1865, 2011.

[38] M. Gopal. *Control Systems: Principles and Design*. McGraw-Hill Education (India) Pvt Limited, 2002.

[39] Philip J Davis. *Circulant matrices*. American Mathematical Soc., 2013.

Acronyms

SCN suprachiasmatic nucleus. 1

TTFL transcriptional translational feedback loop. 7

VIP vasoactive intestinal peptide. 9